5.2.5.1 Vadose Zone: 0 to 10.7 m (0 to 35 ft). This section focuses on U-238, Tc-99, and nitrate simulation results for those locations showing elevated concentrations or trends in the vadose zone at depths less than 10.7 m (35 ft). In general, this region encompasses the waste zone and surficial sediment down to the first basalt interface. Since multiple lysimeters can be at different elevations for an individual well location, lysimeters are referred to in this subsection using a combined well name lysimeter number identifier. See Section 2.3.2 for a complete list of lysimeters in the SDA.

5.2.5.1.1 Uranium-238—From Section 4, lysimeters at Wells PA-01, PA-02, W08, and W23 show substantially elevated concentrations relative to an estimated background concentration of 3.86 pCi/L for the vadose zone. This background concentration is added onto simulation results in the following time histories. The first set of time histories shown in Figure 5-32 is for lysimeters at Wells PA-01, PA02, W08, 98-4, and W25; all five wells are located in the east-central portion of the SDA. At first impression, the simulation results show almost no agreement; however, this difference is explained by the relationship of the gridblocks containing the lysimeters to the locations where U-238 is released from the source model into the vadose zone model. For example, Figure 5-32 also shows a simulated-concentration time history for U-238 for a gridblock that is one gridblock north of the location containing Well PA02-L16. This latter gridblock location is assigned the Pad A waste stream. The time history at this location shows better agreement with observed monitoring results. The concentrations are slightly underpredicted, but are well within the same order of magnitude. Lysimeters in Wells PA01 and W08 also are not in gridblock locations that have a U-238 source release superimposed on them; for similar reasons, these wells show poor agreement with observed concentrations. Lysimeters in Wells 98-4 and W25 show similar behavior, with location relative to gridblocks where waste streams are applied as being important. The lysimeter in Well 98-4 corresponds to the gridblock one cell west of the Pit 4 waste stream and shows reasonable agreement with monitoring data, which is similar to the estimated background. The lysimeter in Well W25, however, just barely corresponds to the westernmost gridblock receiving the Pit 4 waste stream, and the simulated results overpredict monitoring results, which again are similar to the estimated background concentration. With a model as coarsely discretized as the RI/FS model, some locations will show good agreement and some locations will not, depending on where mass is loaded into the vadose zone model from the source model. Also, simulated concentrations represent an average for the entire gridblock, whereas monitoring results represent point data that will vary spatially.

The simulated concentration time history is shown in Figure 5-33 for the three lysimeters in Well W23, located in the western portion of the SDA. This gridblock corresponds to the source-release area of Trenches 1 through 10, which does have U-238 mass imposed on it. As a result, simulated concentrations are nonzero for this location and, although low compared to the observed concentrations, are within an order of magnitude of the monitoring results.

To avoid giving the erroneous impression that U-238 is underpredicted everywhere, vertical cross sections, which include source-release locations, in the second-level refined grid are presented in Figure 5-34. Figure 5-34 shows the locations of the cross sections—two west-east and one south-north. The additional blue shading on the locations of the cross sections indicates source-release gridblocks, with the darker shading showing those locations with higher source-release fluxes, and the lighter shading showing those locations with lower source-release fluxes. Figures 5-35, 5-36, and 5-37 show the cross sections from the indicated locations for a simulation time corresponding to Calendar Year 2004. Monitoring results from this time period are posted on the plot at their approximate location. Also posted beneath these two values is the number of monitoring results that were available from this lysimeter from an arbitrary 2-year period before and after the indicated time. Only samples with detections are posted. Lithologic divisions can be discerned in the cross sections. Land surface is the uppermost solid line and shows slight variations in surface elevation. Solid lines also indicate the bottom of the surficial sediment and the A-B interbed.

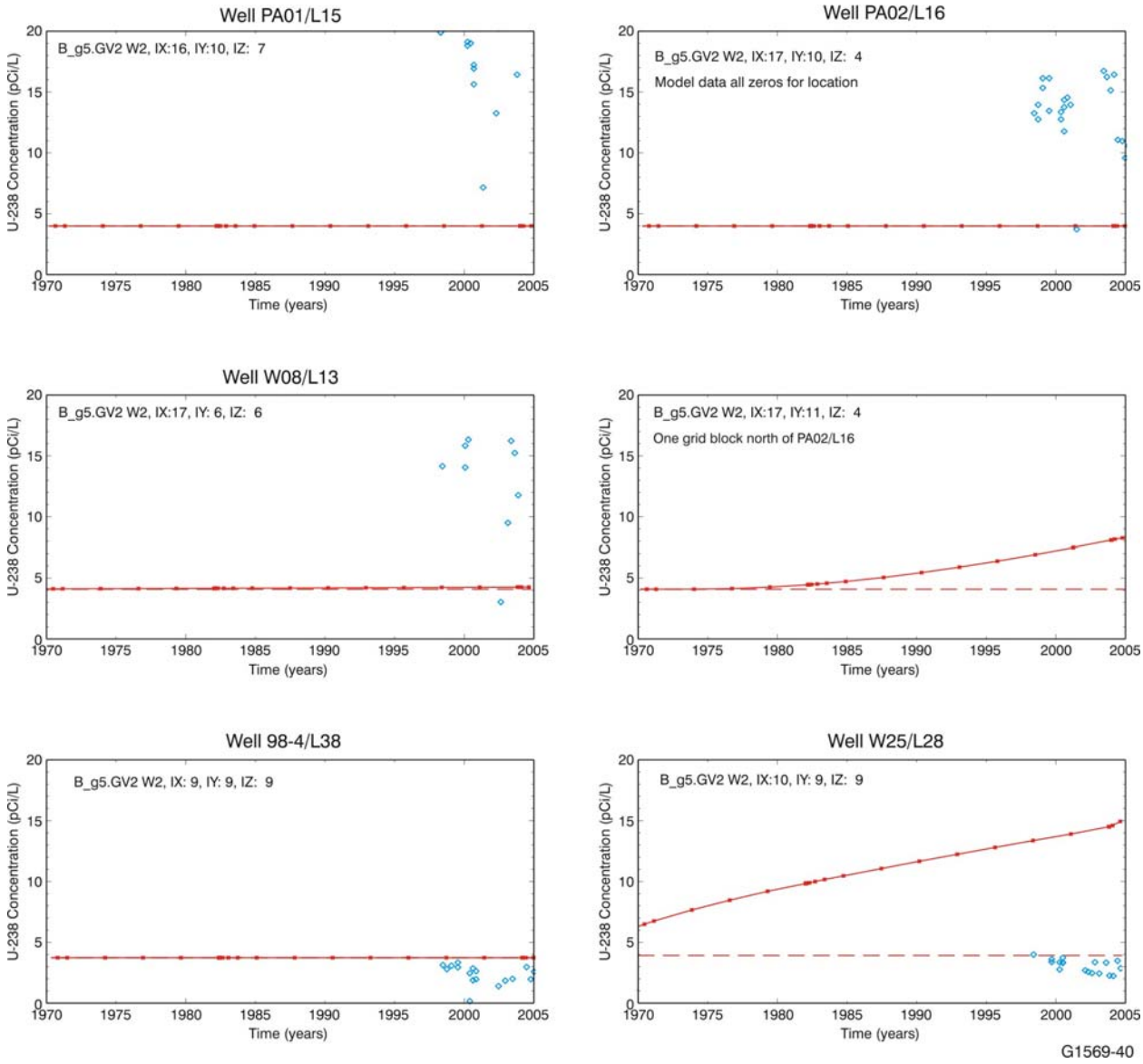

Figure 5-32. Time-history comparison of simulated (red line) and observed (blue diamonds) concentrations for uranium-238 in the lysimeters at Wells PA01, PA02, W08, W98-4, and W25. Background concentration is indicated by the dashed line.

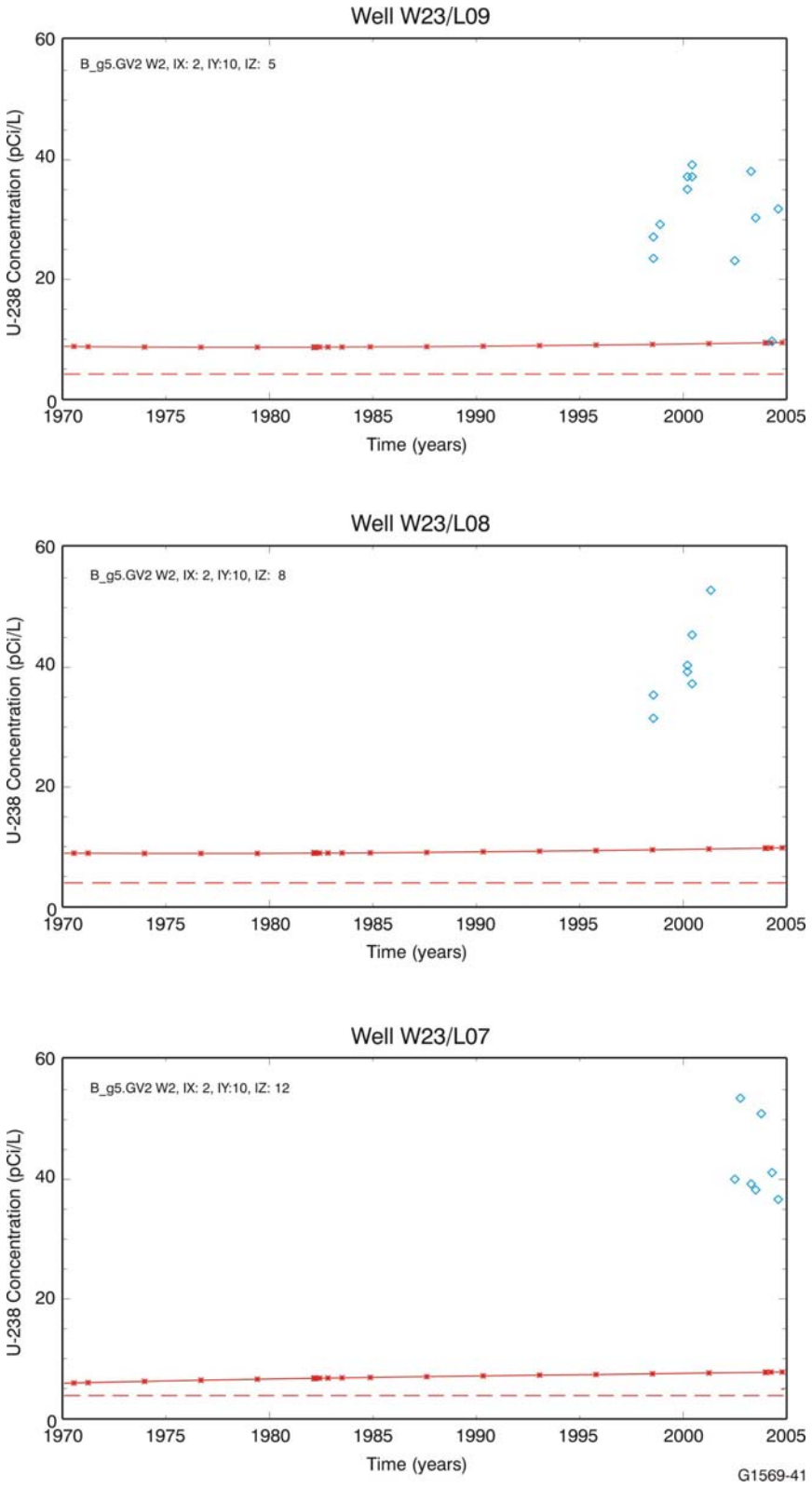

Figure 5-33. Time-history comparison of simulated (red line) and observed (blue diamonds) concentrations for uranium-238 in the lysimeters at Well W23. Background concentration is indicated by the dashed line.

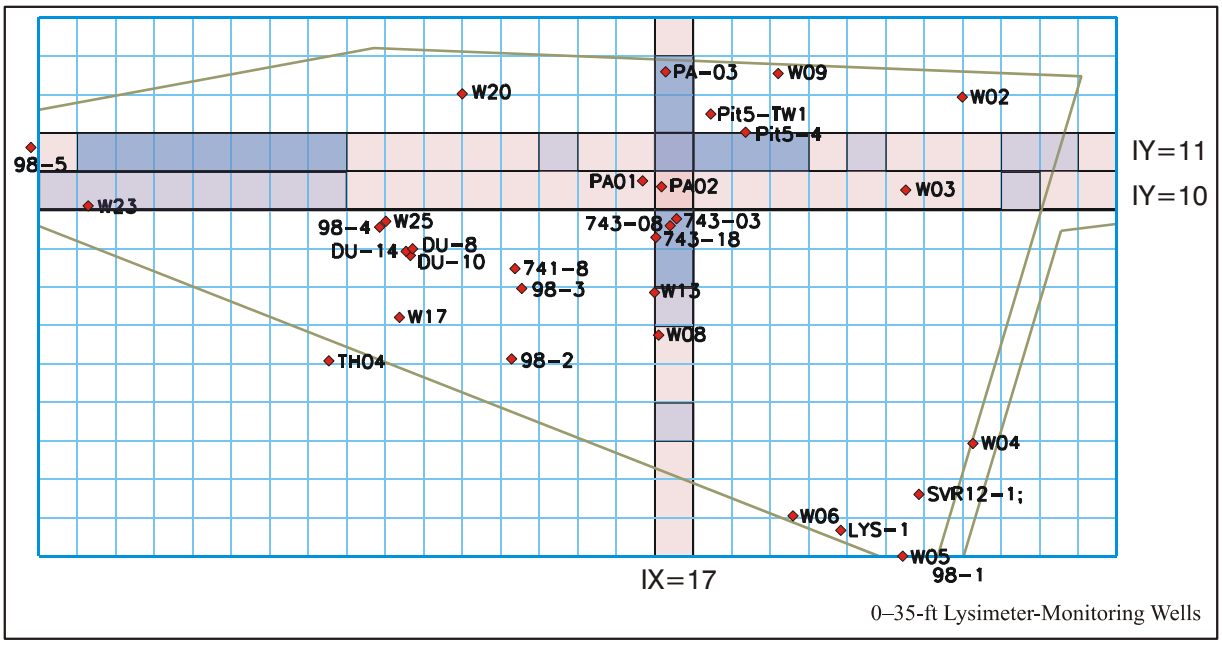

Figure 5-34. Locations of cross sections in the second-level refined grid vadose zone domain. Darker blue shaded gridblocks indicate locations of primary uranium-238 mass loading from the source-release model.

Cross sections in Figures 5-35, 5-36, and 5-37 clearly show the effect of discretization and where U-238 mass is assigned in the model. The effect of the U-238 mass assignment relative to the location of Well PA02 also can be seen in the cross sections. The southernmost Pad A waste stream gridblock shows up in cross sections of both the W-E Section: Plane 11 (see Figure 5-35) and the S-N Section: Plane 17 (see Figure 5-37). Well PA02 is in the gridblock just to the south, and shows very little simulated U-238 mass in contrast to monitoring results for Well PA02, which show U-238 is elevated. In addition, simulation results in the cross sections show that the majority of the U-238 remains within the lower part of the surficial sediment and selectively migrates downward, with some influence from gaps in the A-B interbed.

5.2.5.1.2 Technetium-99—Only one vadose zone location in the 0 to 10.7-m (0 to 35-ft) depth zone shows an increasing trend for Tc-99. This location is Well W23 and Figure 5-38 shows the simulated results compared to monitoring results for this location. The estimated background concentration for Tc-99 in the vadose zone is 0 pCi/L; therefore, it is not added to the time-history simulation results. Time histories in Figure 5-38 are presented using a logarithmic scale for concentration due to Tc-99 being substantially overpredicted at this location, as well as almost everywhere else in the simulations. Figure 5-39 shows a west-east cross section from the second-level refined grid for simulated Tc-99 concentrations in Calendar Year 2004. The Tc-99 overprediction in the vadose zone model is probably caused by the source-release model overpredicting the release of Tc-99.[d]

d. A task to improve the source-release and fate and transport modeling for Tc-99 is ongoing for incorporation in the Operable Unit 7-13/14 feasibility study to provide a better basis for remedial decisions.

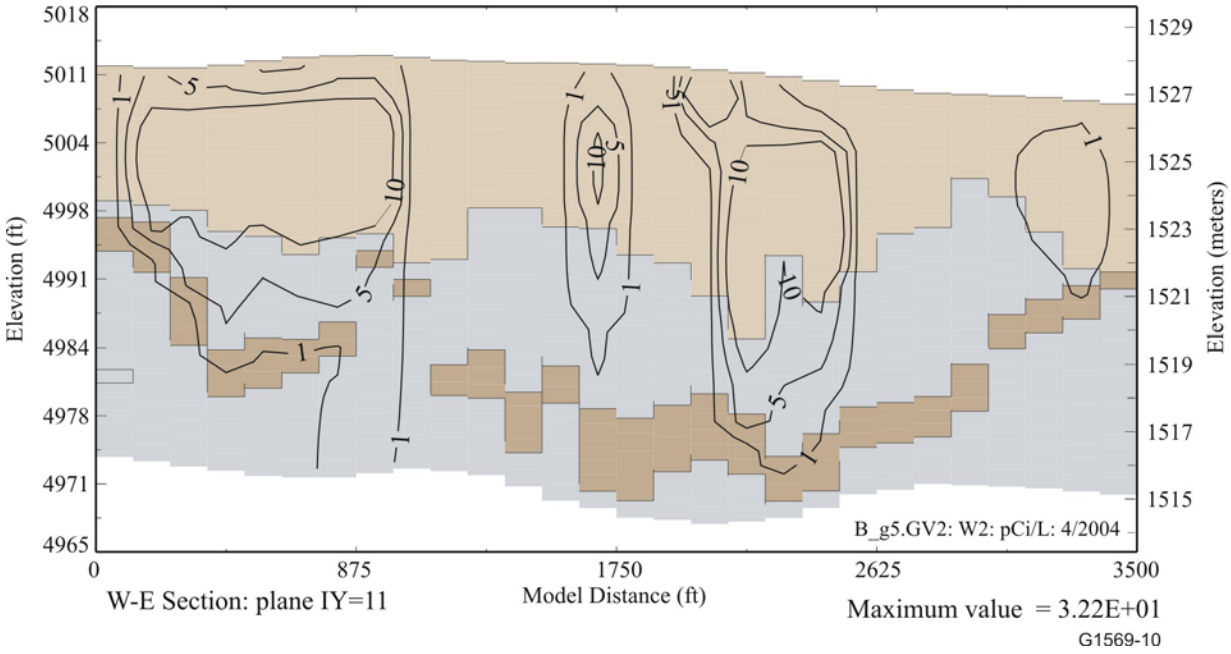

Figure 5-35. Cross section showing simulated uranium-238 aqueous concentrations in Calendar Year 2004 (see Figure 5-34 for the location of cross section).

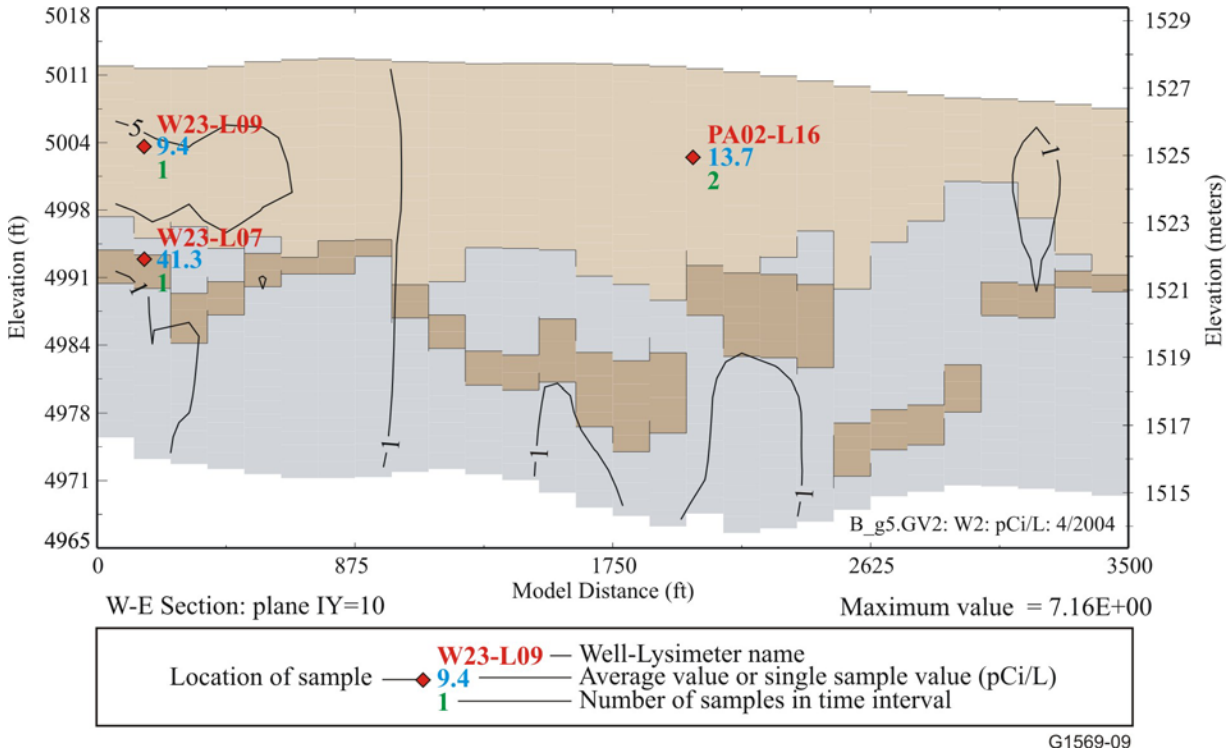

Figure 5-36. Cross section showing simulated uranium-238 aqueous concentrations in Calendar Year 2004 (see Figure 5-34 for the location of cross section).

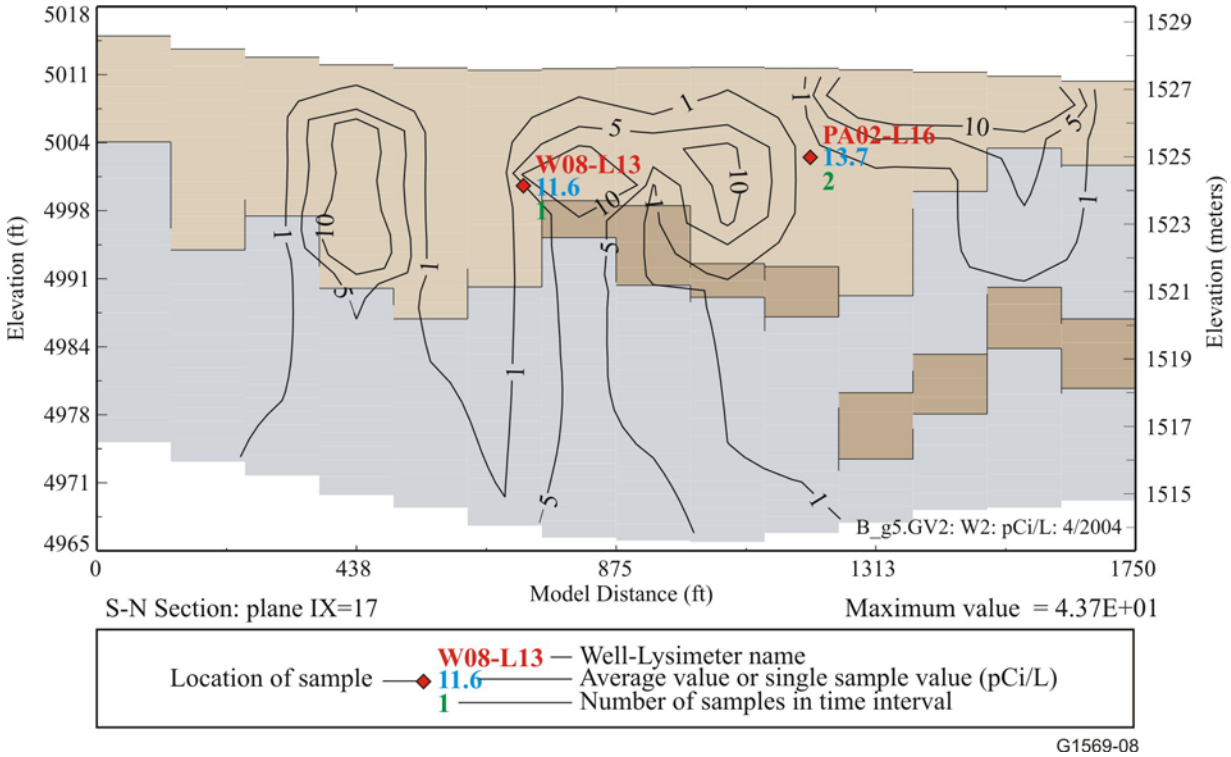

Figure 5-37. Cross section showing simulated uranium-238 aqueous concentrations in Calendar Year 2004 (see Figure 5-34 for location of cross section).

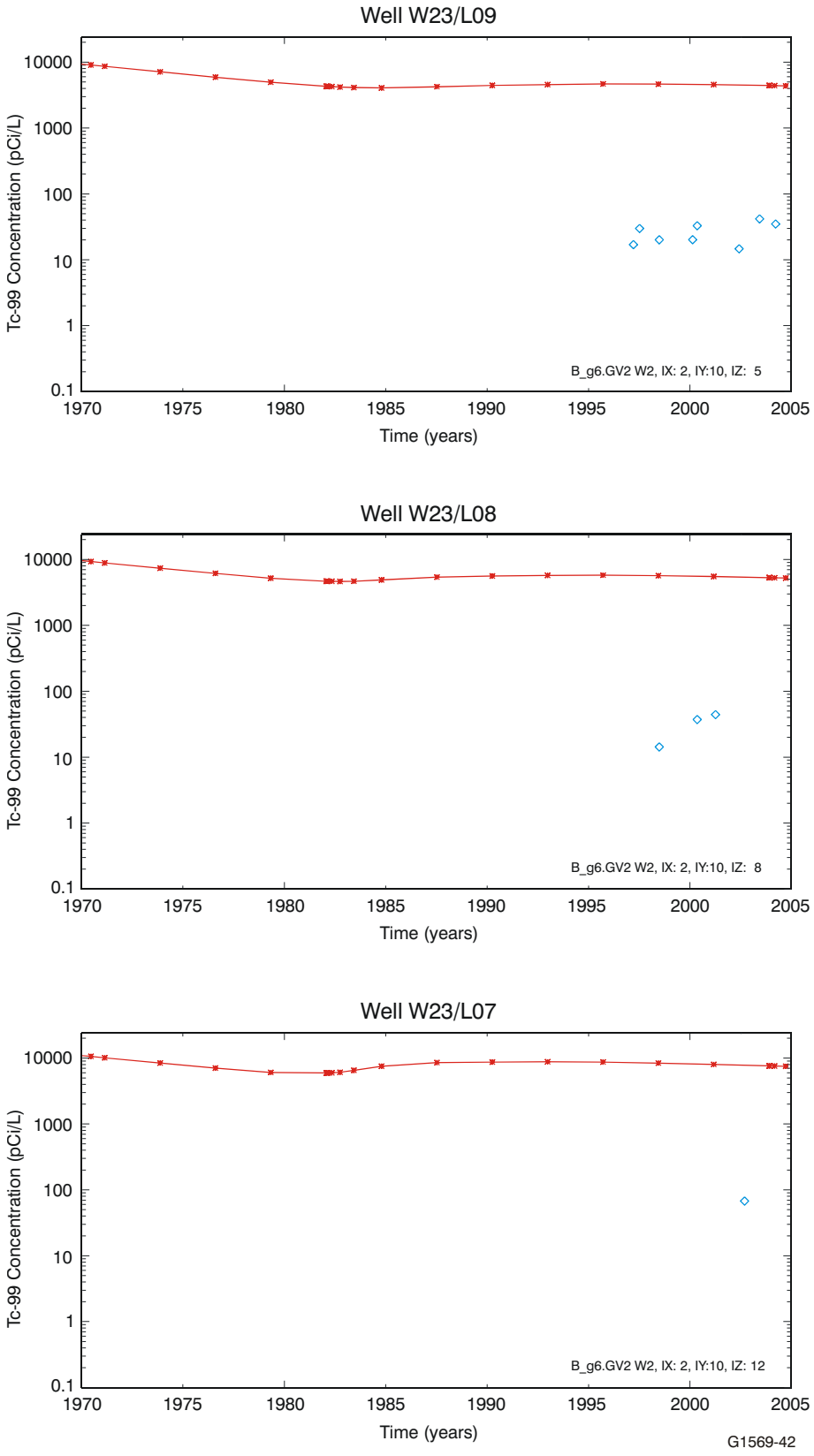

Figure 5-38. Time-history comparison of simulated (red line) and observed (blue diamonds) concentrations for technetium-99 in the lysimeters at Well W23.

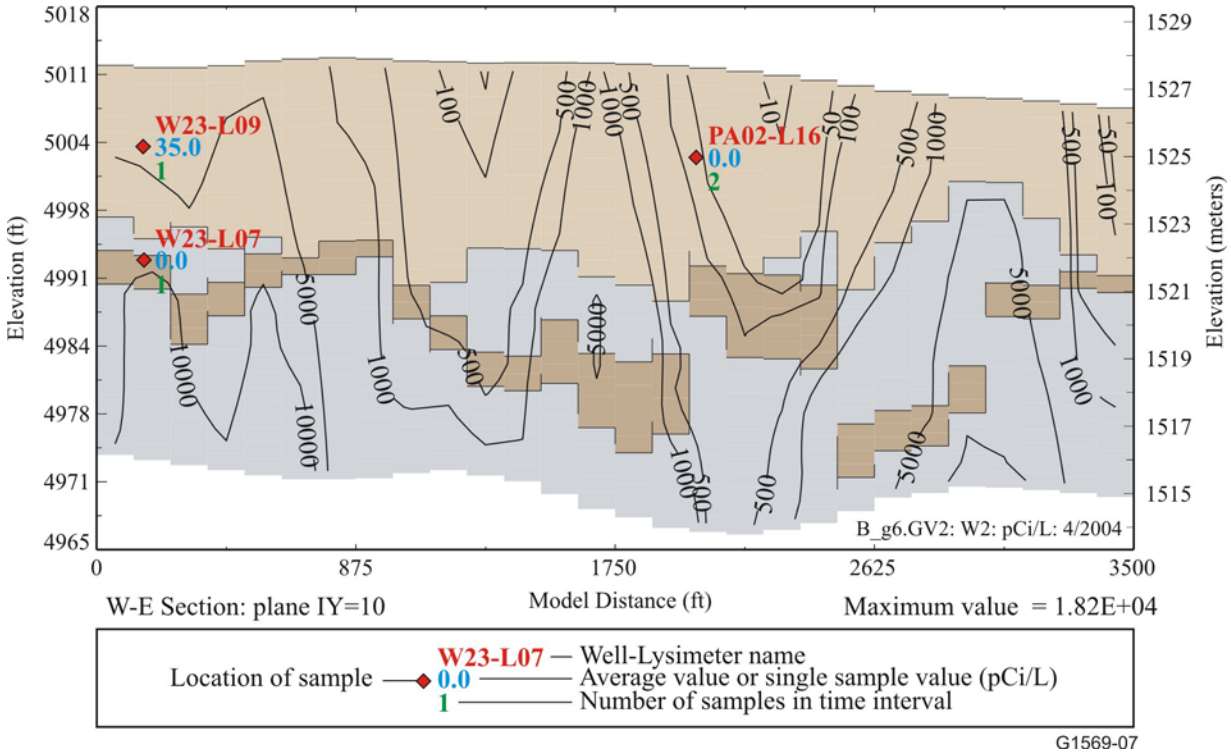

Figure 5-39. Cross section showing simulated technetium-99 aqueous concentrations in Calendar Year 2004.

5.2.5.1.3 Nitrate—Elevated nitrate concentrations were seen at two locations, Wells PA02 and W25 (see Figure 5-40), in the 0 to 10.7-m (0 to 35-ft) zone. The vertical concentration scale is different for the two locations in order to show detail, although both show the simulated concentration to be higher than the observed concentration. In contrast to the U-238 simulation results, even though the gridblock containing Well PA02 does not receive contaminant mass from the source-release model assigned to it, sufficient mass is assigned to the nearby Pad A waste stream blocks to result in appreciable nitrate appearing in the simulation results at this location. These locations were chosen because they show elevated nitrate concentrations; therefore, the model results at all other locations also would show overprediction, leading toward the conclusion that nitrate simulation results are conservative with respect to maximizing groundwater-pathway concentrations.

5.2.5.2 Vadose Zone: 10.7 to 76.2 m (35 to 250 ft). Similar to the shallow vadose zone in the 0 to 10.7-m (0 to 35-ft) interval, simulated time histories are compared in this section for those monitoring locations from the 10.7 to 76.2-m (35 to 250-ft) interval that have elevated—even if only slightly—U-238, Tc-99, and nitrate concentrations, based on discussions in Section 4.

5.2.5.2.1 Uranium-238—Lysimeters showing slightly elevated U-238 concentrations above background are I1S-DL09, I4S-DL15, D06-DL01, D06-DL02, and TW1-DL04. For the Well D06 location, only the uppermost lysimeter (i.e., Lysimeter DL02) is shown in Figure 5-41. Intervals of 10.7 to 42.7 m (35 to 140 ft) and 42.7 to 76.2 m (140 to 250 ft) are combined for this discussion because so few locations are showing elevated concentrations in the deeper interval.

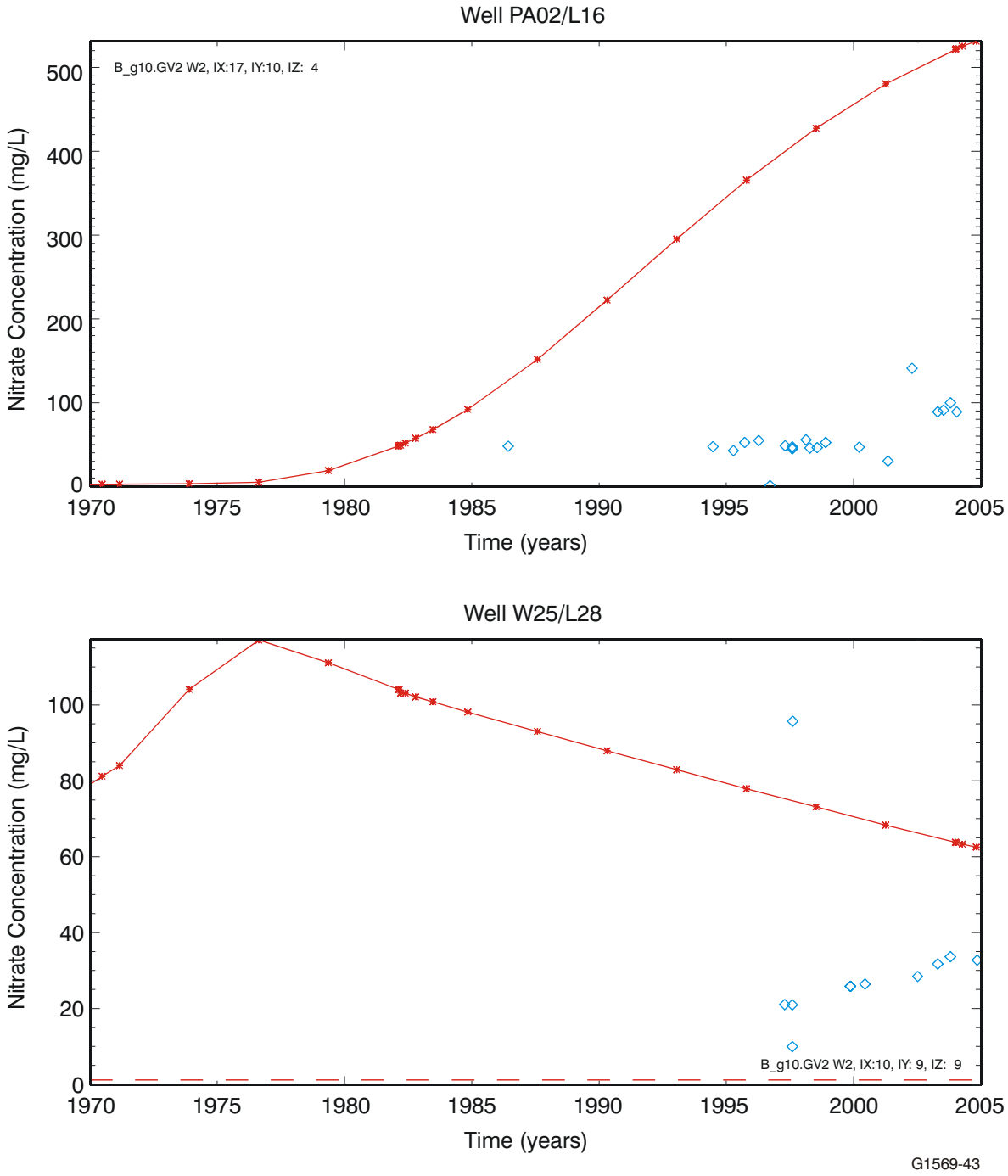

Figure 5-40. Time-history comparison of simulated (red line) and observed (blue diamonds) concentrations for nitrate in Lysimeters PA02-L16 and W25-L08. Background concentration is indicated by the dashed line.

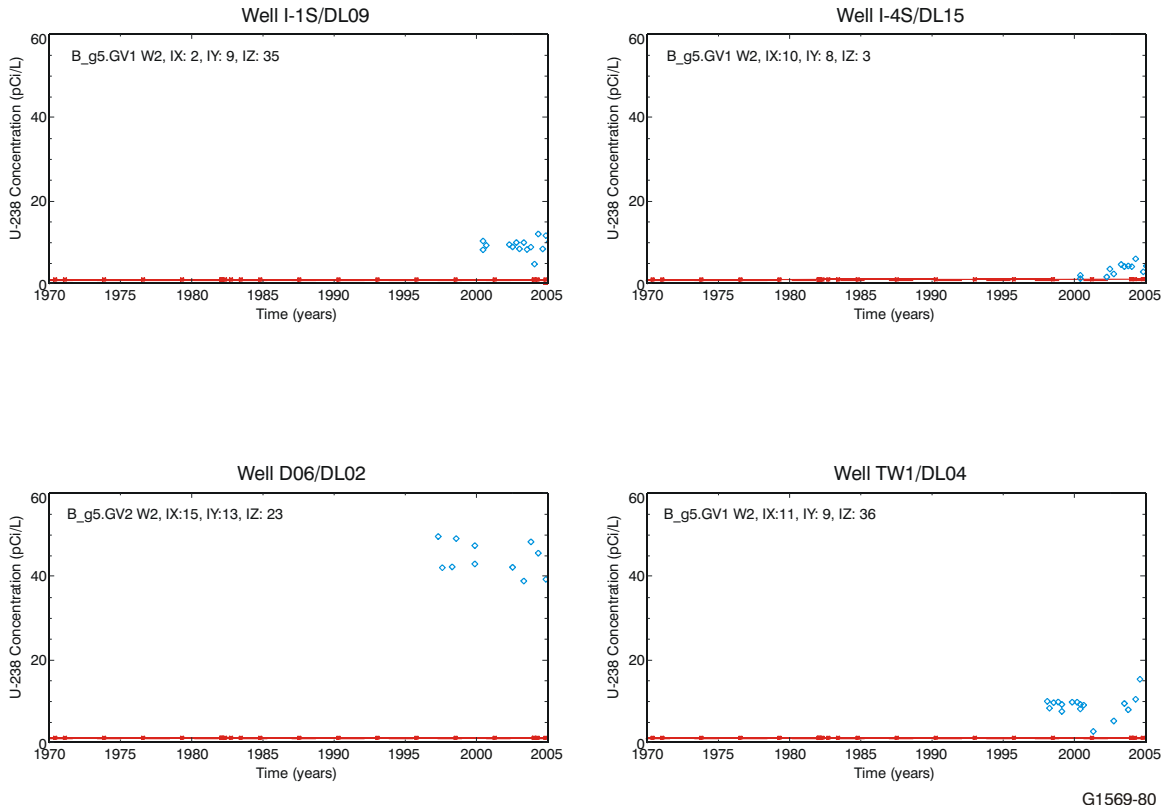

Figure 5-41. Time-history comparison of simulated (red line) and observed (blue diamonds) concentrations for uranium-238 in lysimeters in the 35 to 250-ft depth interval. Background concentration is indicated by the dashed line.

Although simulated concentrations are nonzero, they are very low and essentially plot just at background. Simulations represent averaged concentrations over larger gridblock volumes at this depth—76.2 m (250 ft) on a side—and again cannot be expected to exactly mimic observations at a specific point. Also note that the plots show only locations with elevated concentrations. The other monitoring locations (i.e., the majority) all show nondetects.

5.2.5.2.2 Technetium-99—Elevated concentrations of Tc-99 in the 10.7 to 76.2-m (35 to 250-ft) interval were observed at Wells D06 in Lysimeters DL-01 and DL-02. Simulated Tc-99 concentrations for gridblocks containing these lysimeters are shown in Figure 5-42. These results are plotted with a linear vertical axis because the concentrations are not as overpredicted at this location as they were for the shallower Well W23 location shown previously.

5.2.5.2.3 Nitrate—Elevated concentrations of nitrate in the 10.7 to 76.2-m (35 to 250-ft) interval were observed at Wells I-2S and I-4S. These simulation results are shown in Figure 5-43. Lysimeter I-2S-DL11 shows very high monitoring results for nitrate; therefore, it is not surprising that the model underpredicts in comparison. Lysimeter I-4S-DL15 has lower monitoring results; the model results overpredict for this location.

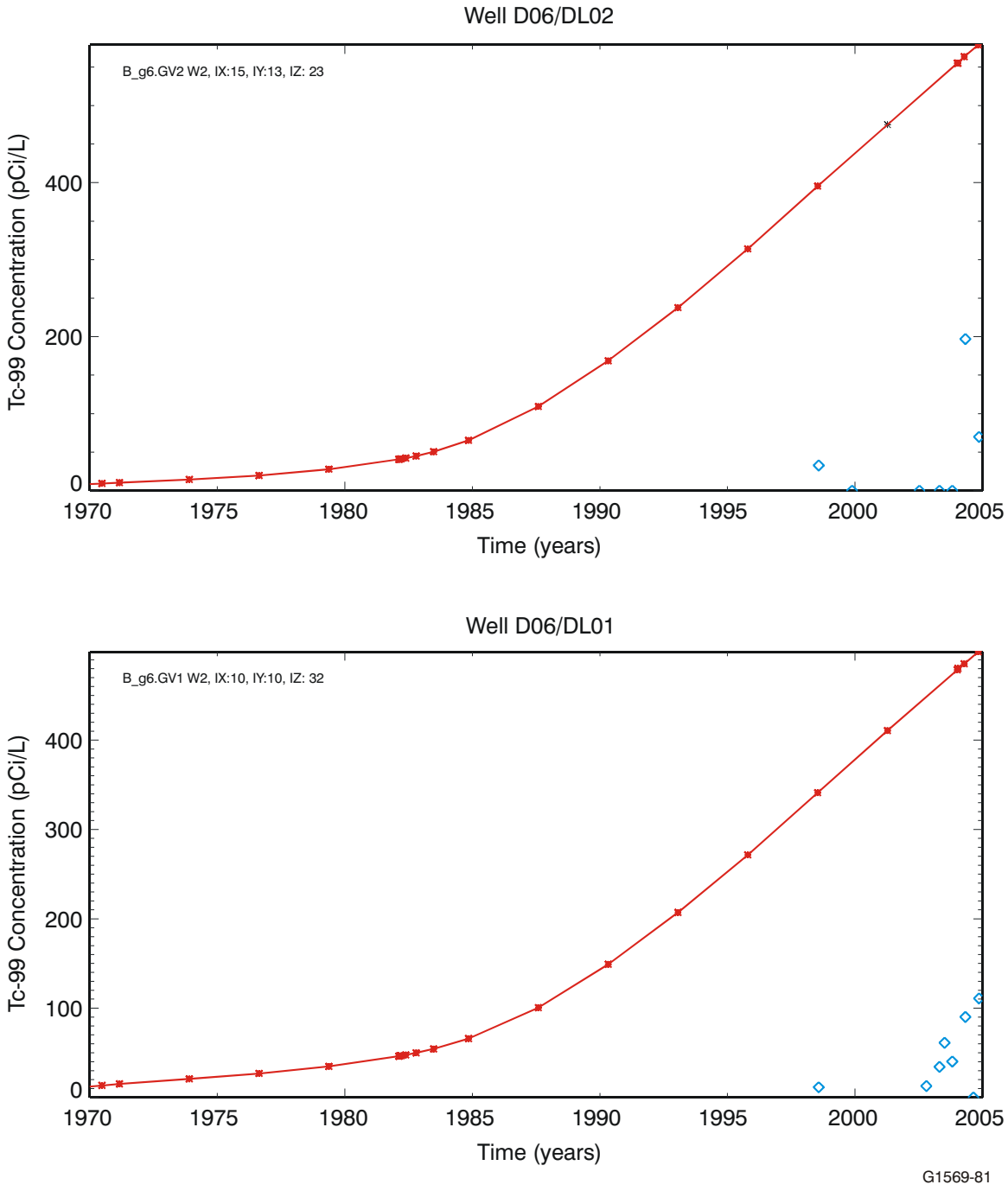

Figure 5-42. Time-history comparison of simulated (red line) and observed (blue diamonds) concentrations for technetium-99 in the lysimeters in the 35 to 250-ft depth interval.

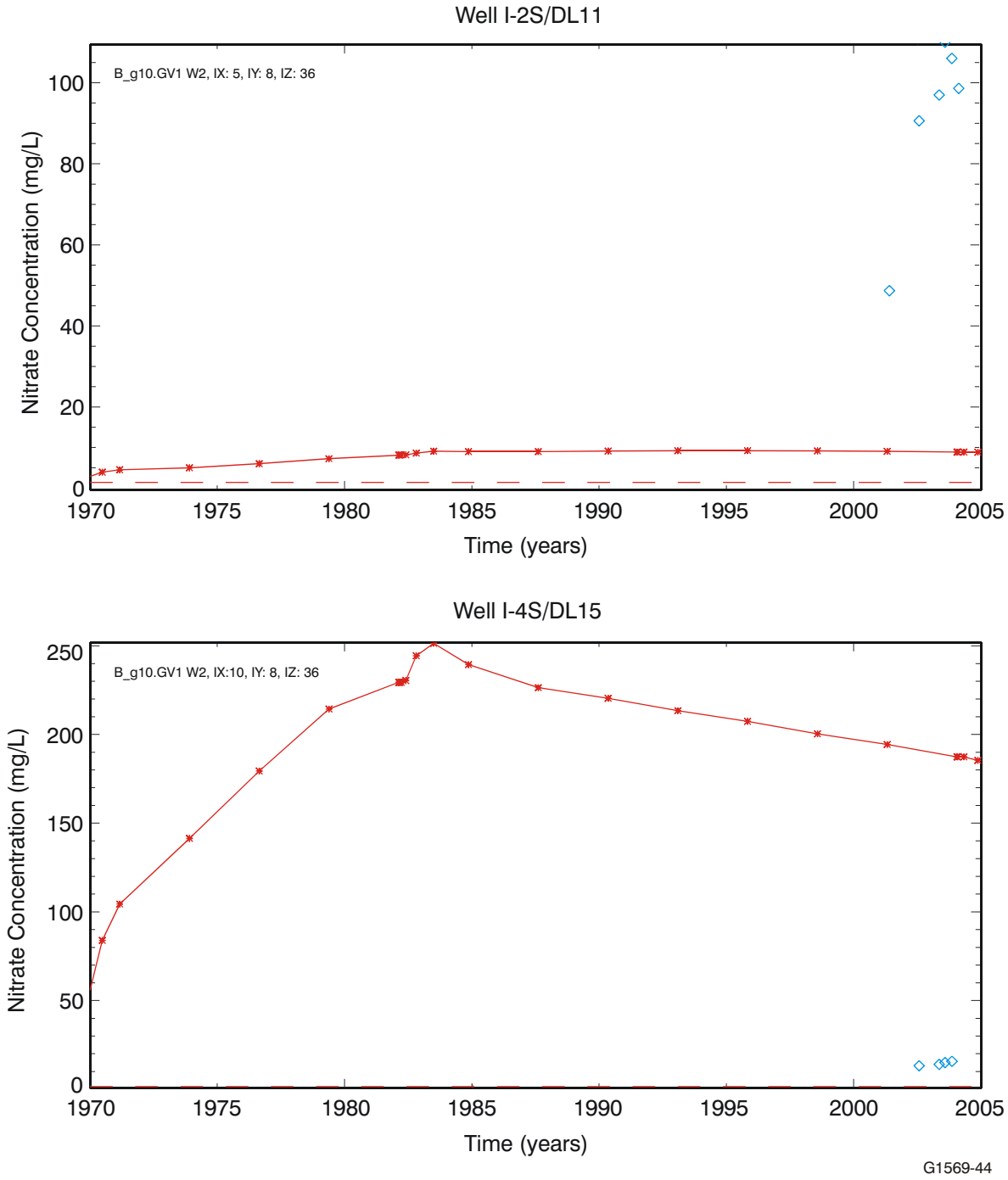

Figure 5-43. Time-history comparison of simulated (red line) and observed (blue diamonds) concentrations for nitrate in lysimeters in the 35 to 250-ft depth interval. Background concentration is indicated by the dashed line.

5.2.5.3 Aquifer. This subsection first compares simulated and observed nitrate and chromium concentrations. These two contaminants are chosen for consistency to allow comparison to ABRA modeling results and because they offer insight into how the model results compare to monitoring data. Both contaminants are conservative in that they do not sorb, and thus, avoid the complication of assigning a K_d. Lastly, time histories for simulated aquifer concentrations for all contaminants in the RI/FS model that have detections from aquifer monitoring are compared to the observations.

5.2.5.3.1 Comparison of Simulated and Observed Nitrate Concentrations— This subsection shows comparisons of simulated results and monitoring results for nitrate as elemental nitrogen. Time histories, contour plots, and vertical profiles through the aquifer domain are presented to show spatial resolution.

Calibration to the observed aquifer nitrate concentrations was not attempted for these simulations. Rather, simulations for both the vadose zone and the aquifer were developed based on best-available information. Then simulations were run once in a forward mode.

Nitrate is a ubiquitous chemical in groundwater. Background concentrations must be considered, when making comparisons, even though it is assumed for RI/FS modeling that contaminant concentrations near the SDA are not influenced by upgradient sources. A background concentration of 1.0 mg/L was added to simulated values in the time-history plots shown in Figure 5-44. This background concentration appears appropriate for the local RWMC area and is within the range of background concentrations typical for the INL Site (i.e., 0.4 to 5.0 mg/L) as presented in Section 4. The time-history plots are all shown with a consistent time axis and a consistent concentration axis, except for Well M17S, which has an one-order-of-magnitude-larger concentration axis to show the simulated results. Simulation results representing all wells, except Well M4D, are taken from the second gridblock down in the aquifer model. This depth best corresponds to the location of well screens for SDA vicinity wells (Magnuson and Sondrup 2006). Well M4D is unique in that it is screened much deeper; therefore, simulated concentrations from deeper in the model are used. In general, the simulation results show slightly lower predicted concentrations in the aquifer than those in the ABRA model due to a combination of reduced inventory and changes in transport through the vadose zone. Figure 5-45 illustrates that nitrate is sometimes overpredicted and sometimes shows no contribution from SDA sources when compared to the monitoring data. Also evident in the monitoring data is that the mean local background estimate has some degree of variability around it.

A contour plot of the simulated nitrate concentrations in Calendar Year 2004 is shown in Figures 5-46 and 5-47 for the refined and base aquifer-simulation domains, respectively. Again, concentrations are taken from the second gridblock down from the aquifer model. The estimated local background of 1.0 mg/L is not added to the simulation results in Figures 5-46 and 5-47. Simulated results show that nitrate is predicted to move to the east–southeast within the area of the refined domain due to topography influences in the vadose zone and slightly south–southeastern water velocities under the eastern portion of the SDA and Transuranic Storage Area. In the larger base domain, control of the regional gradient is exerted and the simulated plume moves south–southwest.

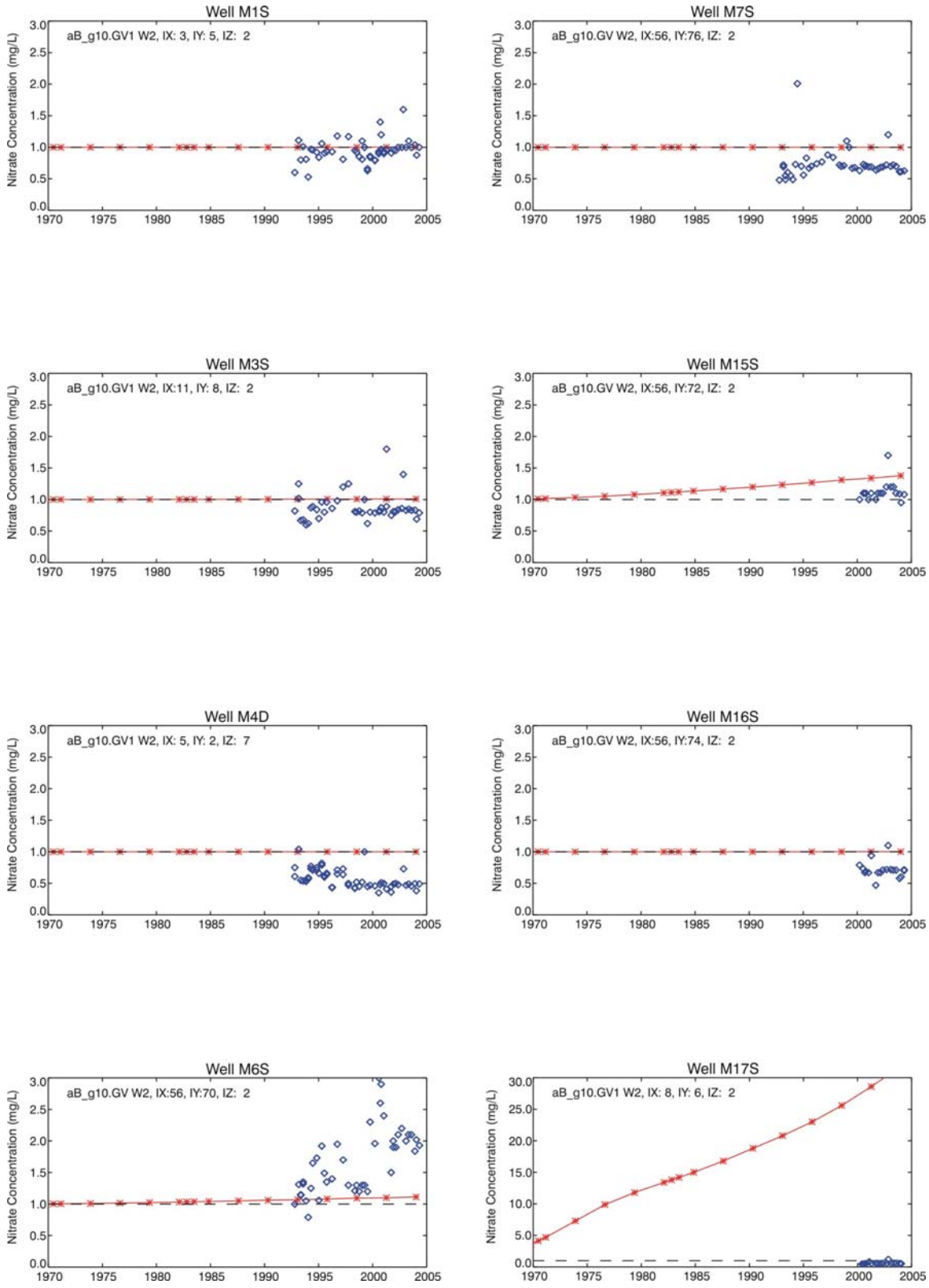

Figure 5-44. Comparison of simulated (red line) and observed (blue diamonds) nitrate (as N) concentration time histories for aquifer monitoring wells near the Subsurface Disposal Area. Background concentration is indicated by the dashed line.

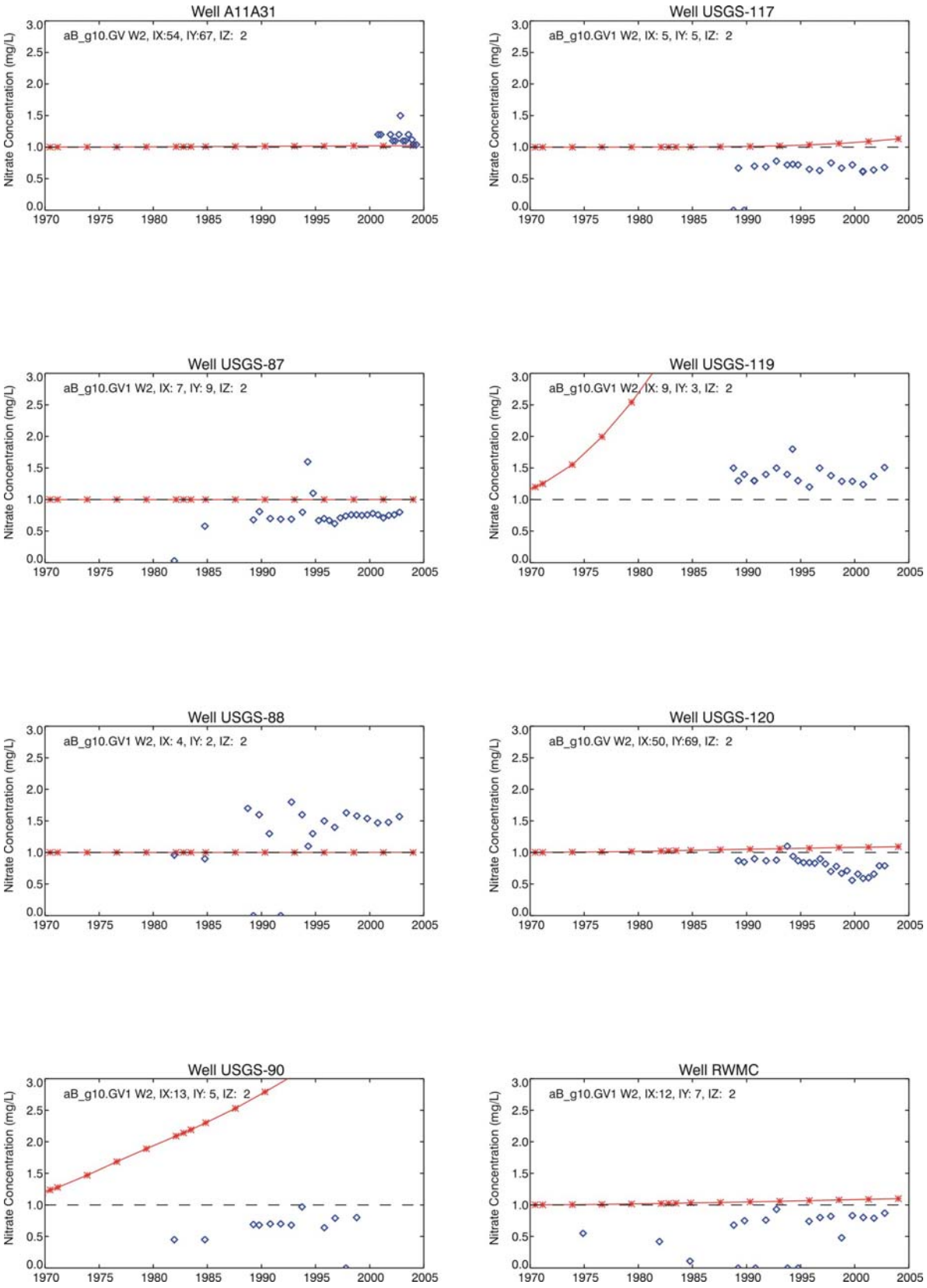

Figure 5-44. (continued).

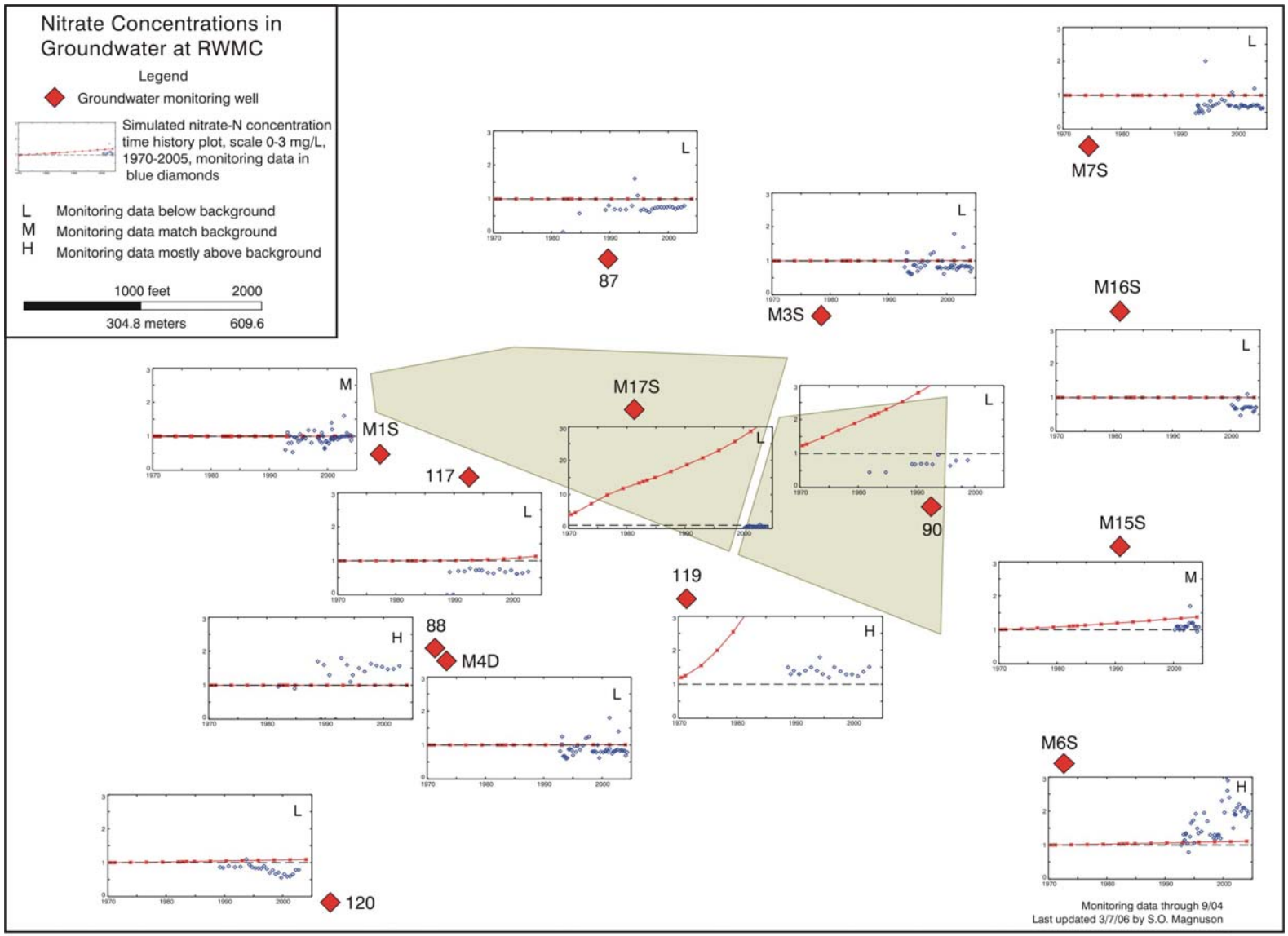

Figure 5-45. Simulated and observed nitrate concentrations superimposed onto monitoring locations near the Radioactive Waste Management Complex. Background concentration is indicated by dashed line.

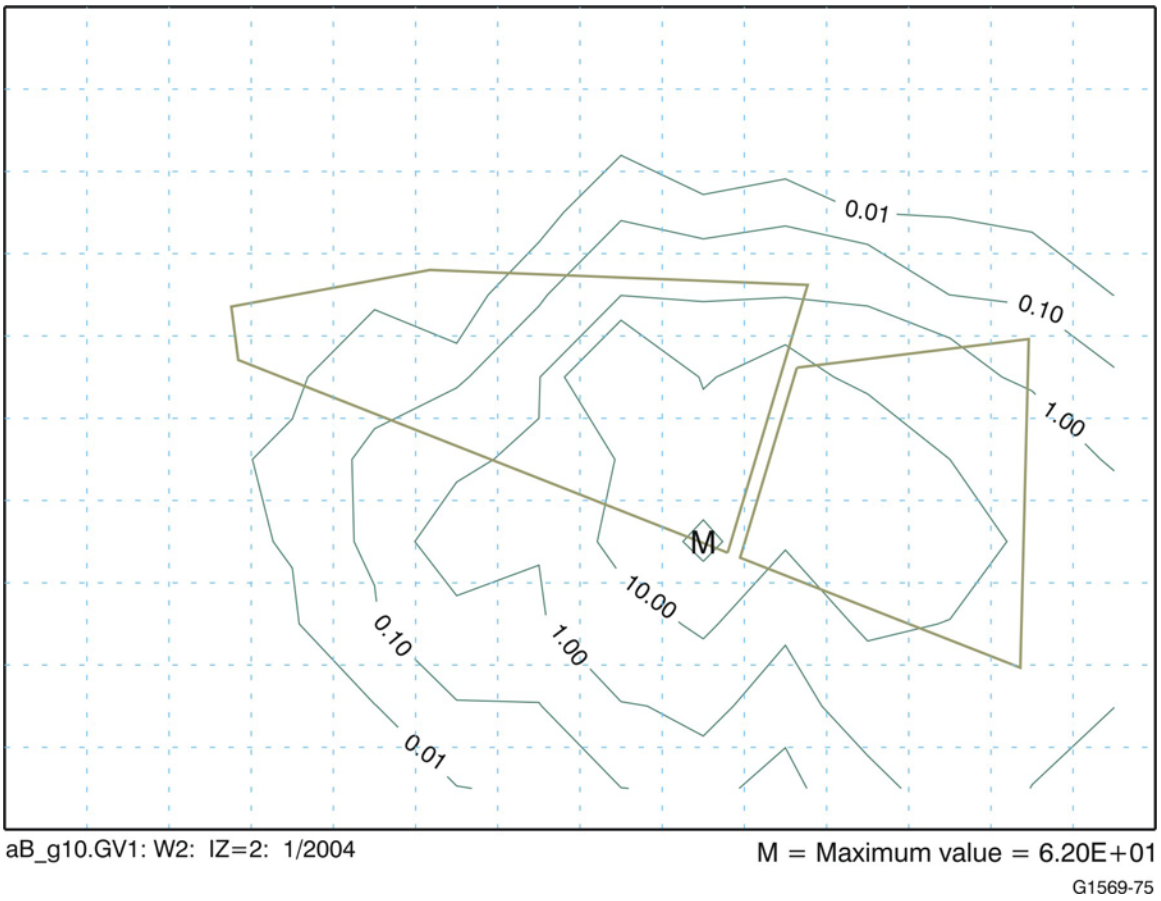

Figure 5-46. Simulated aquifer nitrate concentrations (mg/L) for the year 2004 for the refined aquifer domain. The results do not include any additional contribution from local background concentrations.

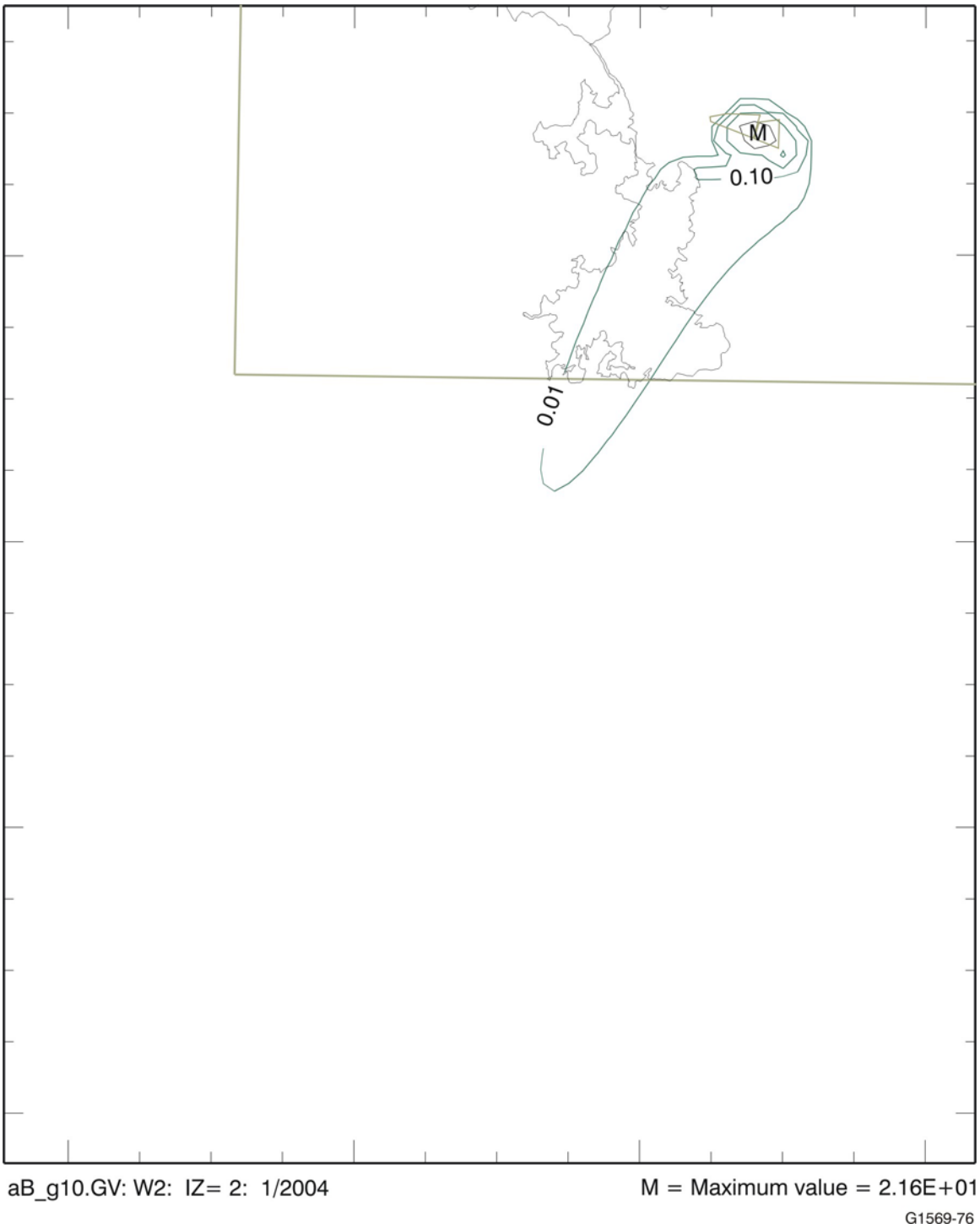

Figure 5-47. Simulated aquifer nitrate concentrations (mg/L) for the year 2004 for the base aquifer domain. The results do not include any additional contribution from local background concentrations.

The predicted movement of nitrate east–southeast within the aquifer model-refined domain can be seen more easily in Figure 5-45, where time histories from Figure 5-44 are portrayed in spatial relation to their well locations. Elevated nitrate concentrations are predicted by current time for Wells M17S, USGS-119, USGS-90, and M15S, which are all beneath the SDA or south-southeast. Well M6S would have a higher predicted concentration, but it is outside the refined area; therefore, the predicted concentration is subject to averaging over a much larger gridblock volume, which dilutes the simulated concentration. In terms of monitoring data, some patterns can be interpreted when compared to the local background estimate of 1.0 mg/L. For purposes of comparison, monitoring results are grouped into four classes with an indication found in the upper right of each time-history plot. An "L" indicates the monitoring data were mostly below the background, an "M" indicates the monitoring data mostly match the background, and an "H" indicates the monitoring data are mostly higher than the background. Following this categorization, Wells USGS-87, M3S, M7S, M16S, USGS-90, M17S, USGS-117, M4D, and USGS-120 all show concentrations mostly below background. Wells M1S and M15S match the local background, Wells USGS-119 and USGS-88 are elevated compared to the local background, and Well M6S has the highest concentrations above the local background estimate. Grouped in this fashion, monitoring data also show a tendency for nitrate concentrations to be elevated in several wells south of the SDA, with one grouping including Wells USGS-119, M15S, and M6S, which are in the direction of predicted local transport to the southeast.

Most of the monitoring data are consistent with the conceptual model and the numerical implementation. The aquifer flow system is dominated by a low-permeability region south and southwest of the SDA that directs flow eastward around the low-permeability system. In comparing simulation results to monitoring results, concentrations are overpredicted in Well M17S (inside the SDA), in Well USGS-119 (immediately south of the SDA), and in Well USGS-90 (east of the SDA). Predicted concentrations slightly overpredict observed concentrations at Well M15S (east of the Transuranic Storage Area).

Concentrations are underpredicted at Well M6S (southeast of the SDA). The simulation results at the grid location corresponding to Well M6S are subject to additional dilution due to being outside the refined area. Without this dilution, the agreement would be better. The majority of other locations outside this predicted contaminant plume essentially shows no simulated impact above local background concentration. Obviously, the system is more complex than has been represented in the model. However, the model does provide a foundation for explaining most of the observed behavior and, thus, meets a goal of general representativeness.

Vertical profiles of simulated nitrate concentrations at the gridblock location with the maximum simulated concentration in Calendar Year 2004 (see Figure 5-46) are shown in Figure 5-48 for four different dates. These plots do not have the background concentration added to the simulation results. This same location remains the location of maximum concentration until Calendar Year 2120, when it shifts southward with the center of mass. Note that the horizontal-concentration scale changes in the profile for Calendar Year 2997. Contours of the simulated concentration for the same times from the corresponding north-south cross section in the refined aquifer domain are shown in Figure 5-49. Only Calendar Years 2004, 2066, and 2110 are shown because the simulated concentration for Calendar Year 2997 is less than 1 mg/L.

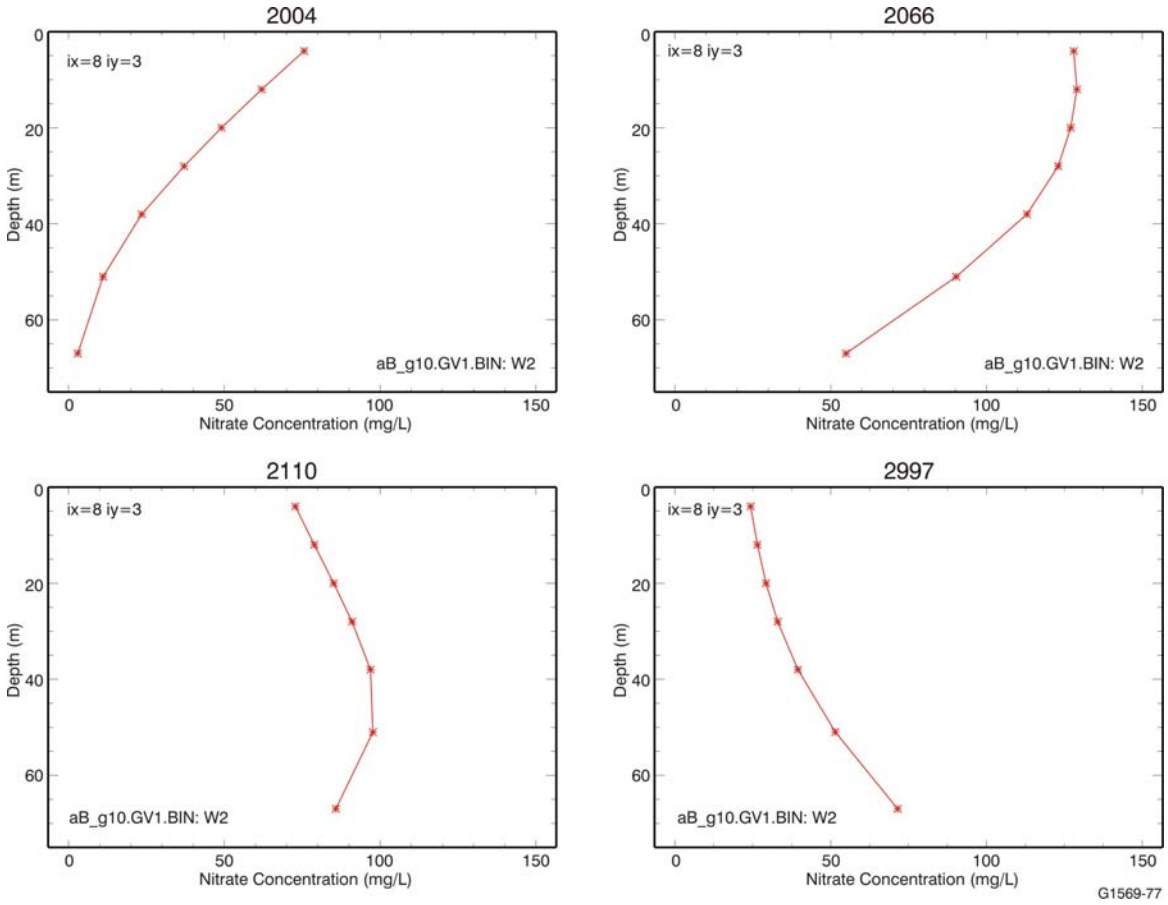

Figure 5-48. Simulated aquifer nitrate concentration profiles beneath the Subsurface Disposal Area. The year is shown at the top of each plot.

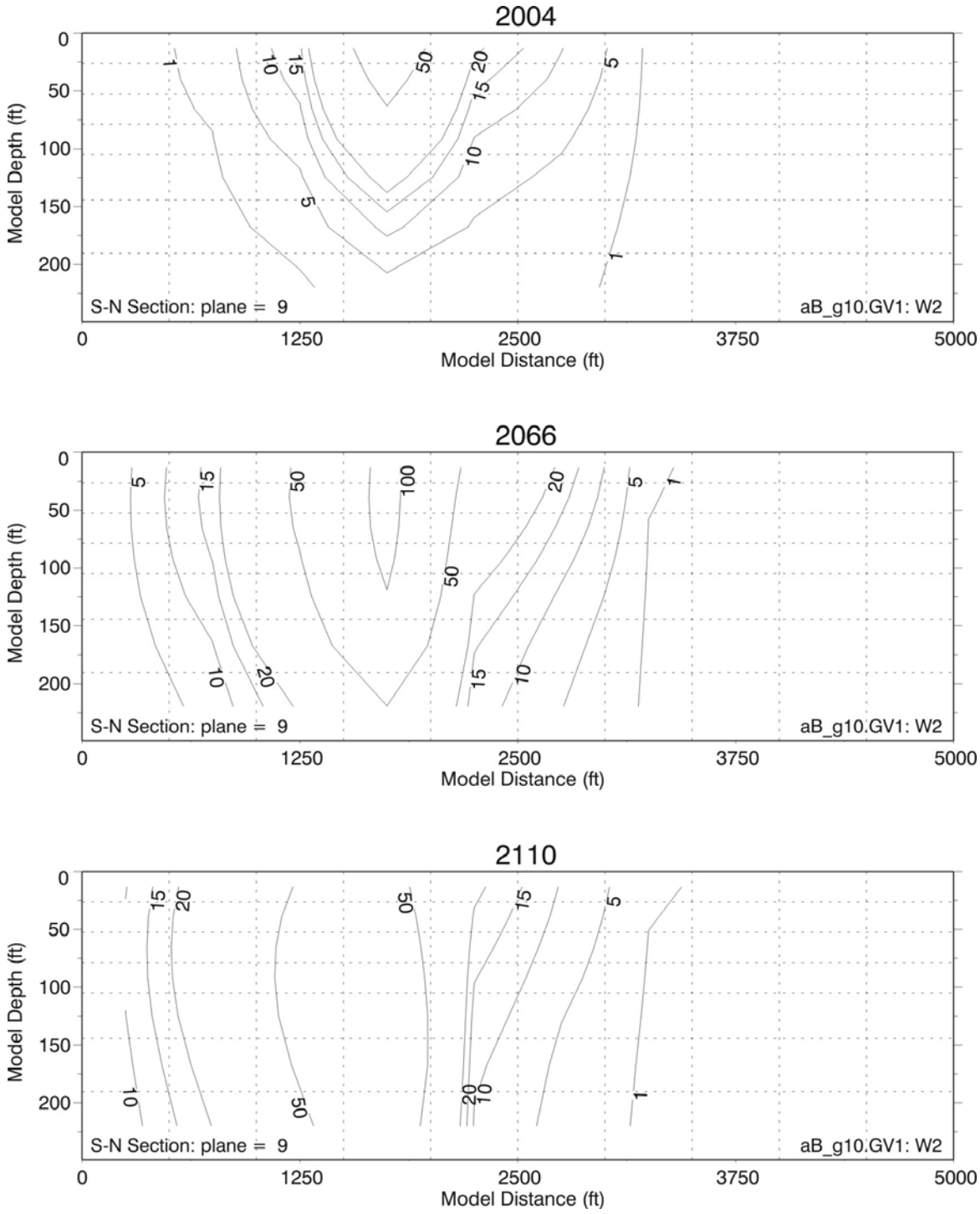

Figure 5-49. Simulated aquifer nitrate concentrations (mg/L) for north-south cross sections through the location of maximum simulated concentration at times corresponding to profiles shown in Figure 5-48.

Understanding the dynamic behavior of simulated profiles requires knowing (1) the contaminant-loading history from the vadose zone simulation at this location, (2) that water flux from the vadose zone is relatively constant, and (3) that the low-permeability region in the aquifer results in slow horizontal velocities, which increases the effect of contaminant flux coming into the model from the vadose zone. A one-to-one correspondence from the bottom of the vadose zone to the top of the refined domain in the aquifer exists. Nitrate loading from the vadose zone model for the gridblock location profiled in Figure 5-48 is shown in Figure 5-50. During the period up to approximately Calendar Year 2050, contaminant flux to the aquifer is increasing. A profile from this period (i.e., Calendar Year 2004) shows consistently decreasing simulated concentrations with depth in the aquifer. Shortly after this period, nitrate flux from the vadose zone begins to decrease while water flux stays the same. This begins to result in lower concentrations at the surface (Calendar Year 2066), possibly indicating that a slight downward gradient has developed in the aquifer simulation within the low-permeability region. By Calendar Year 2110, this reversal in the concentration gradient has almost penetrated to the bottom of the simulation domain. At a much later time (i.e., Calendar Year 2997), the concentration gradient is reversed, with the highest concentration at the bottom of the domain, although concentrations at this later time are much lower. This simulation behavior of the concentration not always being greatest at the uppermost gridblock has implications when extracting concentrations from the model for risk assessment. It would not necessarily always be conservative to use the concentrations from the uppermost gridblock in the aquifer domain. In this baseline risk assessment, concentrations are taken from the second gridblock down. Section 5.2.5.3.3 shows similar vertical profiles for other contaminants to further illustrate this point.

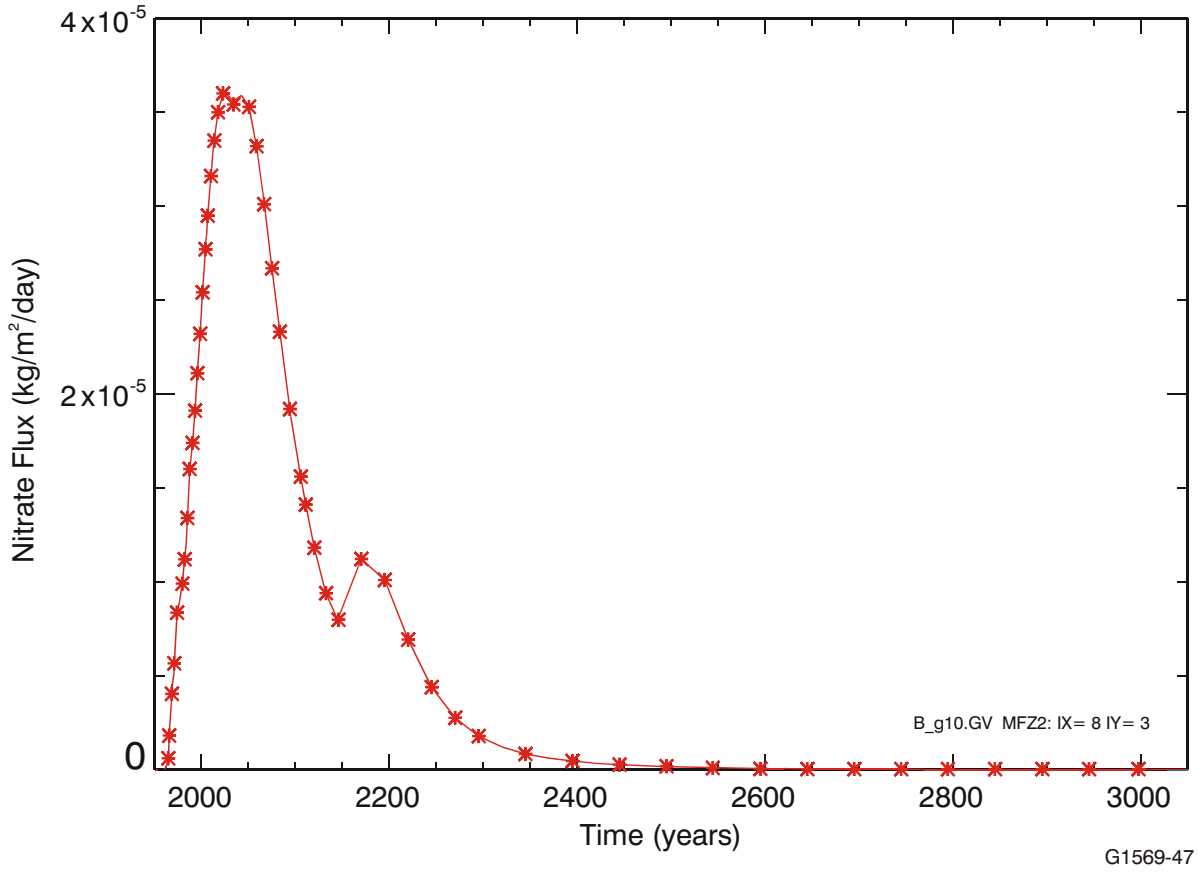

Figure 5-50. Time history of the simulated nitrate flux from the vadose zone simulation at the grid location profiled in Figure 5-48.

5.2.5.3.2 Comparison of Simulated and Observed Chromium Concentrations—

Chromium is another contaminant buried in the SDA for which transport was simulated. In these transport simulations, chromium was assumed to remain in the mobile hexavalent state. Though chromium is not considered a contaminant of potential concern in the RI/BRA, subsurface model predictions for chromium are compared to measured values because sufficient monitoring data are available to support the comparison (see Section 4). Figure 5-51 illustrates time histories of simulated chromium concentrations compared to observed aquifer concentrations. The monitored concentrations are inferred to represent hexavalent chromium also. Similar to the time-history plots for nitrate concentrations, the simulated chromium concentrations are added onto the upper end of the aquifer background concentration range of 1 to 22 μg/L for the Snake River Plain Aquifer (see Section 4). Only simulated chromium concentrations for Wells M17S and USGS-119 begin to be discernible above background for the 1970 through FY 2004 timeframe presented in Figure 5-51. The maximum simulated chromium concentration anywhere in the aquifer through FY 2004 is 30 μg/L. This concentration is approximately an order of magnitude greater than the maximum simulated chromium concentration through the same period for the ABRA model. Both the ABRA and RI/FS models underpredict observed values.

Field data for chromium show considerable variability, similar to nitrate. Locations showing the most consistent elevated concentrations are Wells M1S, M15S, and M6S. Two of these are in the direction of interpreted and simulated flow to the east–southeast in the locally refined portion of the aquifer domain.

5.2.5.3.3 Comparisons of Simulated and Observed Concentrations for Dissolved-Phase Radionuclide Constituents—

This subsection presents comparisons of time histories of simulated results from the base-case simulation for those dissolved-phase radionuclides that have detections in the aquifer from monitoring. These contaminants are I-129, Tc-99, Am-241, Np-237, Pu-238, and Pu-239. Results are presented graphically as time-history comparisons to field monitoring results at grid locations representing SDA aquifer monitoring wells (see Figures 5-52 to 5-57). In contrast to results presented previously for nitrate and chromium, contaminants in these figures are anthropogenic and have no background concentrations to be added to simulation results, except for I-129 with a local background of 0.05 pCi/L. This latter background is indistinguishable in Figure 5-52. Monitoring results for radionuclide contaminants of potential concern that represent 3σ detections, or greater, are included as blue diamonds on the time-history plots along with a whisker-style indication of their associated 1σ uncertainties. In cases where analyses were performed but no contaminants of potential concern were detected, nondetects are plotted in green at the extreme lower-bound inventory of the plot. Simulation results are portrayed as a continuous line with black asterisks. Simulation results representing all wells, except Well M4D, are taken from the second gridblock down in the aquifer model. Well M4D is unique because it is screened much deeper; therefore, simulated concentrations from deeper in the model are used. The second gridblock extends from 8 to 16 m (26 to 52 ft) in the aquifer domain and is similar to most of the screened intervals in the monitoring wells. Thus, simulated concentrations represent concentrations at a depth of 12 m (39 ft) below the water table.

Results in Figures 5-52 through 5-57 highlight the erratic nature of detections compared to the majority of nondetect results, and those results lend credence to the assumption that these detections are not representative of transport and the simulation results need not mimic them. These sporadic detections include low-level actinide concentrations that are just at instrument detection limits and may be false positives.

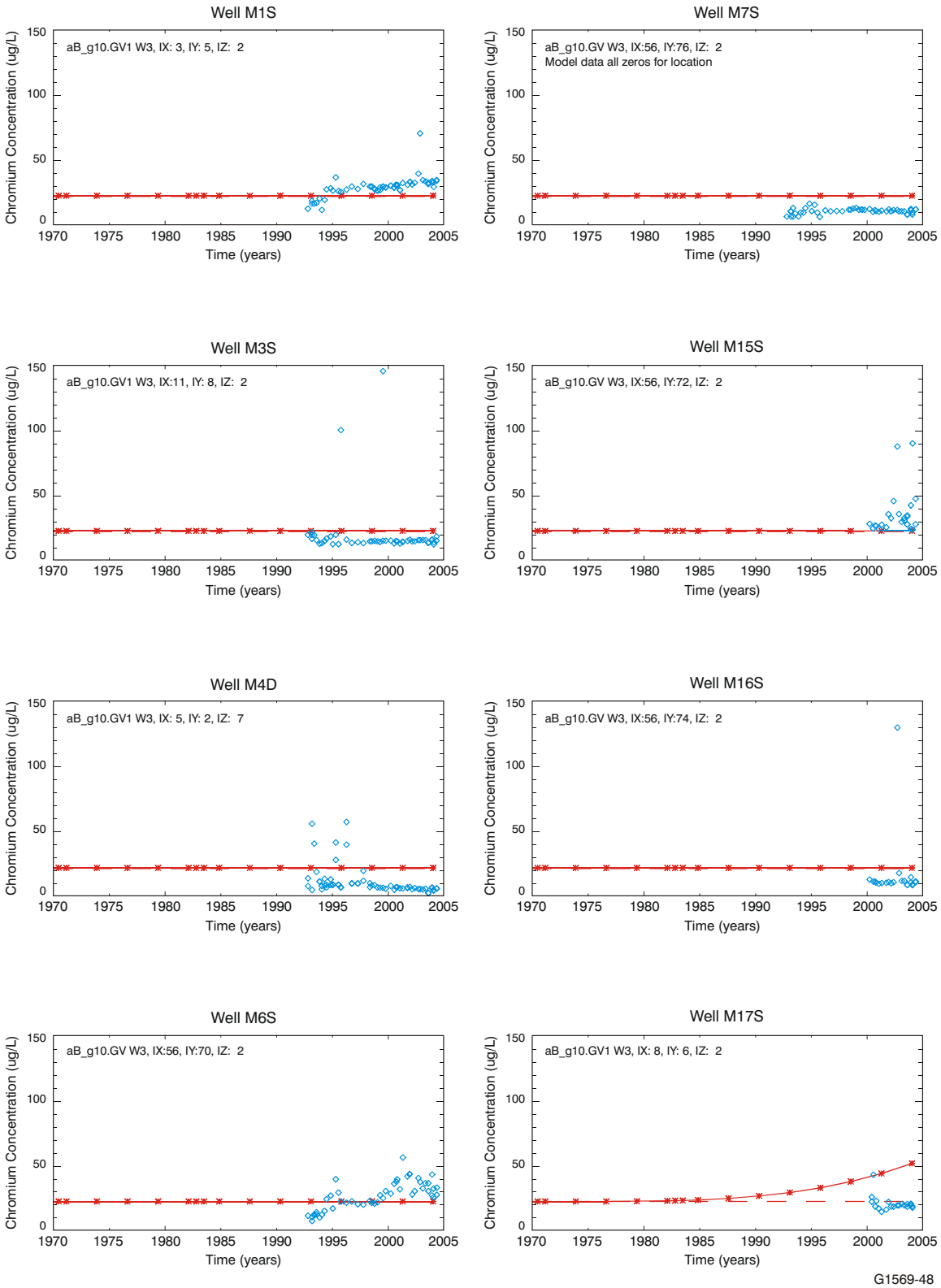

Figure 5-51. Comparison of simulated (red line) and observed (blue diamonds) chromium concentration time histories for aquifer monitoring wells near the Subsurface Disposal Area. Background concentration is indicated by the dashed line.

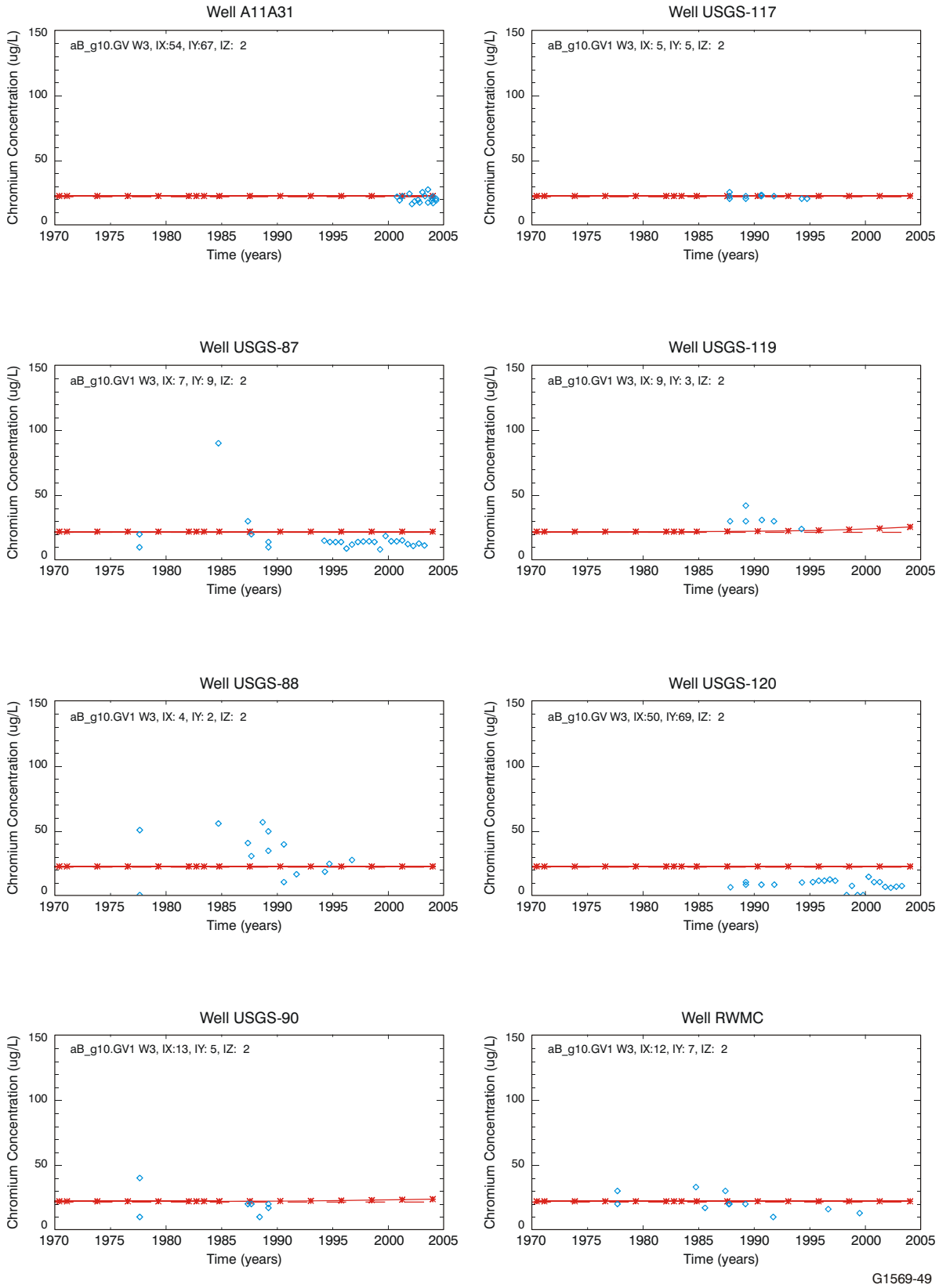

Figure 5-51. (continued).

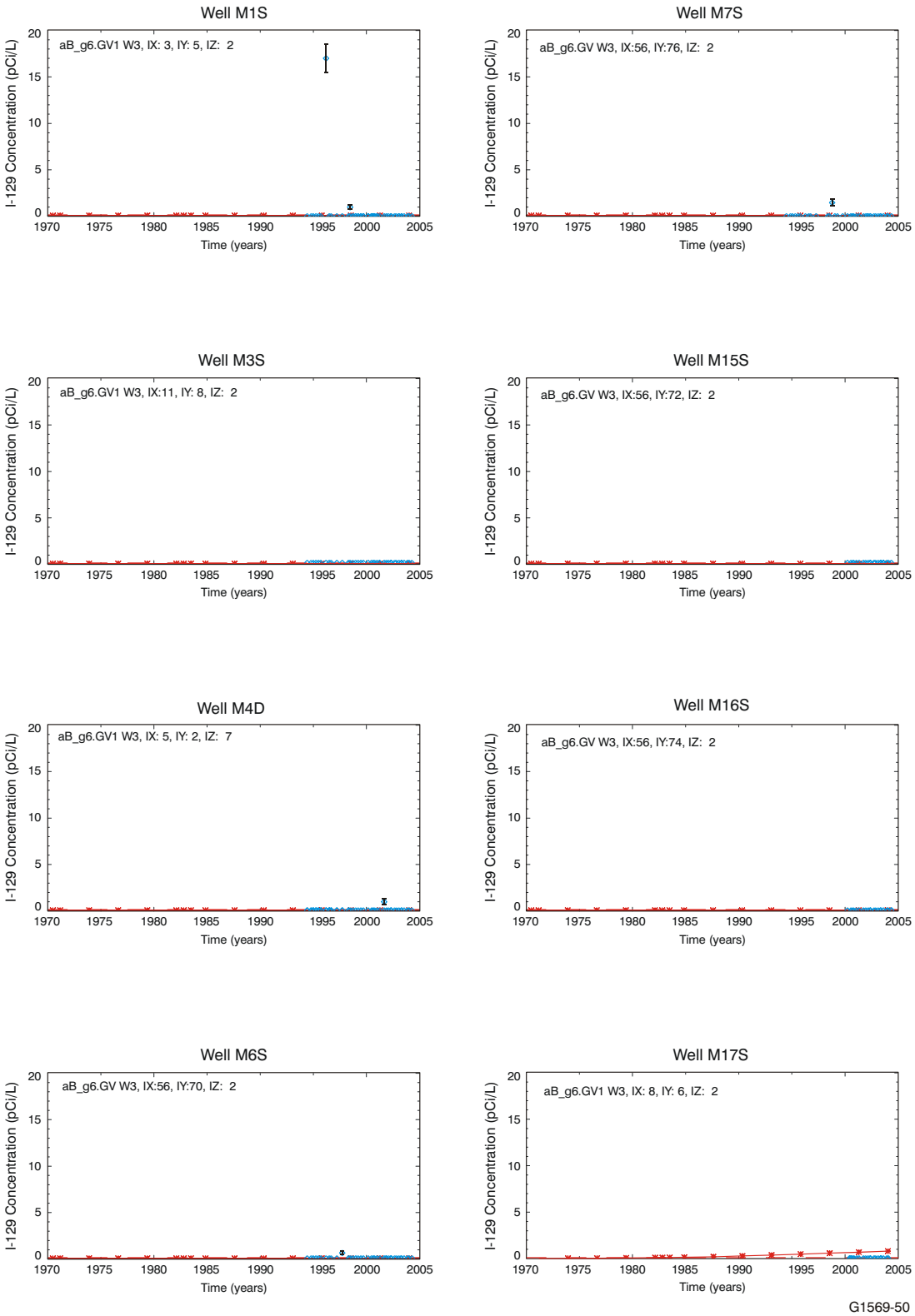

Figure 5-52. Comparison of simulated (red line) and observed (blue diamonds) iodine-129 concentration time histories for aquifer monitoring wells near the Subsurface Disposal Area. Background concentration is indicated by the dashed line.

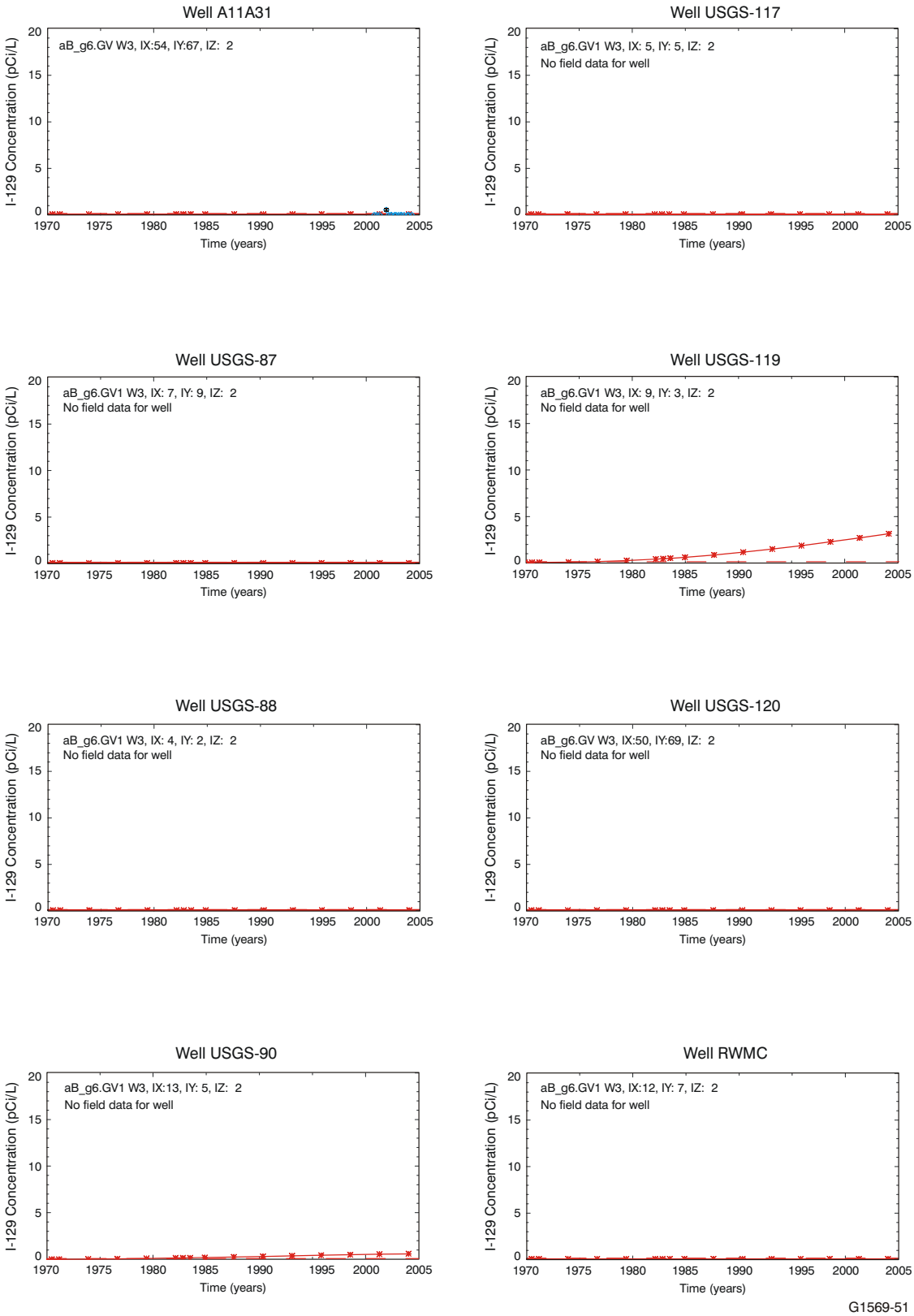

Figure 5-52. (continued).

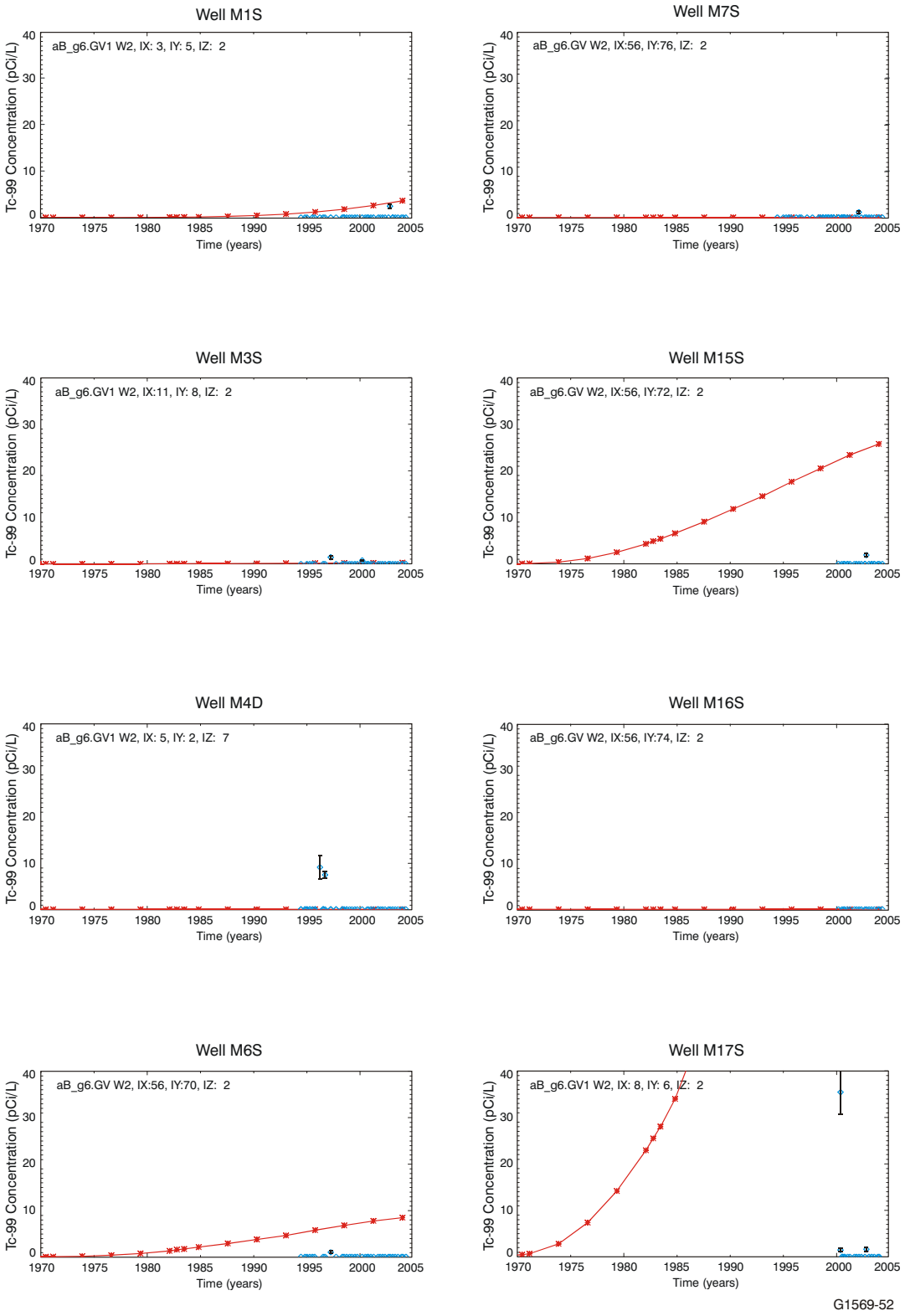

Figure 5-53. Comparison of simulated (red line) and observed (blue diamonds) technetium-99 concentration time histories for aquifer monitoring wells near the Subsurface Disposal Area.

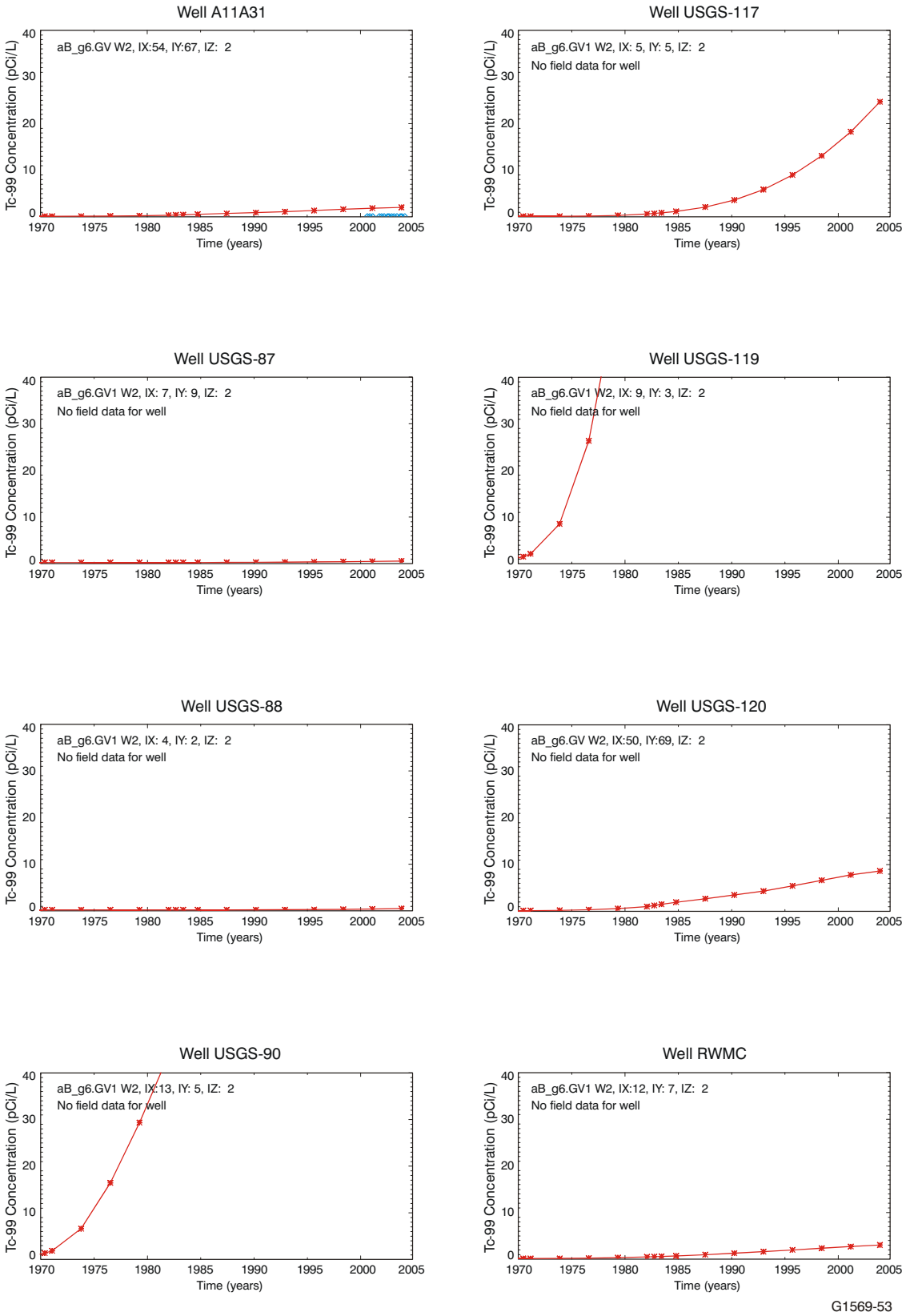

Figure 5-53. (continued).

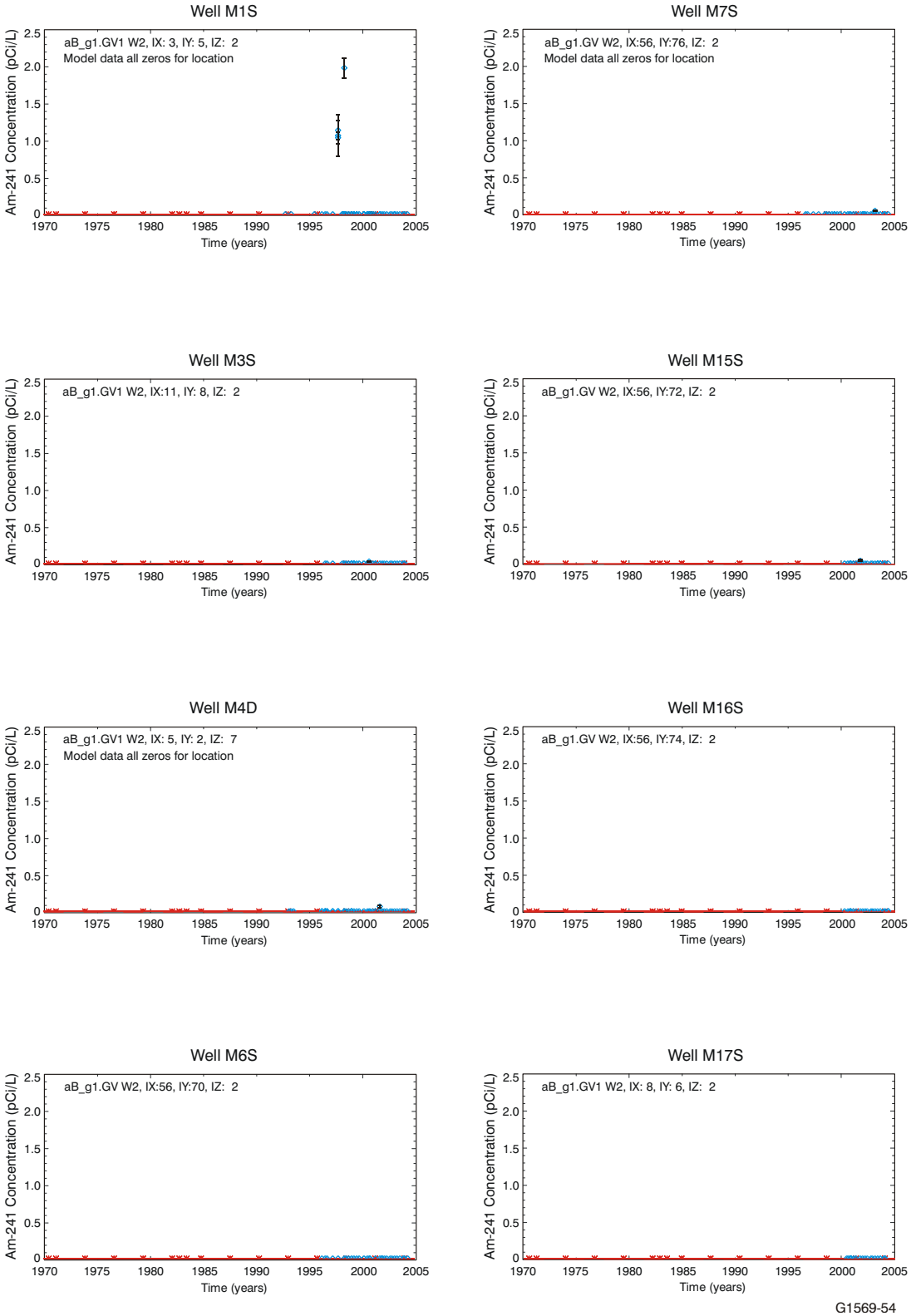

Figure 5-54. Comparison of simulated (red line) and observed (blue diamonds) americium-241 concentration time histories for aquifer monitoring wells near the Subsurface Disposal Area.

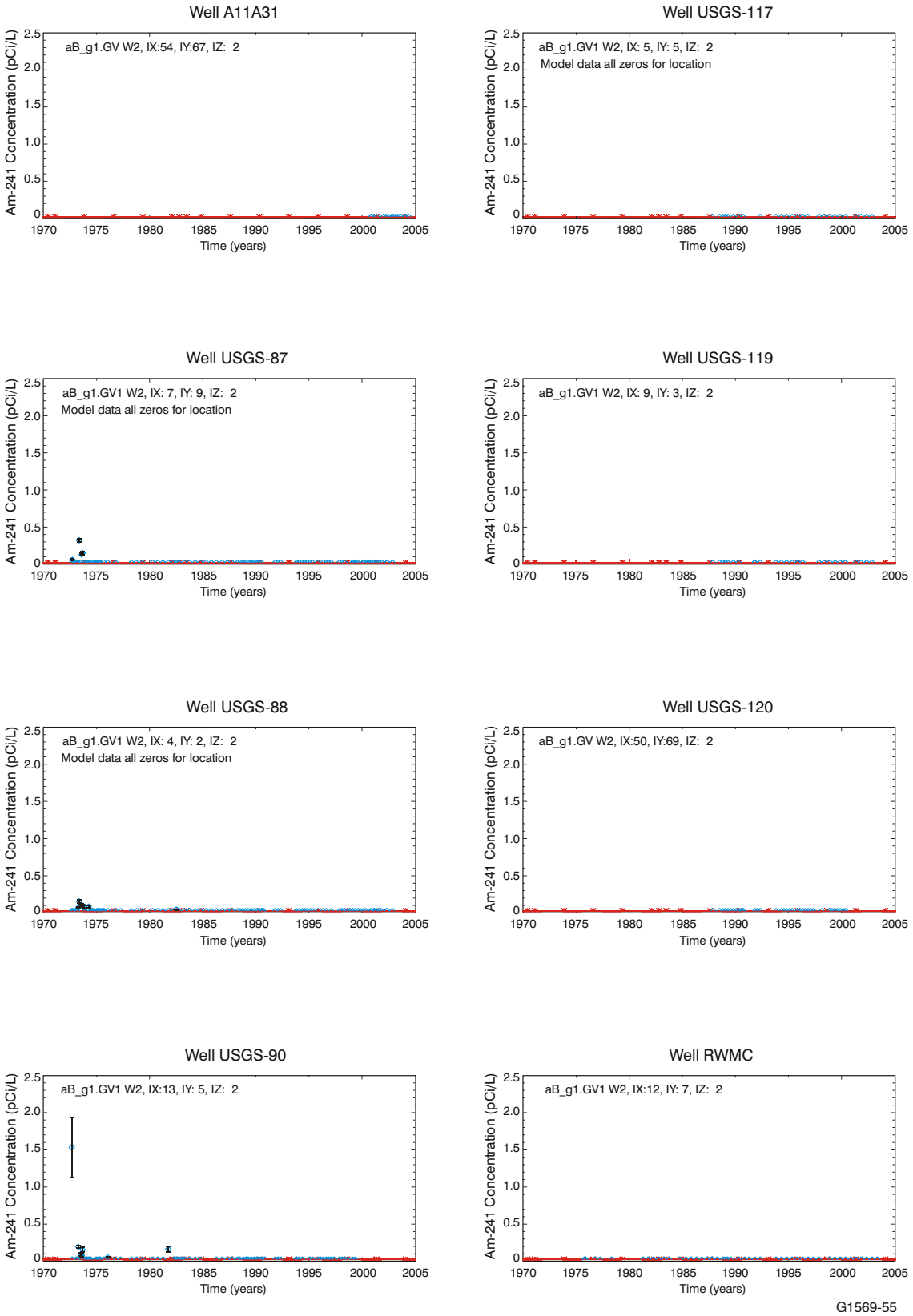

Figure 5-54. (continued).

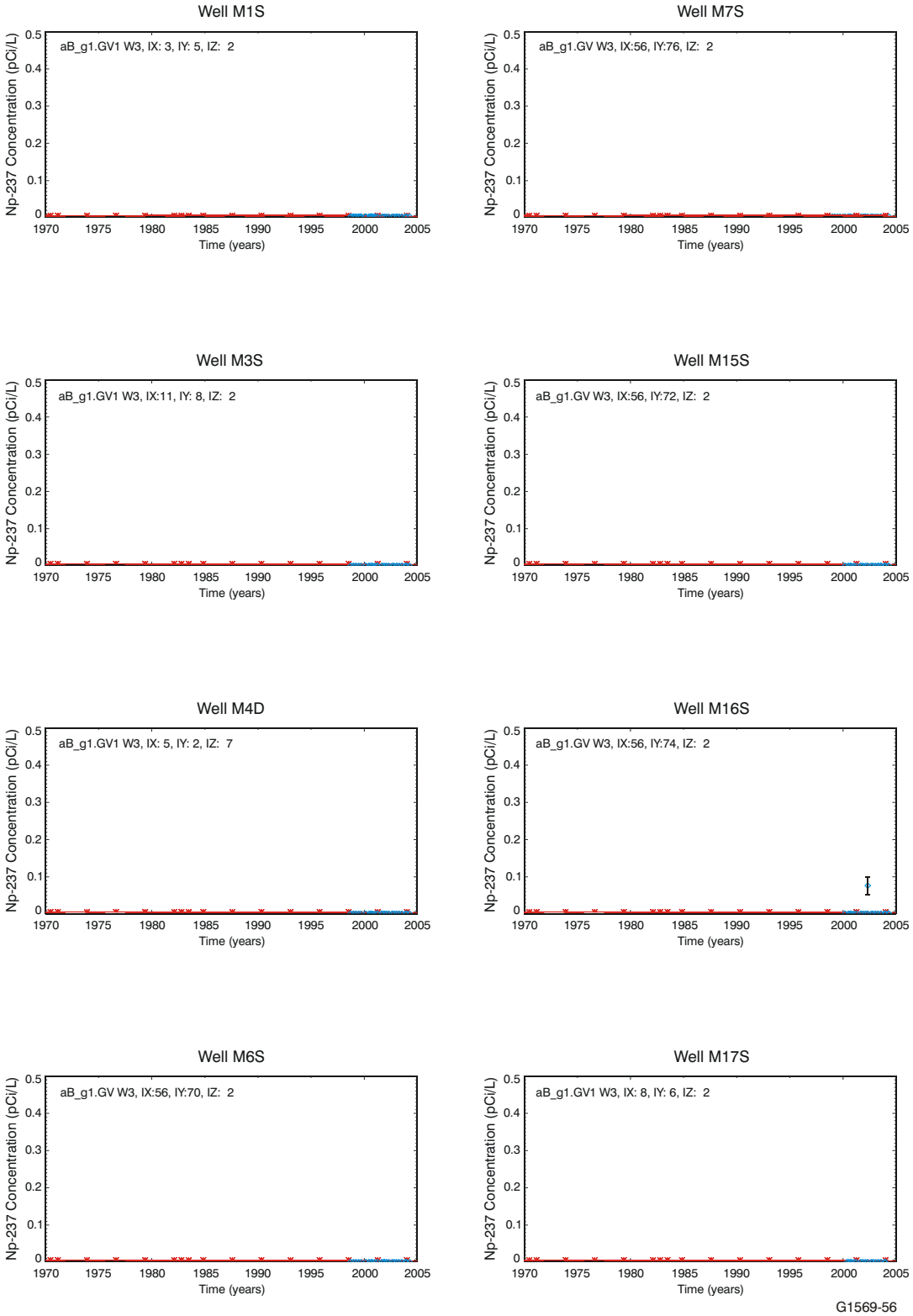

Figure 5-55. Comparison of simulated (red line) and observed (blue diamonds) neptunium-237 concentration time histories for aquifer monitoring wells near the Subsurface Disposal Area.

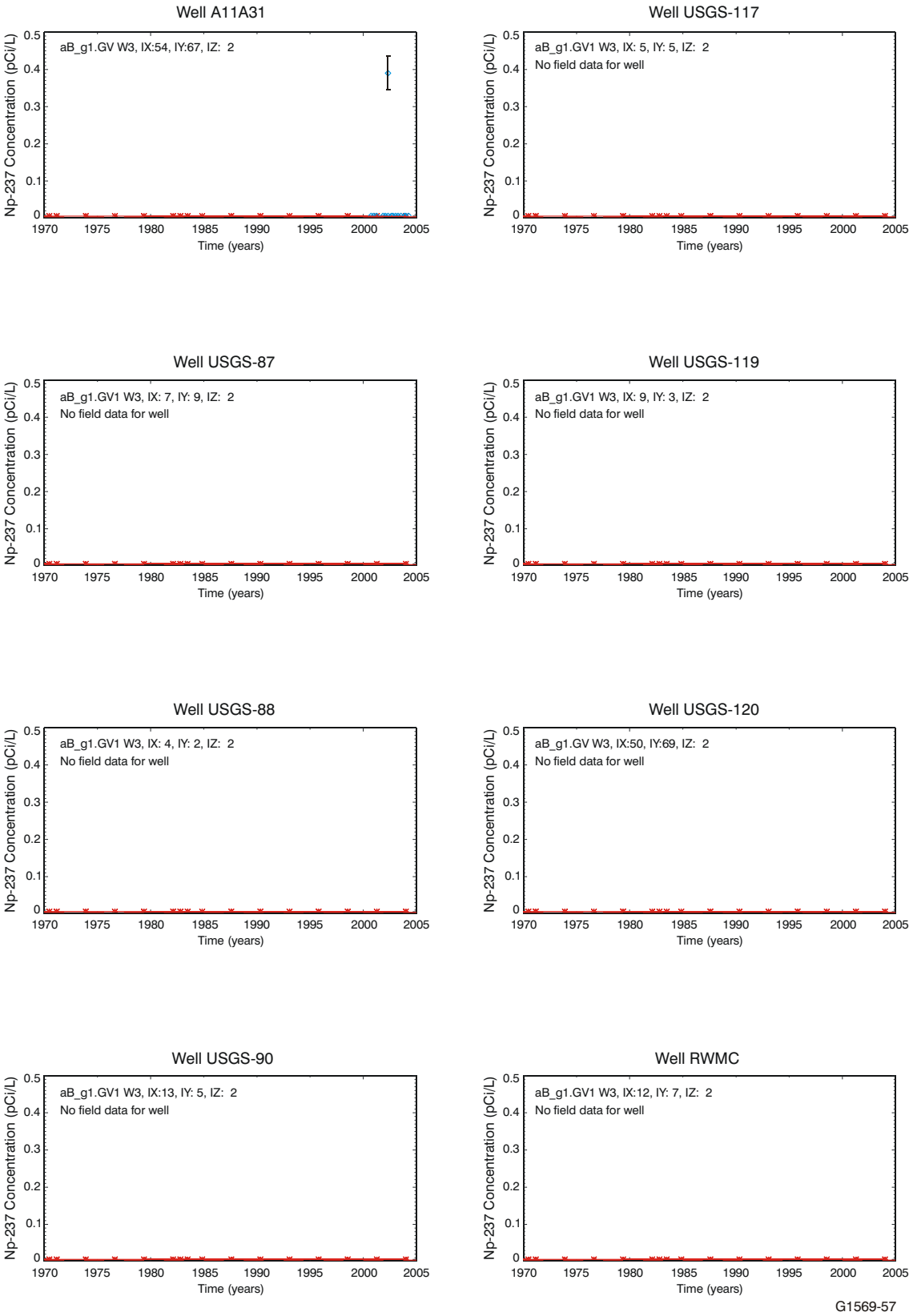

Figure 5-55. (continued).

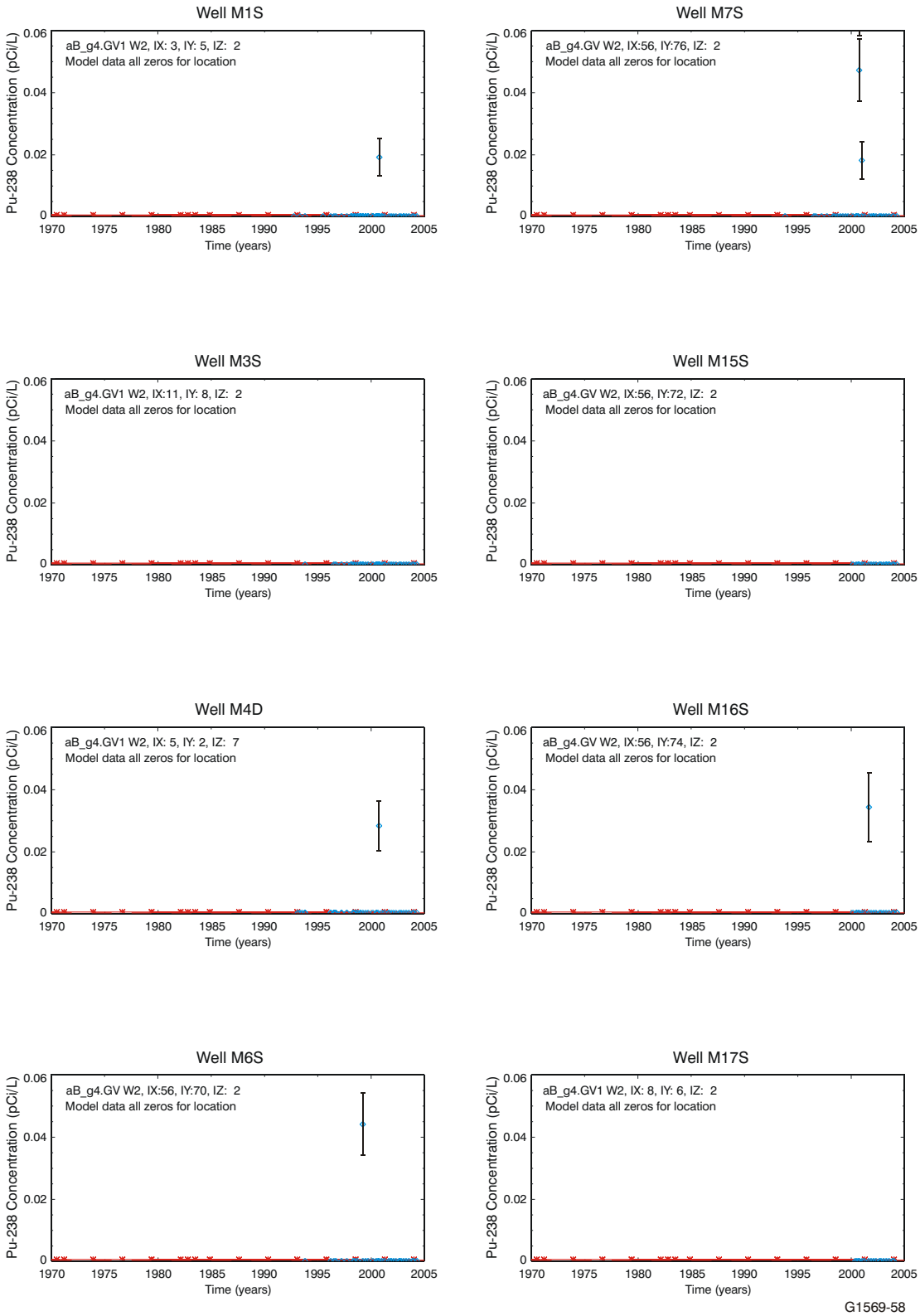

Figure 5-56. Comparison of simulated (red line) and observed (blue diamonds) plutonium-238 concentration time histories for aquifer monitoring wells near the Subsurface Disposal Area.

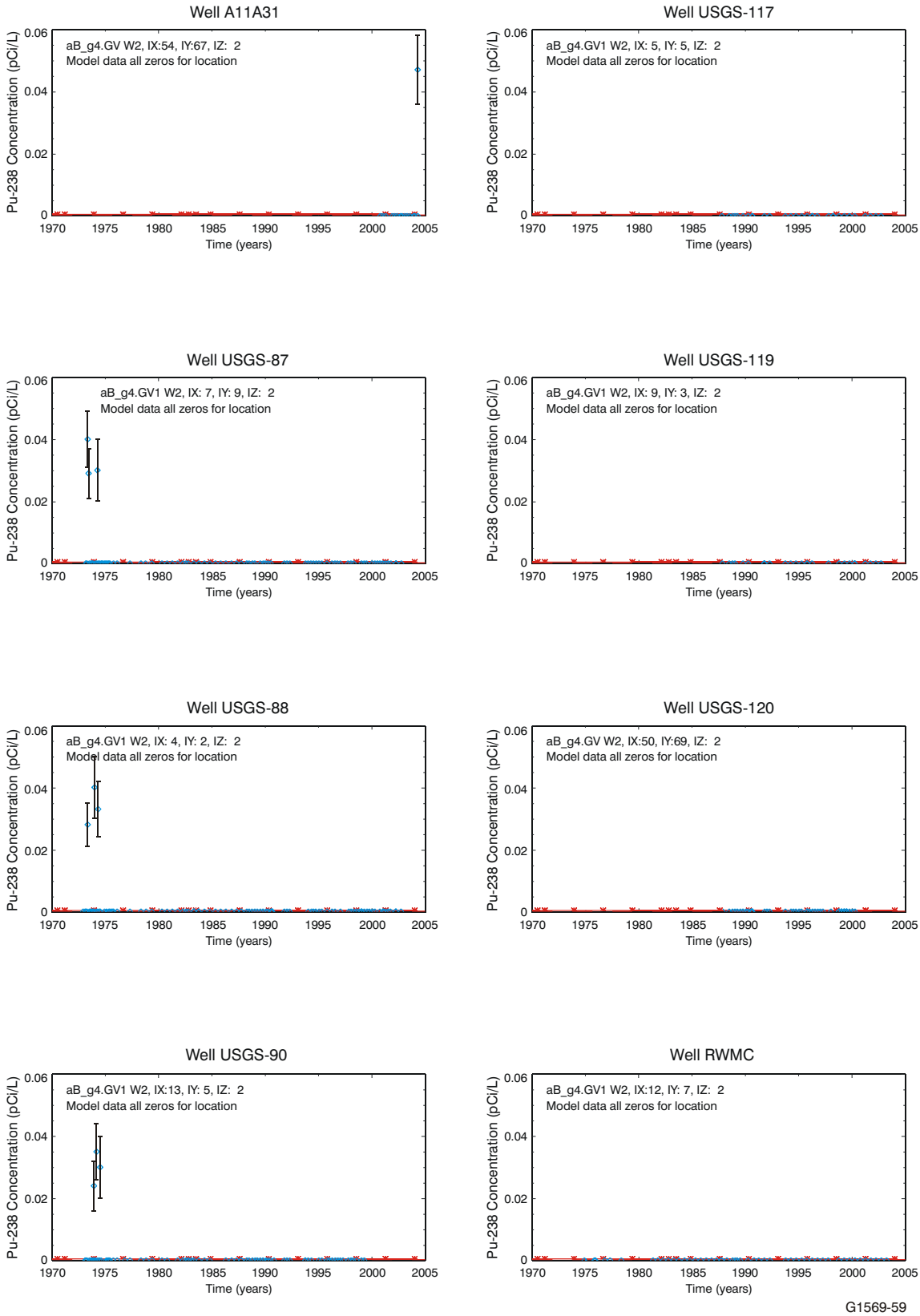

Figure 5-56. (continued).

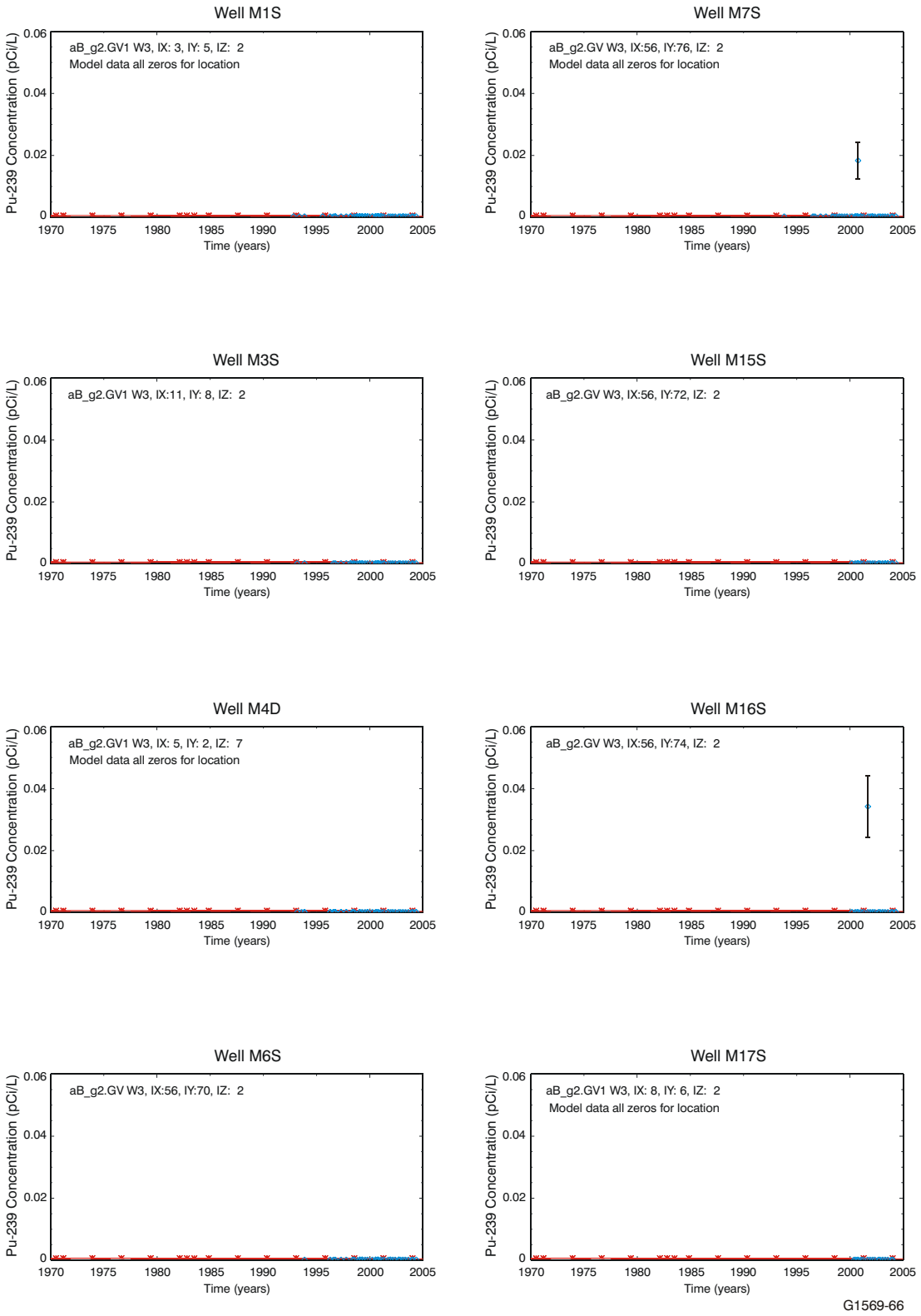

Figure 5-57. Comparison of simulated (red line) and observed (blue diamonds) plutonium-239 concentration time histories for aquifer monitoring wells near the Subsurface Disposal Area.

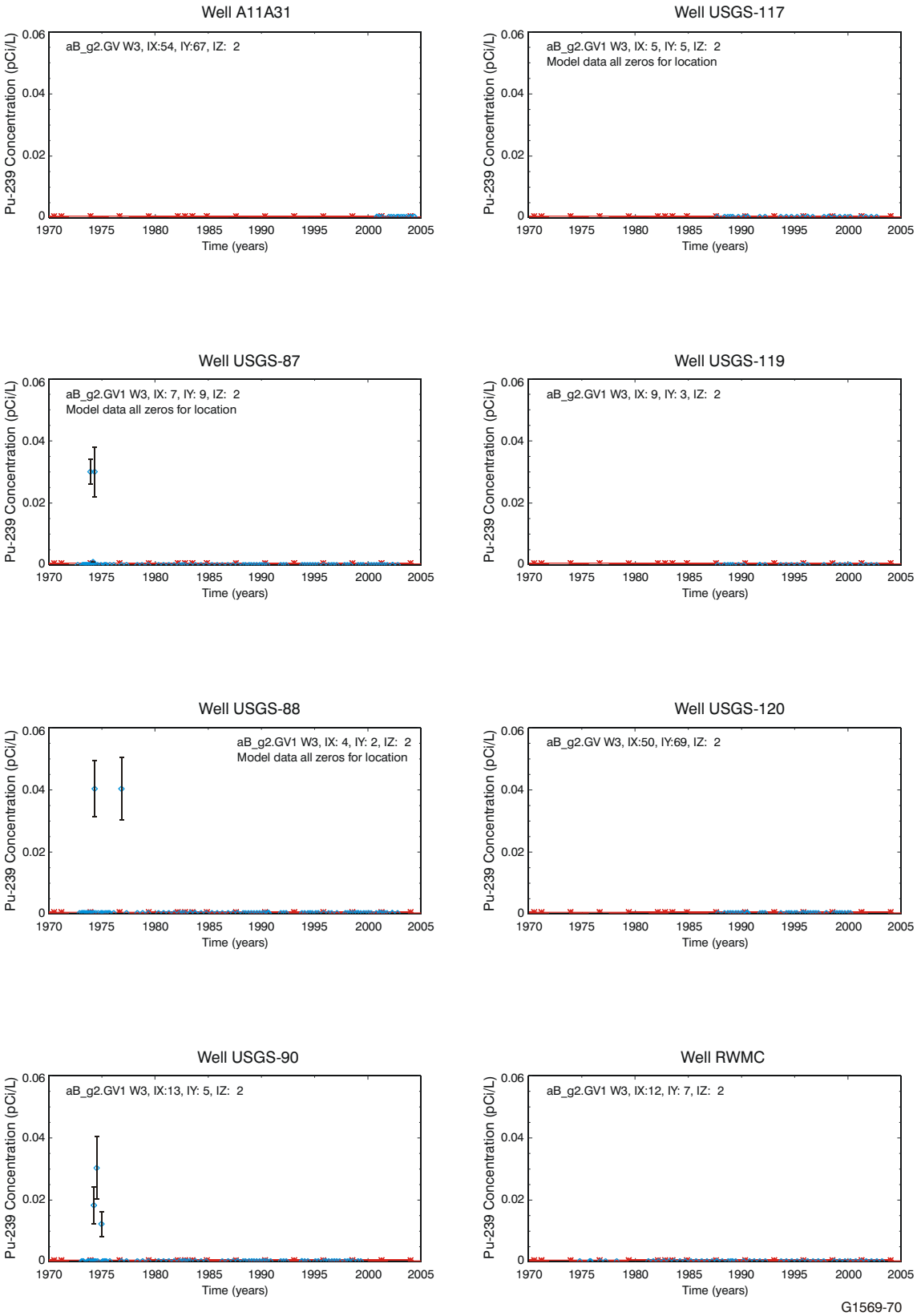

Figure 5-57. (continued).

Table 5-22 lists the maximum simulated concentrations anywhere in the aquifer through FY 2004 for all human health contaminants of potential concern, their long-lived decay-chain progeny, and chromium. No background concentrations are added to any of the simulated results. All of simulated peak values in Table 5-22 occur during FY 2004, indicating that concentrations were still increasing at that time. For comparison, corresponding maximum simulated concentrations through 2001 for the ABRA model and through 1995 from the IRA model are given in the third and fourth columns of Table 5-22. Aquifer background concentrations from Section 4 are shown in the fifth column of Table 5-22 for comparison to simulation results. The last two columns present the range of observed values taken from the nature and extent discussion in Section 4, along with comments concerning some of those values. Observed values from earlier than 1987 are not presented in Table 5-22. Numerous contaminants of potential concern do not have corresponding analyses, as indicated in Table 5-22.

Changes in simulated values between the RI/BRA model and the ABRA model result from numerous causes. The simulated C-14 concentration drops two orders of magnitude primarily due to allowing C-14 to partition into the gaseous phase and diffuse to the atmosphere. This vapor-phase simulation is discussed in Section 5.4. Simulated concentrations for Np-237 and the uranium isotopes have decreased due to an increase in their assigned distribution coefficients. Simulated concentrations for Pu-239 and Pu-240 increased due to increased mobility above the B-C interbed. Plutonium-238 was not treated this way, but shows a slightly increased concentration nonetheless, most likely due to either changes in inventory, changes in water travel time resulting from the topography, or both. Simulated concentrations for the fission products (i.e., Tc-99 and I-129) and activation products (i.e., C-14 and Cl-36) all decreased due to changes in inventory and source-release parameters. All the other contaminants of potential concern have slight changes that are most likely due to inventory changes or changes in assigned parameters for release mechanisms.

When comparing simulated results from the RI/FS model to the range of observed 3σ detections or the background concentrations, several patterns emerge. Simulated aquifer concentrations for fission and activation products are all still overpredicted to varying degrees compared to observed monitoring results, but not as much as they were for the ABRA. This overprediction is more likely caused by inadequacies in the source-release model than in the subsurface flow and transport model. Monitoring results for U-234, -235, and -238 are similar to reported background values. Simulated uranium isotope values are much less than observed values or background values, consistent with the conclusion of no observable impact in aquifer monitoring to date. All other contaminants are predicted to be either not in the aquifer yet or to be present at concentrations below detectable levels. If it is assumed that background concentrations for anthropogenic radioisotopes are zero for those contaminants not explicitly identified in Knobel, Orr, and Cecil (1992), then model results agree with nondetections for this last group of contaminants. This statement disregards sporadic detections of plutonium isotopes and Am-241 as anomalies. At a minimum, for this latter set of contaminants, model results are not in conflict with observed results. Inorganic contaminants (i.e., nitrate and chromium) are both overpredicted when compared to the majority of observed values.

Simulated vertical profiles of C-14 and U-238 concentrations within the aquifer are shown in Figures 5-58 and 5-59 to illustrate behavior for selected contaminants. These vertical profiles are at the same horizontal location as that shown previously in Figure 5-48 for nitrate, which generally contained the maximum concentration for most times. Similar to profiles for nitrate, some times maximum concentration does not occur at the uppermost gridblock for C-14. This is because contaminant flux from the vadose zone model behaved similarly for nitrate and C-14, with a pulse of contaminant followed by clean water. The simulated profile for U-238 shows that the maximum concentration always occurs in the uppermost gridblock, reflecting the long-duration, delayed contaminant flux from the vadose zone model. The overall implication for the baseline risk assessment remains the same: that it is not necessarily conservative to extract concentrations from the uppermost gridblock.

Table 5-22. Comparison of aquifer model concentrations and observed concentrations with no adjustments for background concentrations.

Contaminant[a]	RI/FS Model Concentration[b] (pCi/L)	ABRA Model Concentration[c] (pCi/L)	IRA Model Concentration[d] (pCi/L)	Aquifer Background Concentration[e] (pCi/L)	Range of Detections[f] (pCi/L)[g]	Comments on Detections[g]
Ac-227	2E-11	5E-07	6E-08	NE	No analyses[h]	None
Am-241	7E-17	9E-17	1E-06	0	0.026 to 1.97	None
Am-243	3E-19	7E-24	2E-11	NE	No analyses	None
C-14	8E+01	3E+03	5E+00	NE	1.8 to 42.1	Analysis began in 1994
Cl-l36	4E+00	3E+02	1E+00	NE	All nondetects	Analyses for Cl-36 began in the year 2001; Cl-36 analyses are done semiannually
I-129	1E+01	5E+01	4E+00	0	0.59 to 17.0	None
Nb-94	—	1E-23	1E-14	NE	No analyses	None
Np-237	1E-10	4E-04	8E-04	NE	0.08 to 0.38	None
Pa-231	1E-10	7E-06	1E-06	NE	No analyses	None
Pb-210	1E-17	3E-10	4E-08	NE	No analyses	None
Pu-238	4E-26	0	1E-12	0	0.018 to 0.37	NA
Pu-239	3E-17	5E-28	2E-11	0	0.034 to 4.3	None
Pu-240	3E-17	3E-30	7E-12	0	0.034 to 4.3	None
Ra-226	3E-17	4E-09	1E-08	0.01 to 0.37	4.0 to 12.7	Reported through gamma analysis when detected above laboratory instrument and sample matrix background
Ra-228	7E-19	—[i]	8E-12	0 to 2.7	No analyses	Reported through gamma analysis when daughter products are detected above laboratory instrument and sample matrix background
Tc-99	5E+03	4E+04	5E+01	NE	0.97 to 35.4	None
Th-229	4E-11	1E-06	4E-08	NE	No analyses	None
Th-230	2E-14	3E-06	8E-7	NE	No analyses	None
Th-232	2E-18	6E-13	1E-11	NE	No analyses	None
U-233	8E-08	4E-03	3E-04	NA	No analyses	NA
U-234	4E-10	1E-01	5E-02	1.92	2.0 to 4.3	None

Table 5-22. (continued).

Contaminant[a]	RI/FS Model Concentration[b] (pCi/L)	ABRA Model Concentration[c] (pCi/L)	IRA Model Concentration[d] (pCi/L)	Aquifer Background Concentration[e] (pCi/L)	Range of Detections[f] (pCi/L)[g]	Comments on Detections[g]
U-235	2E-10	2E-02	3E-03	0.15	0.18 to 3.0	None
U-236	9E-09	4E-03	2E-03	NA	No analyses	None
U-238	9E-10	3E-01	4E-02	0.90	1.7 to 2.1	None
Nitrate (as nitrogen-N)	6E+01 mg/L	1E+02 mg/L	1.4E+01 mg/L	0.4 to 5.0 mg/L	0.28 to 3.4 mg/L	None
Chromium (total)	3E+01 µg/L	1E+00 µg/L	1E-01µg/L	1 to 22 µg/L	4.6 to 99.6 µg/L	Most other high chromium values were approximately 40 to 60 pCi/L
Carbon tetrachloride	1E+02 µg/L	—[i]	8E+00 µg/L	0 µg/L	0 to 8 µg/L	None
1,4-Dioxane	1E+02 µg/L	—[i]	—[i]	0 µg/L	No analyses	1,4-dioxane was only recently added to the analyte list
Methylene chloride	1E+01 µg/L	—[i]	1E-01 µg/L	0 µg/L	0 to 6 µg/L	Single detection of 6 µg/L was not believed to be a valid result
Tetrachloroethylene	1E+01 µg/L	—[i]	6E-01 µg/L	0 µg/L	0 to 0.4 µg/L	None

Note: 0.0 pCi/L for radionuclides signifies a nondetectable result (i.e., result is <3σ and <maximum detectable concentration) using traditional radiochemical analyses methods.

a. Observed values from earlier than 1987 are not presented in this table.
b. Maximum simulated concentration at 12-m depth through Fiscal Year 2004.
c. Maximum simulated concentration at 12-m depth through Calendar Year 2001.
d. Maximum simulated concentration at 12-m depth through Calendar Year 1995.
e. Aquifer background concentrations are from Table 4-1 in Section 4.
f. In the Subsurface Disposal Area-vicinity wells since 1987.
g. The range of observed values is taken from the nature and extent discussion in Section 4.
h. See the respective contaminant discussions in Section 4 regarding lack of analysis.
i. Not reported in the IRA or ABRA.

ABRA = Ancillary Basis for Risk Analysis (Holdren et al. 2002)
IRA = Interim Risk Assessment (Becker et al. 1998)
NA = information not available on background concentrations
NE = not established
RI/FS = remedial investigation and feasibility study

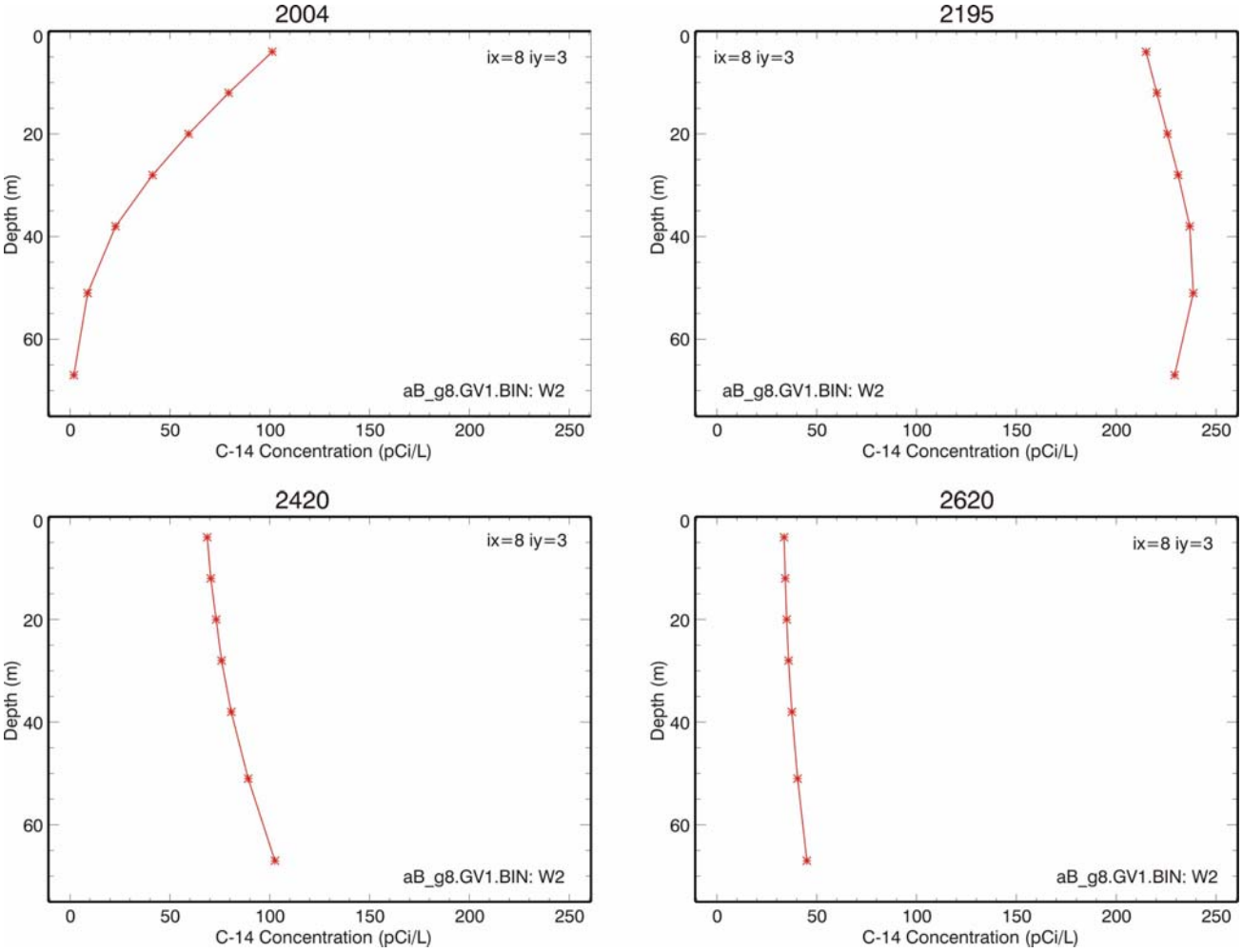

Figure 5-58. Simulated aquifer carbon-14 concentration profiles beneath the Subsurface Disposal Area. The year is shown at the top of each plot.

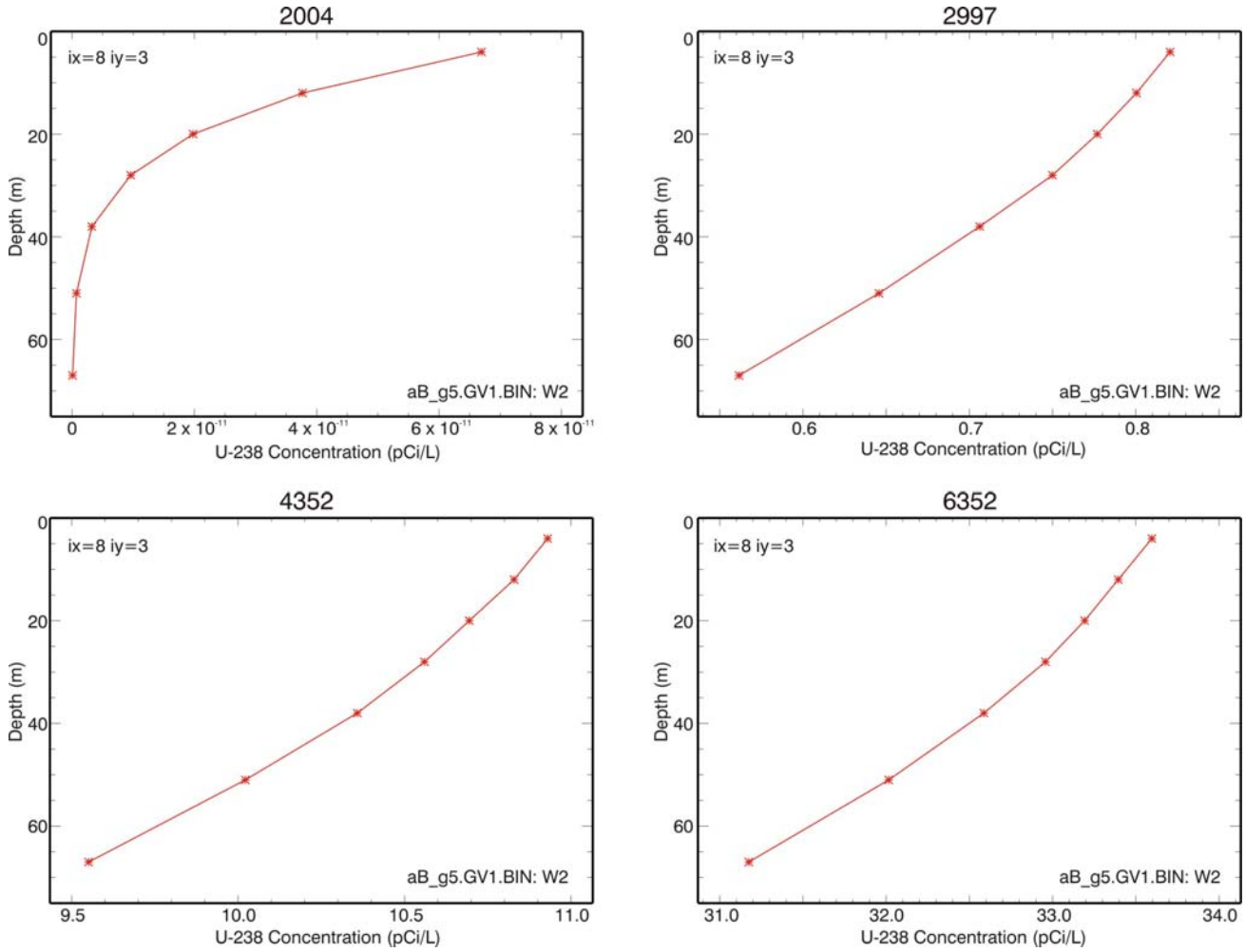

Figure 5-59. Simulated aquifer uranium-238 concentration profiles beneath the Subsurface Disposal Area. The year is shown at the top of each plot.

5.2.6 Baseline Risk Assessment Sensitivity Simulations

This section discusses implementation of simulations for the RI/BRA sensitivity analyses, which were defined in Holdren and Broomfield (2004). Results, when presented, are in terms of water saturations or simulated concentrations. Results are presented for U-238, C-14, and nitrate simulations to demonstrate the impact from a variety of contaminants with sorbing and nonsorbing behavior for most of the sensitivity cases. Exceptions are presentation of Pu-239 and Pu-240 for a case with no sorption in the interbeds and Tc-99 for evaluation of impacts from increasing the fractured-basalt permeability anisotropy ratio. Technetium-99 and I-129 are not shown for most of the sensitivity cases because those results are being revised for the feasibility study. Carbon-14 results presented in these sensitivity simulations use the model that includes both gaseous-phase and dissolved-phase transport described in Section 5.4 and the effect of vapor vacuum extraction described in Section 5.3. Both the time and concentration axes vary on the sensitivity results plots to show adequate detail in the results to discern behavior. The sensitivity results also are presented in terms of impacts to groundwater-pathway risks in Section 6. These sensitivity simulations test assumptions used in the model, and as such, the simulations represent an assessment of conceptual uncertainty.

5.2.6.1 Simulation Nomenclature. Development of a nomenclature to track the simulations was necessary because of the extensive number and types of simulations performed for the RI/BRA and the feasibility study. This nomenclature section is included to allow the reader to recognize headings in the simulation-results figures and involves having unique names for each of the RI/BRA base-case and sensitivity simulations. These headings also serve the purpose of further identifying the specific contaminant from within the simulation group that is portrayed in a figure. Unique names were used in naming all input and output files from a simulation group so that the results can be easily retrieved from project archival storage using keyword searches.

Contaminants were divided into 11 groups for purposes of performing the simulations; those divisions are described in Section 5.1.5 and listed in Table 5-8. Table 5-23 provides the nomenclature for the leading character string in the run names. The first letter is always a "B" for RI/BRA-related simulation or an "F" for a feasibility study simulation. Letters in the remaining positions—two through four—were then used to identify attributes of a sensitivity case. The TETRAD simulator imposes an arbitrary limit of eight characters total for a unique run name. With the last four positions taken up with the group identifier, the unique leading string could only be four characters long to avoid extensive renaming of results, which was necessary in some cases. Table 5-24 shows how these conventions were applied to define names for each of the simulation groups. Table 5-24 gives the application that was being simulated and a detailed description of the simulation group. The "g*" indicates Groups 1 through 11 as appropriate for each name.

Table 5-23. Run-naming nomenclature.

Run Nomenclature	Run Description
Leading B	Baseline risk assessment
u	Upper-bound inventory
i	Infiltration
o	Outside the Subsurface Disposal Area
4	Pit 4
n	No
g	Grout
bc	B-C interbed
l	Low
h	High
k	Permeability
cP	Colloidal plutonium, in the no sorption in the vadose zone interbeds sensitivity case

Table 5-24. Simulation group names and descriptions.

Simulation Group Name	Application	Description
BASE CASE		
B_g*	Baseline risk assessment base case	Best-estimate inventories, average infiltration inside the SDA = 5.0 cm/year, background infiltration outside the SDA = 1.0 cm/year
BASE CASE SENSITIVITY: Hold all values constant as in the baseline risk assessment base case, except as noted.		
Bu_g*	Upper-bound inventories	Upper-bound instead of best-estimate inventories
Bhi_g*	High infiltration in the SDA	Increase infiltration rate to 23 cm/year assigned uniformly across the SDA
Bloi_g*	Low background infiltration	Reduce infiltration rate assigned outside the SDA boundary from 1.0 to 0.1 cm/year
Bnbc_g*	No B-C interbed	Bounding case where B-C interbed gridblocks replaced with fractured basalt
B4ng_g*	No interim actions	Pit 4 inventory not reduced for the Accelerated Retrieval Project and beryllium blocks not grouted
Bnlk_g*	No low-permeability zone in aquifer	Revise low-permeability region in the aquifer from 153 to 712,000 mD
BcP_g*	No sorption in the vadose zone interbeds	Bounding case where sorption of Pu-239 and Pu-240 does not occur in the B-C and C-D interbeds
Bli_g*	Low infiltration in the SDA	Low infiltration inside the SDA beginning in the year 2010

SDA = Subsurface Disposal Area

5.2.6.2 Upper-Bound Inventories. A simulation suite was performed where upper-bound inventories were used instead of best estimates. The only difference in the subsurface flow and transport models was that a different source term was supplied. The entire suite of potential contaminants was simulated. Figure 5-60 shows a comparison of the concentration of U-238, C-14, and nitrate between the base case and the upper-bound inventory simulation. In each case, simulated concentrations are larger, although it takes longer for this to be evident for U-238, which undergoes sorption, thus, the longer time portrayed on the horizontal axis. Note that the concentrations shown in this sensitivity section are for the maximum simulated concentration anywhere in the aquifer, including beneath the SDA, for all simulated times. This is in contrast to risks presented in Section 6, which are based on the maximum simulated concentration anywhere outside the SDA fence after institutional control ends in Calendar Year 2110.

5.2.6.3 No B-C Interbed. The method used to define interbed upper surfaces and interbed thicknesses resulted from a consistent statistical approach that was based on all lithologic data available. To incorporate spatial variability, geostatistical analysis and interpolation methods were implemented and robustly tested by Leecaster (2002) and updated in Leecaster (2004). As with the ABRA model, the RI/FS model used kriging results without imposing any bias into them. In the IRA model, kriging results were modified to enforce gaps in the interbeds in gridblock locations containing wells that showed an interbed was missing at that location.

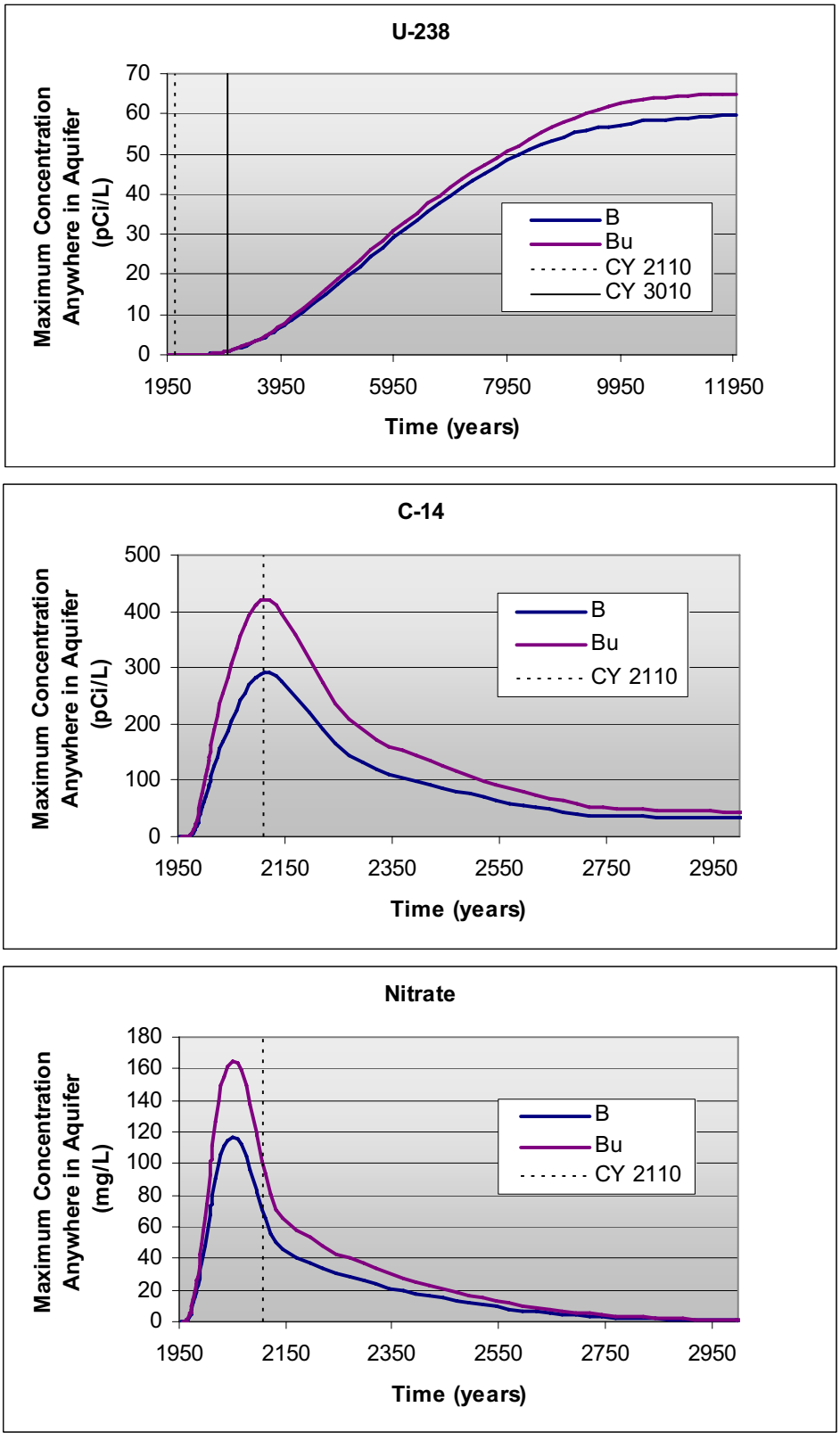

Figure 5-60. Comparison of base case (B) and upper-bound inventory (Bu) maximum simulated concentration anywhere in the aquifer for uranium-238, carbon-14, and nitrate.

To bound the effect of including gaps, a simulation suite was performed where the entire B-C interbed was treated as though it were missing. The gridblocks that were assigned B-C interbed properties for the RI/FS model were assigned properties of fractured basalt instead. This allowed the mobile fraction of Pu-239 and Pu-240 to continue migrating down to the C-D interbed before being affected by the higher distribution coefficient. Upper-boundary conditions for water infiltration rates and contaminant source-term results were unchanged from the RI/FS model. The entire suite of potential contaminants was simulated, except for VOCs (Group 11). As a result of not simulating VOCs, C-14 simulation results for this case do not include the effect of vapor vacuum extraction operations. Figure 5-61 shows a comparison of U-238, C-14, and nitrate concentrations between the RI/FS model and the sensitivity simulation without the B-C interbed. As expected, in each case, the simulated concentrations for the sensitivity case show an earlier breakthrough due to the absence of the B-C interbed, with the largest change in results for U-238, where the lack of sorption in the B-C interbed exaggerates impact. Magnitudes of peaks do not change substantially with U-238 and C-14 both increasing. The nitrate peak concentration decreases slightly, possibly due to interactions between where nitrate is released into the vadose zone model and the location where nitrate would otherwise have been redirected when transiting the B-C interbed.

5.2.6.4 High Infiltration inside the Subsurface Disposal Area. Water infiltration rates are assigned at the upper boundary of the vadose zone simulation domain. These amounts of water also are input into the source-term model and impact the contaminant release. Uncertainty in assigned infiltration rates is acknowledged. To bound the effect of the infiltration rate being greater than was assigned, a sensitivity simulation was performed whereby the infiltration rate everywhere inside the SDA boundary was assigned a value of 23 cm/year (9 in./year), both in the source-release model and in the vadose zone flow and transport model, beginning in 1952. The water infiltration rate outside the SDA boundary remained at the background estimate of 1.0 cm/year (0.4 in./year). The 23-cm/year (9-in./year) infiltration rate is the same as the total annual average precipitation on the INL Site and represents conservative upper-bound inventories on the possible net infiltration into the subsurface. The entire suite of potential contaminants was simulated.

Figure 5-62 shows a comparison of U-238, C-14, and nitrate concentrations between the base case and the sensitivity simulation with a high-infiltration rate inside the SDA. As expected, in each case, the simulated concentrations for the sensitivity case show higher concentrations and reach peak values sooner than the base-case simulated concentrations. Conceptually, water that contacts waste results in higher concentrations uniformly in the groundwater pathway. Results of this sensitivity case demonstrate this aspect of the conceptual model.

In addition to the effect on groundwater-pathway concentration results, this sensitivity simulation lends itself to assessing the impacts on simulated interbed saturations. Figure 5-63 illustrates the resulting maximum simulated water saturations in the B-C and C-D interbeds for the high-infiltration case. Water saturations in Figure 5-63 can be compared to those for the base case (see Figure 5-24). The extent of high saturation areas greater than 0.9 is considerably larger, especially in the B-C interbed. Better agreement with locations that had shown perched water in the western half of the SDA is shown.

5.2.6.5 Pit 4 Inventory Not Removed and No Beryllium Block Grouting. The base-case model included removing a portion of the Pit 4 inventory, based on the assumption that the Accelerated Retrieval Project was completed. Likewise, the grouting of beryllium blocks also was included. This sensitivity study considered a case where neither of these actions occurred. The entire suite of potential contaminants was simulated.

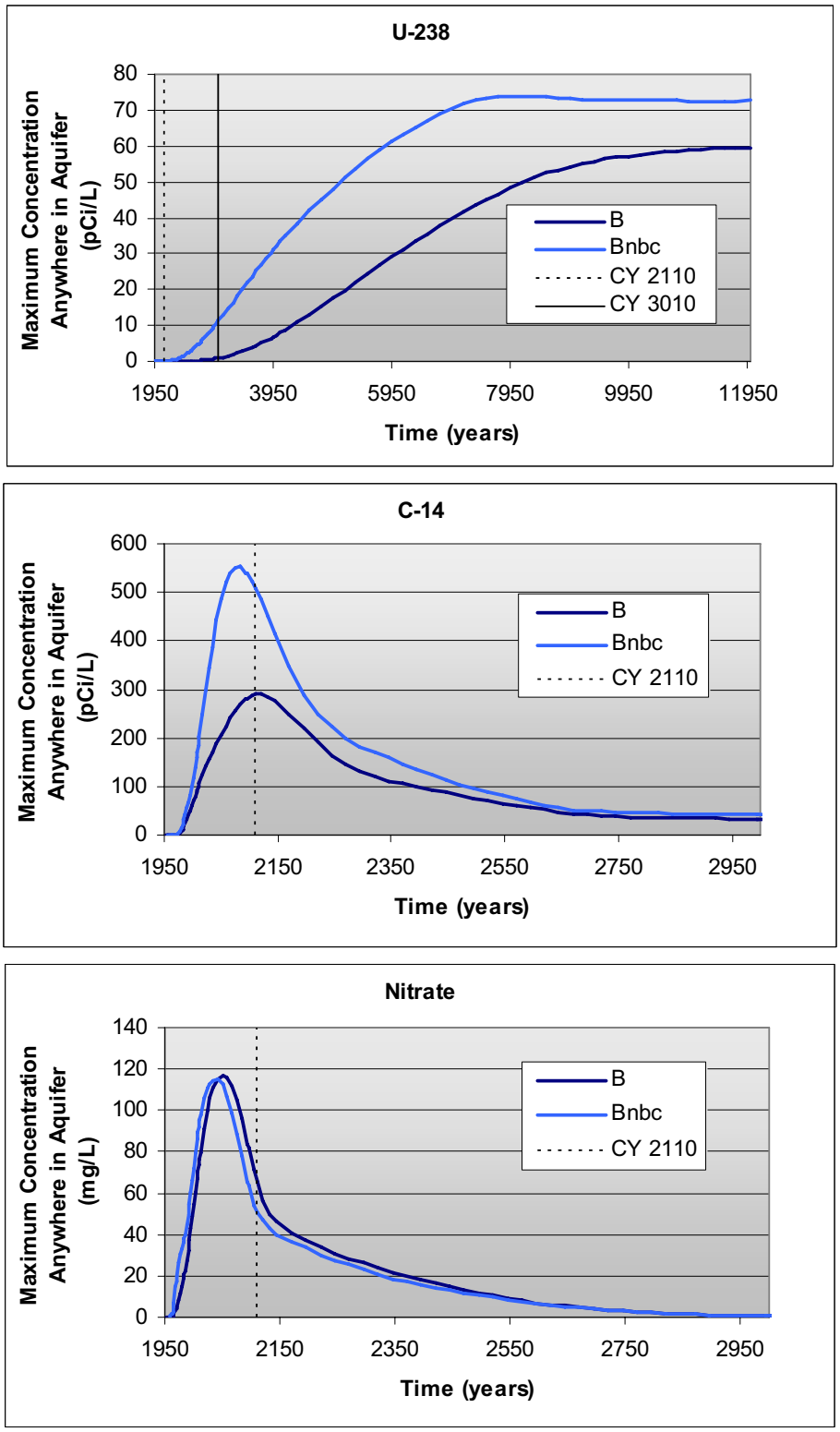

Figure 5-61. Comparison of the base case (B) and the no-B-C-interbed (Bnbc) maximum simulated concentrations anywhere in the aquifer for uranium-238, carbon-14, and nitrate. The carbon-14 results do not include the effect of vapor vacuum extraction operations.

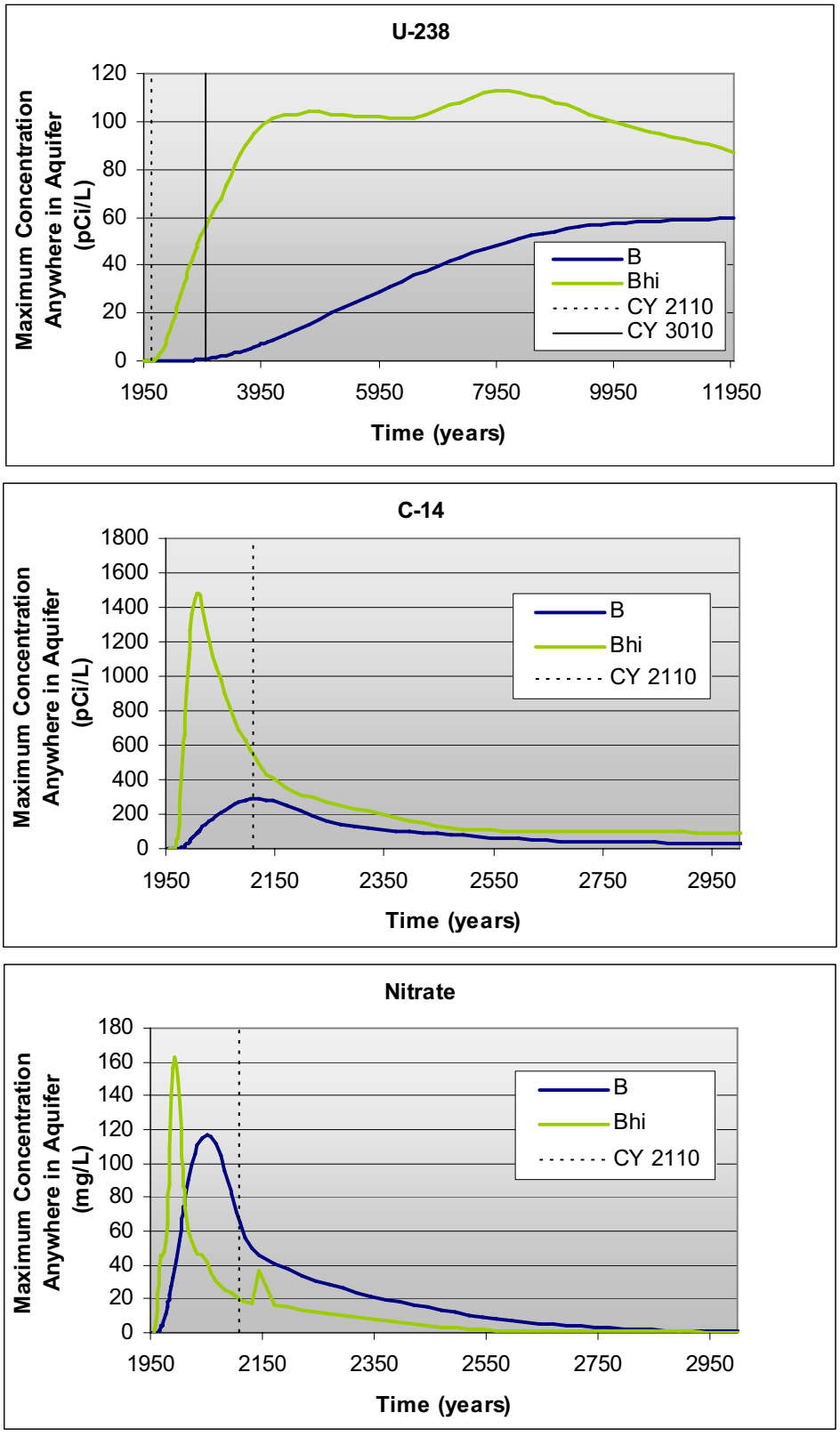

Figure 5-62. Comparison of base case (B) and high infiltration inside the Subsurface Disposal Area (Bhi) maximum simulated concentration anywhere in the aquifer for uranium-238, carbon-14, and nitrate.

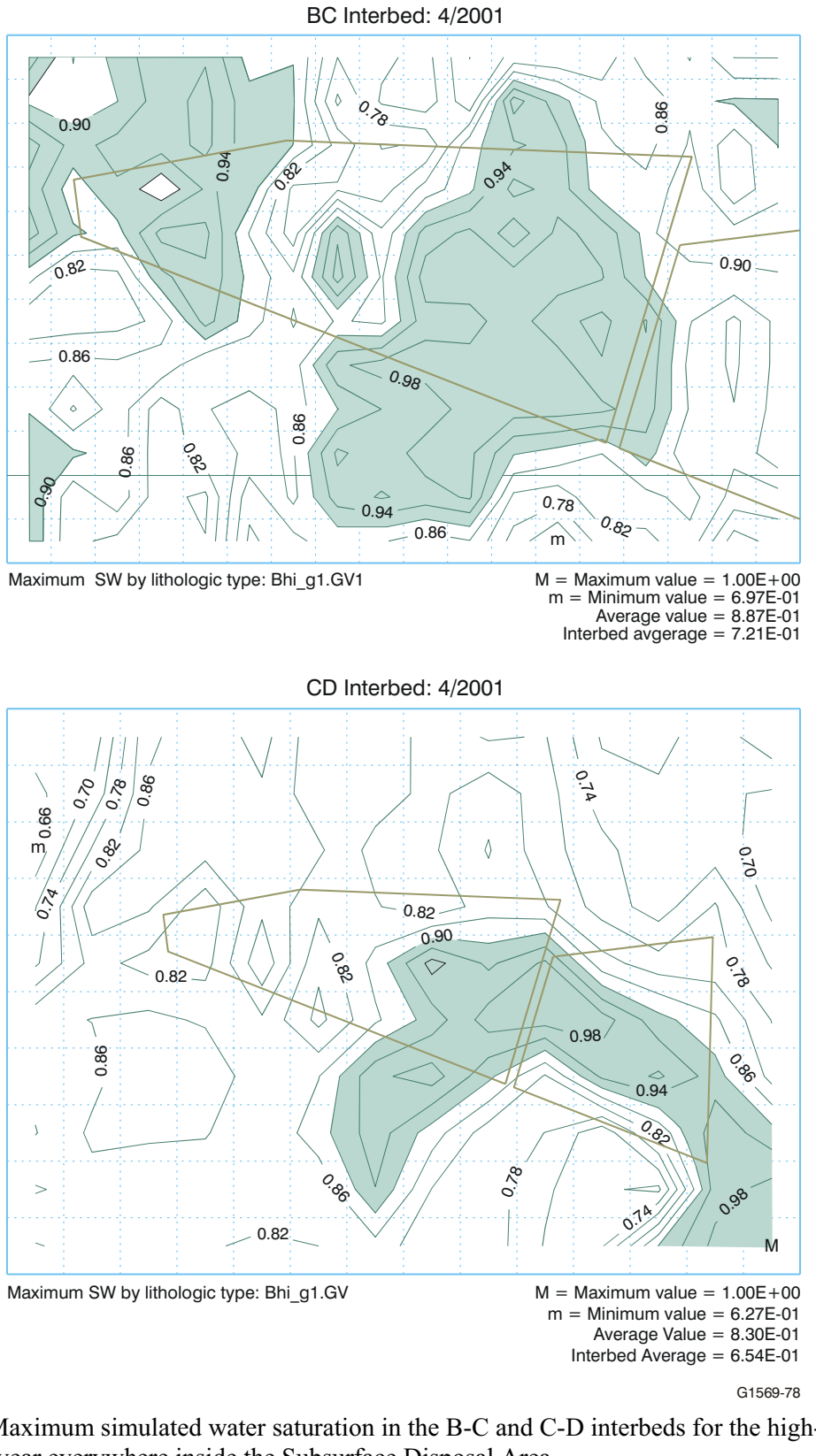

Figure 5-63. Maximum simulated water saturation in the B-C and C-D interbeds for the high-infiltration rate of 23 cm/year everywhere inside the Subsurface Disposal Area.

Figure 5-64 shows a comparison of U-238 and C-14 concentrations between the base case and sensitivity simulation with the Pit 4 inventory not reduced and without beryllium block grouting. Nitrate is not shown because no change to the source-release modeling for this sensitivity case was included. The simulated U-238 concentrations for the sensitivity case are essentially the same because, although there is a larger inventory available for release in the sensitivity case, the solubility limit for U-238 keeps the source-release term almost equivalent between the two cases. The simulated C-14 concentration is slightly higher for the sensitivity case because of a greater release from the source model due to a larger inventory.

5.2.6.6 Low Background Infiltration. The infiltration rate outside the SDA was assigned a value of 1.0 cm/year (0.4 in./year) for the RI/FS model. In this sensitivity case, a background infiltration rate that is an order of magnitude lower was assigned to test the impact on simulated groundwater-pathway concentrations. This lower rate was assigned because ongoing investigations may lead to the conclusion that the 1.0 cm/year (0.4 in./year) background infiltration rate is too high. The lower background infiltration rate was used for initial conditions for this sensitivity simulation and was continued for infiltration outside the SDA beginning in 1952. The entire suite of potential contaminants was simulated.

Figure 5-65 shows a comparison of U-238, C-14, and nitrate concentrations between the base case and the sensitivity simulation with a lower background infiltration rate outside the SDA. For each of these three contaminants, simulated concentrations arrived slower in the sensitivity case, showing the effect of slower velocities in the vadose zone that result from less water overall in simulations. Peak concentrations for U-238 and nitrate increased, likely due to less dilution with less water overall coming into the aquifer from the vadose zone domain. However, the C-14 concentrations decreased, with the decrease likely due to specific interactions between where C-14 is released into the vadose zone model and reductions in velocity.

5.2.6.7 Fractured Basalt Anisotropy. This case was not specified in Holdren and Broomfield (2004). The need for this case arose when it was discovered that by using a fractured basalt anisotropy ratio of 300:1 for the horizontal-to-vertical permeability, some additional lateral water movement above the C-D interbed occurred that resulted in some water and contaminants contacting the horizontal no-flux boundary in the southeastern corner of the vadose zone simulation domain. For some short-duration periods before the end of institutional control in the year 2110, this lateral movement results in the peak concentration in the aquifer occurring beneath this extreme southeastern gridblock location in the vadose zone model domain. If the boundary were farther away, additional dilution would have occurred if the water and dissolved contaminants had continued to migrate horizontally. The impact of water contacting this boundary and not being able to move farther was investigated for the mobile fission and activation contaminants (Group 6) and found to be negligible. The evaluation was performed using comparisons of contaminant fluxes with additional fractured basalt anisotropy ratios of 30:1 (i.e., the ABRA value), 3:1, and 1:1. Magnuson and Sondrup (2006) presents the results and discussion.

5.2.6.8 No Low-Permeability Region in Aquifer. This case was not specified in Holdren and Broomfield (2004), and updates results of a similar assessment done after IRA modeling (Magnuson 1998) where the effect of not including the low-permeability zone in the aquifer was simulated. In the RI/FS model, the low-permeability region in the aquifer is assumed to be continuous and have substantially slow movement of water within the aquifer beneath the SDA. This slower movement results in less dilution of influxing vadose zone contaminants than would otherwise occur. Simulating only the aquifer portion of the groundwater pathway for this sensitivity simulation was necessary because the vadose zone simulation was unaffected.

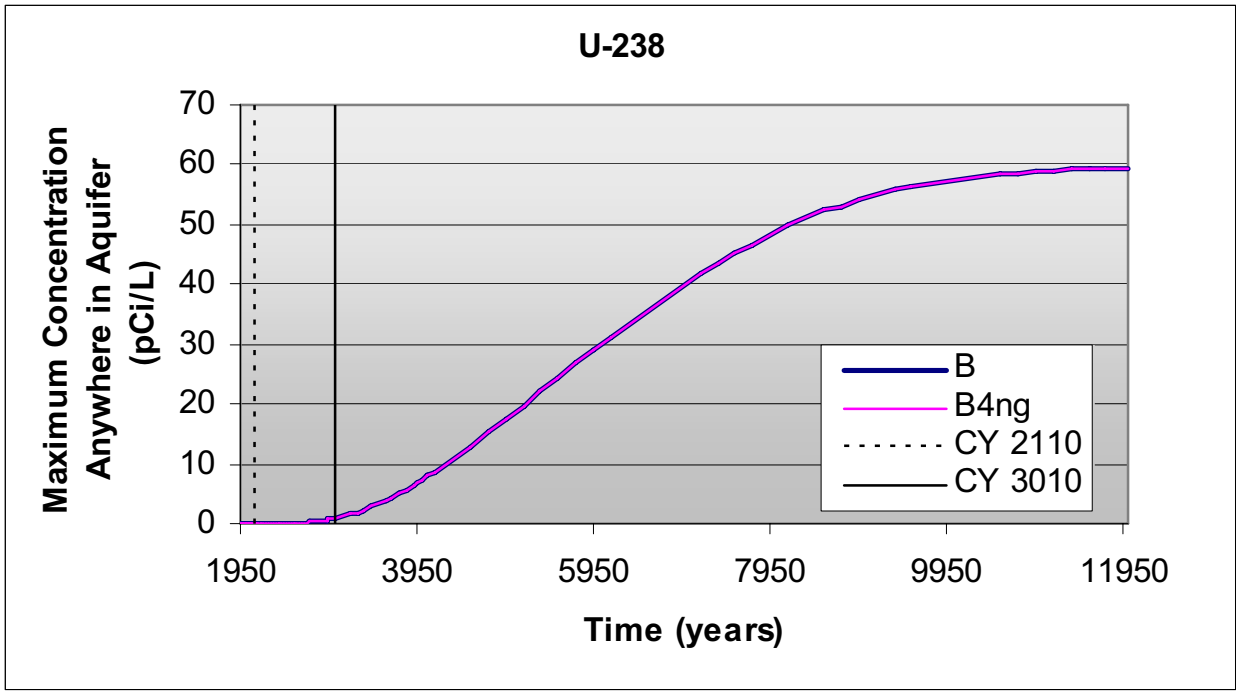

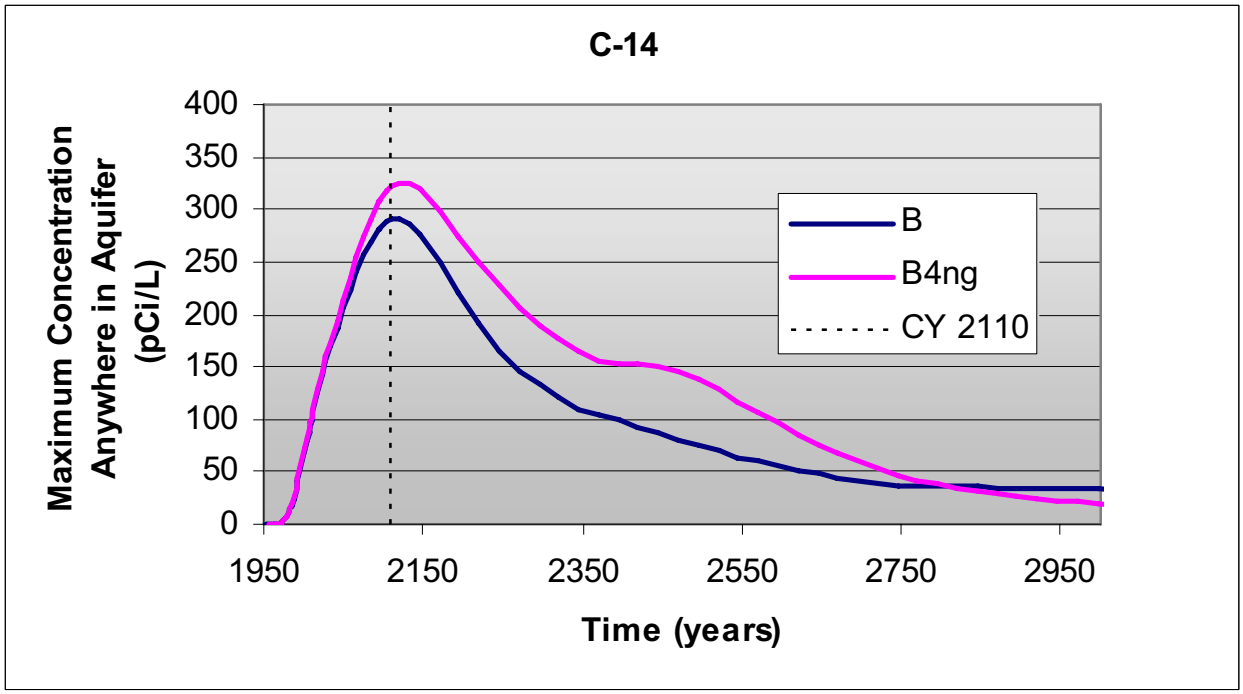

Figure 5-64. Comparison of the base case (B) and Pit 4 inventory not removed and no beryllium block grouting (B4ng) maximum simulated concentration anywhere in the aquifer for uranium-238 and carbon-14. Nitrate is not shown because no change to the source-release modeling was included for this case.

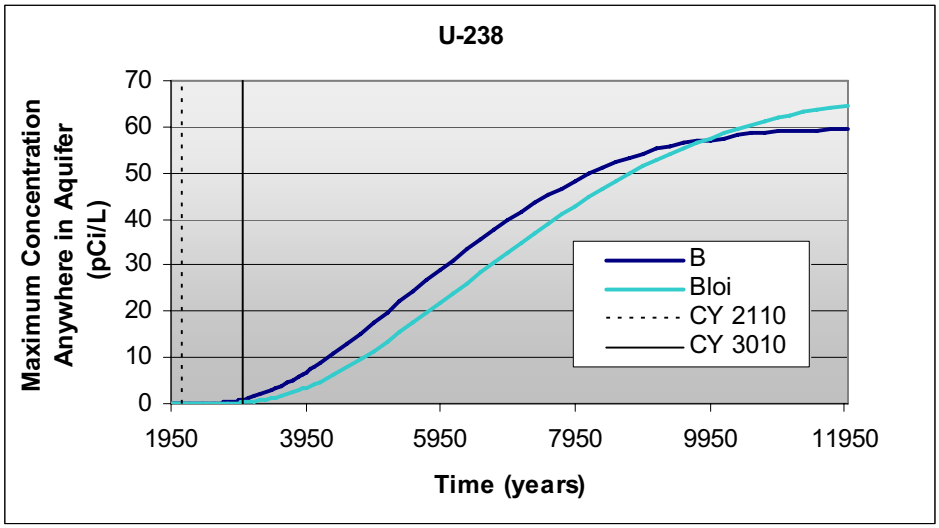

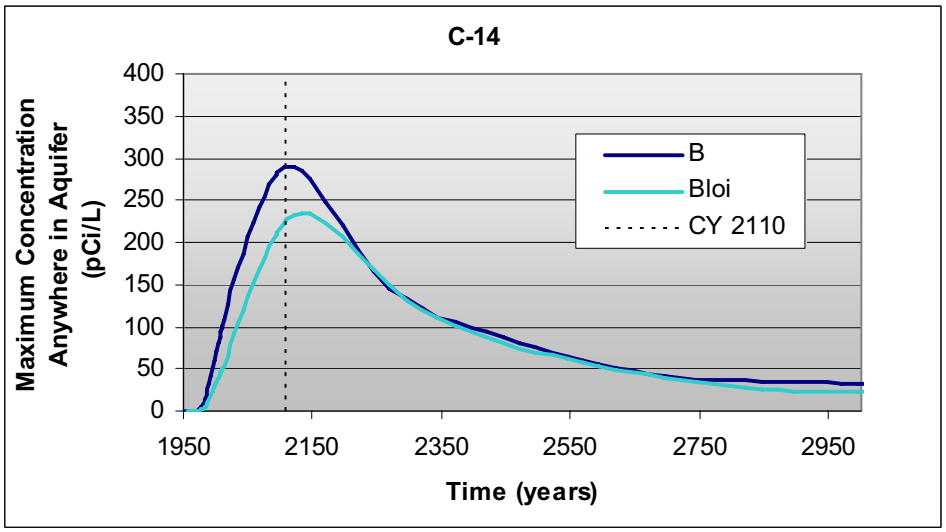

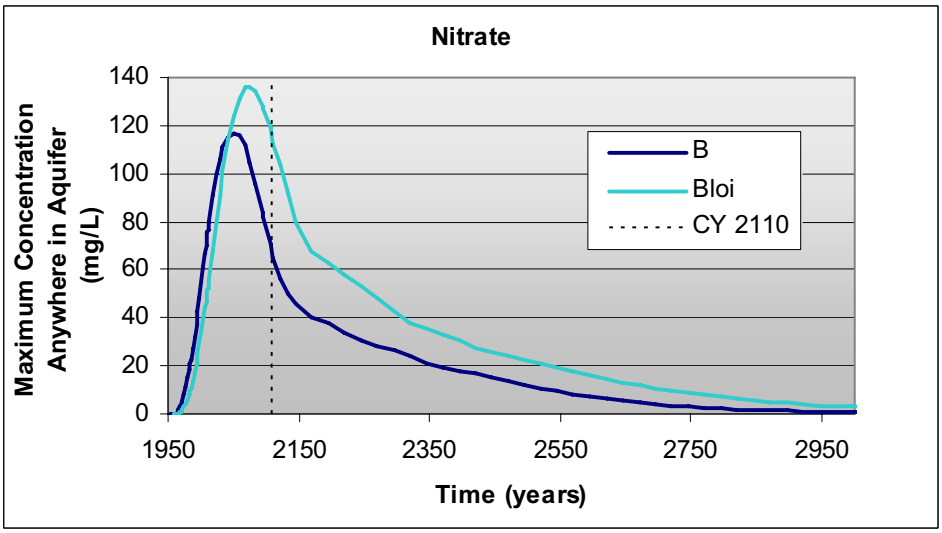

Figure 5-65. Comparison of base case (B) and low background infiltration (Bloi) maximum simulated concentration anywhere in the aquifer for uranium-238, carbon-14, and nitrate.

Figure 5-66 shows a comparison of U-238, C-14, and nitrate concentrations between the base case and the sensitivity simulation without the low-permeability region in the aquifer. Simulated concentrations, without the low-permeability region in the aquifer, are markedly reduced. This reduction in concentration when the low-permeability region is absent demonstrates a conservative aspect of the RI/FS model.

5.2.6.9 Low Infiltration Inside the Subsurface Disposal Area. This case also was not specified for the RI/BRA in Holdren and Broomfield (2004). This case simulates the effect of a low-infiltration rate of 0.1 cm/year (0.04 in. /yr) occurring inside the SDA beginning in the year 2110 and is included to show a counterpoint to high infiltration inside the SDA sensitivity case. Section 6 discusses the effect on risk.

Figure 5-67 shows a comparison of U-238, C-14, and nitrate concentrations between the base case and the sensitivity simulation with low infiltration inside the SDA beginning in the year 2010. The time history for the U-238 comparison is shown with the concentration axis in logarithmic scale to allow sensitivity case concentrations to be seen because they are so much lower. On a linear concentration scale, the sensitivity case concentrations would plot as a flat line essentially at the zero concentration value. In all three plots, the base case results and the sensitivity case results are exactly the same until the year 2010, when a lower infiltration rate inside the SDA is simulated. Simulated concentrations for C-14 and nitrate show decreased simulated aquifer concentrations, although at later times the base-case nitrate results are lower due to nitrate getting flushed out of the vadose zone faster with the higher infiltration rate. This sensitivity case also shows the effect of water contacting waste, similar to the case of high infiltration inside the SDA—water contacting the waste increases simulated groundwater-pathway concentrations, while additional water included in a simulation (i.e., water that does not contact the waste) dilutes groundwater-pathway concentrations.

5.2.6.10 No Sorption in Vadose Zone Interbeds. This case also was not specified for the RI/BRA in Holdren and Broomfield (2004). In the base case, 3.7% of the Pu-239 and Pu-240 inventory for Rocky Flats Plant waste streams was mobile and moved through the surficial sediment and the A-B interbed without sorption. Sorption of mobile plutonium did occur in the base case in the deeper, nearly continuous B-C and C-D interbeds. This subsection presents an extreme bounding sensitivity case that completely eliminates sorption of plutonium in both the B-C and C-D interbeds. Advective spreading during transit of vadose zone results in some dilution as the contaminant flux is more widely spread as it enters the aquifer model domain. Other than the spreading in the vadose zone model, this sensitivity case is roughly equivalent to spreading the source term laterally and leaching it directly into the aquifer. In both the base case and this sensitivity case, the majority of plutonium (i.e., 96.3%) undergoes sorption in the surficial sediment and interbeds with the assigned distribution coefficient of 2,500 mL/g.

Figure 5-68 shows peak simulated aquifer concentrations anywhere along the southern INL Site boundary and at the extent of the southern model domain as a function of time for the base and no sorption in the vadose zone interbeds sensitivity case. As with other results, these concentrations are extracted from the second gridblock down from the top of the aquifer domain. Simulated concentrations from the base case are very low, with INL Site boundary maximums of 7E-13 pCi/L for Pu 239 and 1E-13 pCi/L for Pu-240. With the extreme bounding case of no sorption in the vadose zone, the fraction of the mobile fraction of plutonium from the source model migrates past the deeper B-C and C-D interbeds and into the aquifer, resulting in simulated concentrations that are approximately 15 orders of magnitude higher than base-case concentrations at the INL Site boundary.

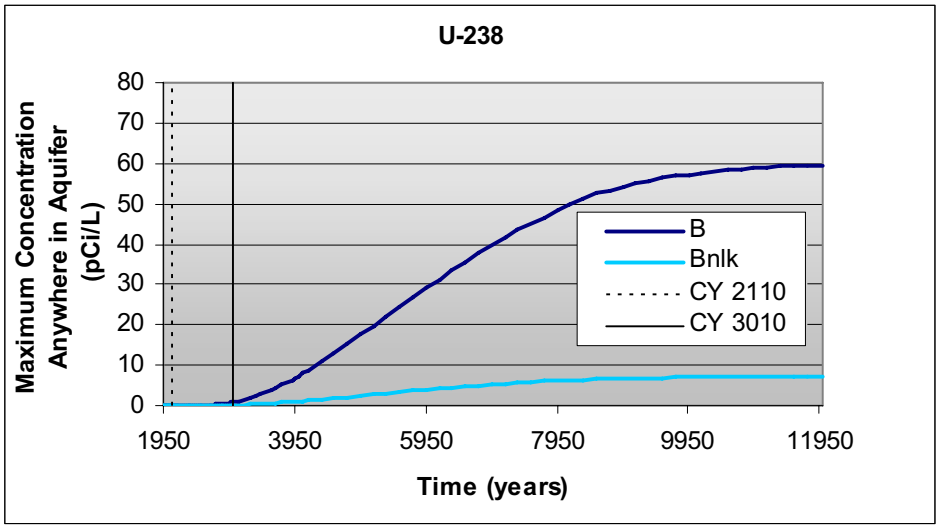

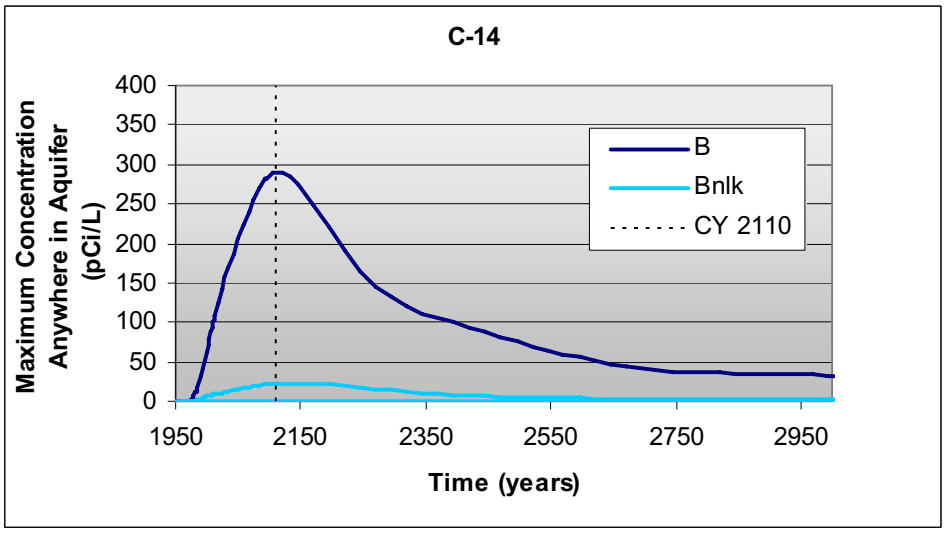

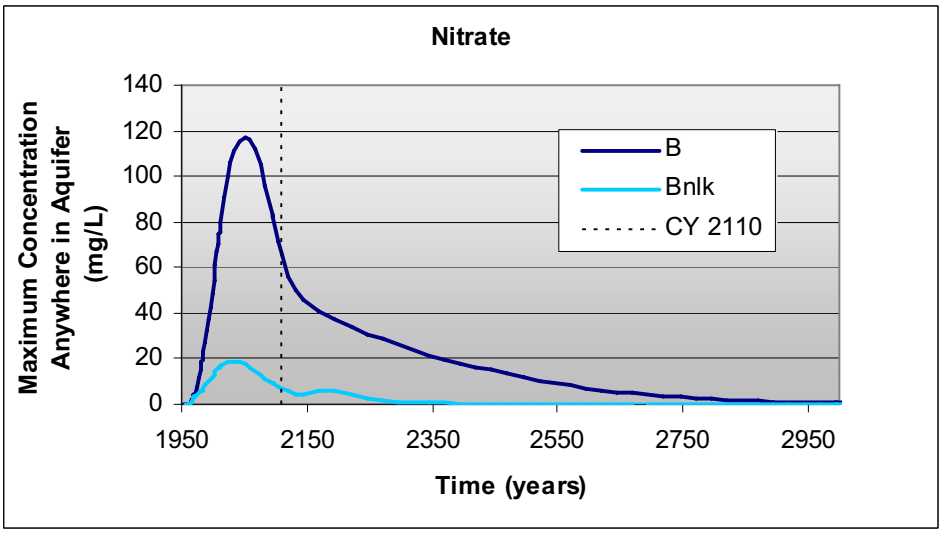

Figure 5-66. Comparison of base case (B) and no low-permeability region in aquifer (Bnlk) maximum simulated concentration anywhere in the aquifer for uranium-238, carbon-14, and nitrate.

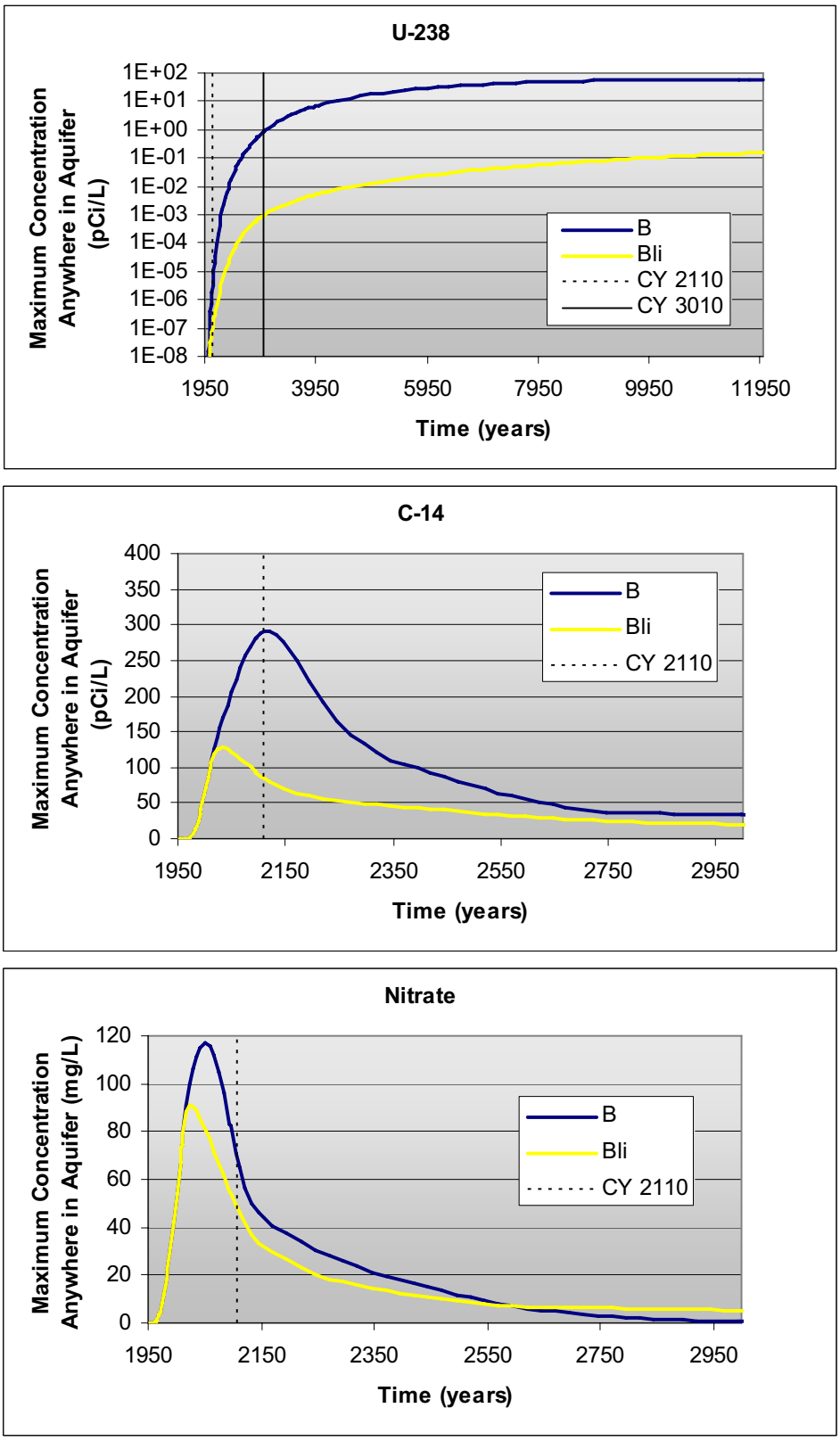

Figure 5-67. Comparison of base case (B) and low infiltration (Bli) inside the Subsurface Disposal Area maximum simulated concentration anywhere in the aquifer for uranium-238, carbon-14, and nitrate.

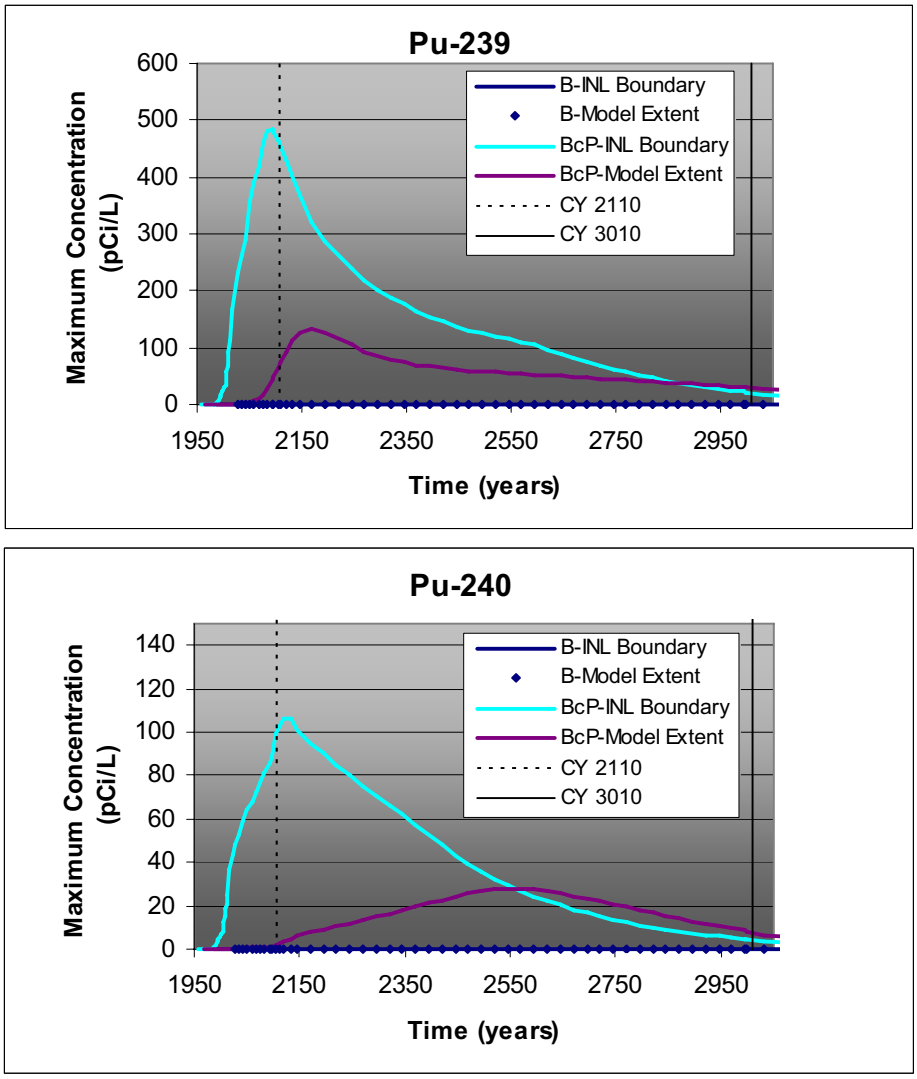

Figure 5-68. Comparison of the base case (B) and the no sorption in the interbeds (BcP) maximum simulated concentration anywhere in the aquifer along the INL Site boundary and at the extreme southern extent of the model domain for plutonium-239 and plutonium-240.

Comparing simulated values through the current time to monitoring results demonstrates the lack of credibility of these results. The maximum simulated concentration results anywhere in the aquifer through the year 2004 for the case without sorption in the interbeds were 3E+05 pCi/L for Pu-239 and 7E+05 pCi/L for Pu-240. Detections of plutonium in the aquifer (see Section 4) show an overall maximum of 4.3 pCi/L in Well M4D in 1993. Although other detections are found, they are at a low level near the minimum detectable concentration and occur very sporadically. The no-sorption sensitivity case results dramatically overpredict even the maximum monitoring results by five to six orders of magnitude. Stated another way, if the sensitivity case were at all credible, there would be easily detectible plutonium in any aquifer well in the SDA vicinity. Since this is not the case, the sensitivity simulation results are not credible because there is no basis in reality for the results.

5.2.6.11 Combined Sensitivity Simulation Results. This section presents the maximum simulated aquifer concentration results for U-238, C-14, and nitrate for all the sensitivity simulations on common plots (see Figure 5-69) to facilitate comparison of impacts to simulated groundwater concentrations between simulations.

For U-238, the larger impacts result from the following sensitivity cases:

- High infiltration inside the SDA
- No B-C interbed
- No low-permeability region in the aquifer
- Low infiltration inside the SDA.

Results for low infiltration inside the SDA plot just above the zero value on the concentration axis. The first two listed cases result in earlier arrival of U-238 to the aquifer, but eventually lead to similar overall simulated concentrations. The latter two sensitivity cases delay the arrival of U-238 and lead to substantially lower simulated aquifer concentrations. The remaining cases (i.e., upper-bound inventory and low infiltration outside the SDA) have much smaller impacts, as can be seen in Figure 5-69. Simulation results for the Pit 4 inventory not removed and no beryllium block grouting cases are not shown on Figure 5-69 because they are essentially the same as the base case. Larger impacts on simulated U-238 concentrations are related to the amount of water contacting the waste for the cases of high and low infiltration inside the SDA, to lack of sorption in the no B-C interbed case, and to increased dilution in the no low-permeability region in the aquifer case.

For C-14, larger impacts result from the cases of high infiltration inside the SDA, the upper-bound inventory, and the no low-permeability region in the aquifer. Results from the other cases are clustered closer around the base case. Larger impacts result from the amount of water contacting the waste (high infiltration inside the SDA), increased dilution in the aquifer (no low-permeability region in the aquifer), and the increased inventory (upper-bound inventory).

For nitrate, larger impacts result from the cases of high infiltration inside the SDA, the upper-bound inventory, and the no low-permeability region in the aquifer. Results from the other cases, while differing slightly more on a relative basis from the base case than for C-14, are still similar in terms of their peak simulated aquifer concentrations. Larger impacts result from the same three sensitivity cases as C-14.

Overall, common results can be summarized when comparing impacts of the sensitivity cases on simulated concentrations of U-238, C-14, and nitrate. Consistently large impacts come from the cases of high infiltration inside the SDA and no low-permeability region in the aquifer. The upper-bound inventory case also impacts nitrate and C-14. In conclusion, the amount of water contacting the waste, the inventory, and the inclusion or noninclusion of the low-permeability region in the aquifer and contaminant dilution have the dominant effect on simulated groundwater-pathway concentrations.

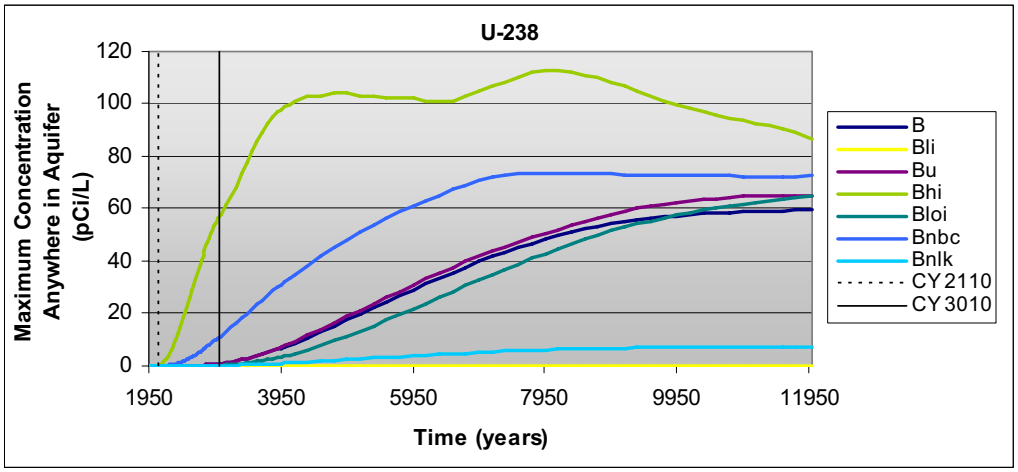

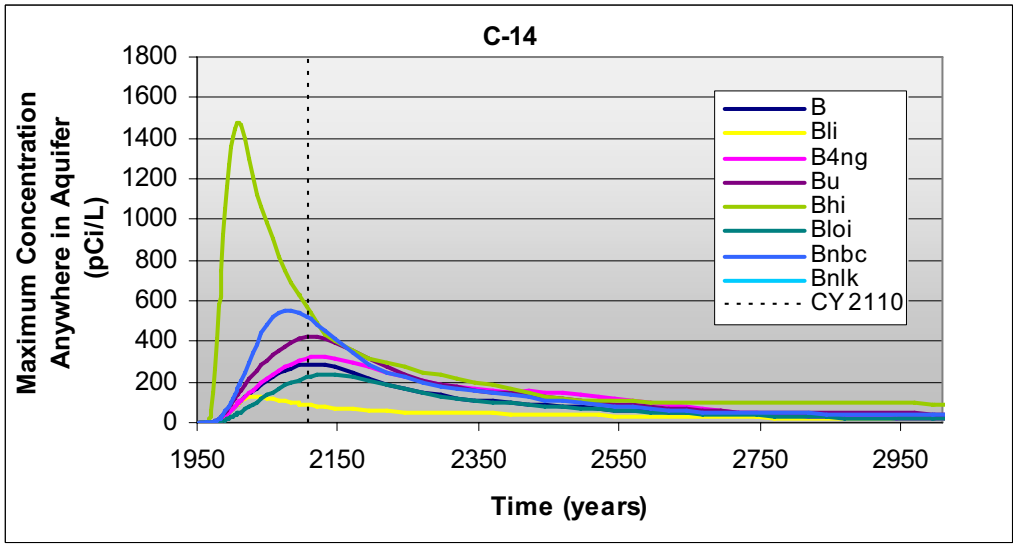

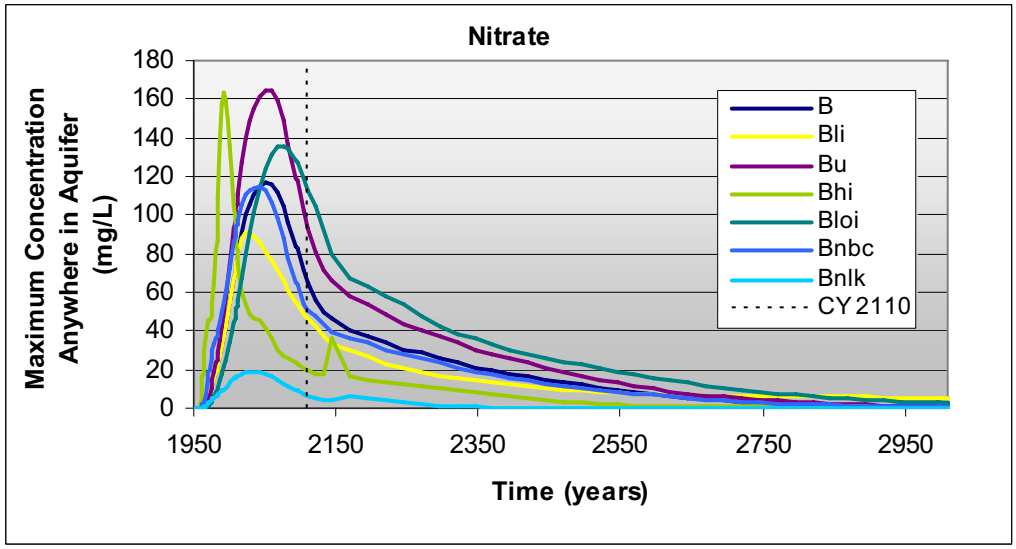

Figure 5-69. Combined sensitivity results for maximum simulated concentration anywhere in the aquifer for uranium-238, carbon-14, and nitrate.

5.3 Volatile Organic Compound Modeling

This section describes the model that simulates transport of VOCs and discusses results of base-case simulations. The VOC transport model uses the same basic model developed for dissolved-phase contaminants described in Section 5.2. All aspects of the dissolved-phase model for simulating water movement in the vadose zone and aquifer are the same for the VOC transport model. However, because VOCs are transported in the subsurface in multiple phases and by a number of complex, interrelated processes, additional capabilities of the model were necessary that were not required for flow or dissolved-phase transport modeling. A separate calibration also was necessary to determine additional parameters associated with VOC release and transport. This section describes only those aspects of the model that are unique to VOCs.

The VOC model was used to simulate groundwater-pathway concentrations for 1,000 years, instead of the 10,000 years that was used for all other contaminants. At 1,000 years, simulated concentrations in the aquifer had decreased substantially (at least an order of magnitude) beneath peak concentrations for all VOCs.

5.3.1 Volatile Organic Compound Transport Model Development

The objective of VOC modeling was to construct a model that could adequately reproduce the observed migration of VOCs from the SDA—and predict with a high degree of confidence—future concentrations of VOCs in the air, vadose zone, and aquifer. This section describes features of the vadose zone model that are distinct to the migration of VOCs and includes VOC transport properties and a complete list of assumptions. Although the source-release model is described in Section 5.1, details pertinent to understanding model calibration are presented again for completeness.

5.3.1.1 Conceptual Model of Volatile Organic Compound Transport. Volatile organic compounds are transported through the subsurface by two primary mechanisms: advection and diffusion. Advection refers to passive transport of contaminants with the bulk movement of a mobile phase (i.e., gaseous, aqueous, or oleic). Diffusion is a spreading process that moves contaminants from areas of high concentration to areas of low concentration by intermolecular collisions. Partitioning occurs between all phases and is assumed to be an equilibrium process.

In the SDA, significant movement of a liquid oleic phase is unlikely because of the high viscosity of the treated waste. Even if liquid VOCs were present, the relatively small amount that might separate from the treated waste would be likely to residualize near the source. The high volatility of VOCs and the relatively dry nature of the INL Site suggest that vapor transport is an important transport mechanism, especially in the basalt portions of the vadose zone. Gaseous movement of VOCs occurs primarily through diffusion and advection. Gaseous advection occurs primarily in the fractured basalt. Aqueous-phase VOCs migrate with infiltrating water, following established flow paths primarily in the sediment and fractured basalt. The basalt matrix acts primarily as a storage site for both aqueous- and gaseous-phase VOCs.

5.3.1.2 Volatile Organic Compound Transport Model Assumptions. This section lists assumptions unique to the VOC transport model:

- All VOC contaminants of potential concern were assumed to be contained in sludge. This is true for all of the tetrachloroethylene and 1,4-dioxane and 99.5% of the carbon tetrachloride, but only 51% of the methylene chloride was sludge. The other 49% of methylene chloride was contained in paper, rags, trash, dirt, and concrete.

- The VOC release rate (i.e., source term) was controlled by drum failure and diffusion through sludge, except for the methylene chloride that was not sludge; this portion was released by diffusion and no credit was taken for drum containment.
- In the year 2000, 50% of the original VOC mass had been released, and 50% remained in the pits (Sondrup et al. 2004).
- The vadose zone basalt is represented as a dual-continua (i.e., dual porosity and permeability) media to account for transport and storage in both the fractures and the matrix.
- Interphase mass transfer is linear and reversible.
- Partitioning between the aqueous and gaseous phases is adequately described using Henry's Law.[e]
- Distribution coefficients are homogeneous in the interbeds, and sorption is negligible in basalt.
- Aqueous-phase VOCs migrate with infiltrating water, following established flow paths.
- Gaseous movement of VOCs occurs through diffusion and advection.
- Gaseous diffusion can be represented by Fickian diffusion, using an effective diffusion coefficient that includes a tortuosity factor.
- Gaseous advection is the result of density gradients and pressure gradients. Pressure gradients are caused by barometric pressure fluctuations, positive-pressure air drilling, and vapor vacuum extraction operations. Gaseous advection due to thermal gradients is negligible.
- Barometric pressure fluctuations can be adequately represented using a square-wave approximation. Fluctuations caused by the passage of pressure fronts are important, while higher frequency variations due to wind gusts or diurnal temperature changes can be neglected.
- All air-drilled wells were drilled at the same speed and the same air injection rate. Air recovery during drilling was 100% above the depth of 18 m (60 ft) below land surface, and 0% below 18 m (60 ft). This only applies to wells drilled before 1994.
- Base-case simulations assume the Operable Unit 7-08 vapor vacuum extraction with treatment system will operate 10 months (i.e., January through October) of each year, from 2005 through 2009, and will extract from wells in use at the end of 2004. Actual data from all other vapor vacuum extraction activities (i.e., 2-week test [1989], 4-month test [1990], treatability study [1993], and Operable Unit 7-08 operations from January 1996 through January 2005) are included.
- Eighty percent of VOC waste in the Accelerated Retrieval Project retrieval area was removed in January 2004, and containment of the remaining 20% failed in January 2004 (see Section 5.1.1 for an explanation).
- Injection and extraction wells are located in the center of the gridblock they occupy.
- Contaminant degradation was not included in the model.

---

e. Henry's Law: a fact in physical chemistry: the weight of a gas dissolved by a liquid is proportional to the pressure of the gas.

- Calibration of the VOC transport model was performed using only carbon tetrachloride. Effects from the presence of other VOCs on partitioning and transport of carbon tetrachloride were inconsequential for calibration.

5.3.1.3 Fate and Transport Processes and Parameters. This section describes the following transport processes and parameters and how they were implemented in the VOC transport model:

- Phase partitioning, including sorption
- Gaseous diffusion and advection
- Aqueous diffusion, advection, and dispersion.

All transport model parameters discussed in this section and others pertinent to VOC transport are presented in Table 5-25.

Table 5-25. Volatile organic compound chemical and transport properties.

Property	Carbon Tetrachloride	Tetrachloroethylene	Methylene Chloride	1,4-Dioxane
Molecular weight (g/mole)	154	166	85	88
Density (kg/m^3)	1,584	1,631	1,335	1,033
Henry's Law constant (nondimensional)	0.75	0.442	0.058	0.00021
Organic carbon partition coefficient, K_{oc} (mL/g)	439	364	8.8	1.23
Free air diffusion coefficient (m^2/day)	0.72	0.69	0.87	1.98

5.3.1.3.1 Phase Partitioning—Typically, VOCs in the vadose zone will partition into all the phases, seeking an equilibrium condition. The relative amount of chemical in two neighboring phases in equilibrium is described by partition coefficients. Partitioning between the vapor and aqueous phases is described by Henry's Law. Henry's Law coefficients, shown in Table 5-25, are simply the vapor pressure of pure compound divided by the aqueous solubility.

Partitioning of VOCs between the aqueous and solid phases often is described using a distribution coefficient, which assumes sorption is linear and reversible. The distribution coefficient for VOCs is simply the product of the organic carbon partition coefficient (mL/g) and the fraction of organic carbon in the soil (dimensionless). The amount of sorption, therefore, depends strongly on the type of geologic material (especially the amount of organic carbon), and the type of chemical constituents dissolved in water. In the model, sorption was assumed to occur in sediment, based on an organic content value of 0.05% reported by Colwell (1988). Sorption in basalt was considered negligible. Organic carbon partition coefficients are shown in Table 5-25.

5.3.1.3.2 Gaseous Transport—Gaseous- or vapor-phase migration in the vadose zone is typically much more rapid than aqueous transport. The rate of vapor transport strongly depends on soil-moisture content. Soil moisture will retard vapor migration by reducing the pore space available for vapor movement and through partitioning of the vapor phase into the aqueous phase. The relatively dry nature of the SDA suggests that vapor transport is an important transport mechanism.

Vapor diffusion in a porous medium is described by Fick's first law, which states the contaminant flux is proportional to the concentration gradient. The proportionality constant is called the effective diffusion coefficient. In a porous medium, contaminant molecules must travel longer diffusion paths because of the structure of the medium and moisture in the pore space. To account for longer diffusion paths, the effective diffusion coefficient is the product of the free-air diffusion coefficient and the gas- or air-filled porosity, divided by a parameter of the medium called the tortuosity. Free-air diffusion coefficients are presented in Table 5-25. Gaseous-phase tortuosity values were an important calibration parameter. Initial estimates of tortuosity were calculated using an expression derived by Millington (1959). These values were adjusted as part of the model calibration process and final values are presented in Table 5-26.

Table 5-26. Final tortuosity values for material types defined and used in the volatile organic compound model.

Material	Tortuosity
Surficial sediment	6
A-B interbed	10
B-C interbed	7
C-D interbed	7
Fractured basalt	1
Matrix basalt	9

Vapor-phase advection can result from pressure, density, and thermal gradients in the subsurface. Pressure gradients can be caused by barometric pressure fluctuations, positive-pressure air drilling, and vapor extraction operations. Although barometric pressure fluctuations were included in the calibration, they could not be included in base-case simulations due to extremely long simulation times caused by the short time step limitation. Effects of not including barometric pressure are discussed in Section 5.3.2.2.

Pressure gradients resulting from air injection during well drilling have the potential to move vapor-phase VOCs because of the high pressures involved and the permeable basalt subsurface. Many wells near the SDA have been drilled with air to bring drill cuttings to the surface. Since 1994, reverse-air circulation, which uses a dual-wall drill stem, has been used because it recovers most of the injected air. Before 1994, more than 40 wells were drilled without reverse-air circulation. A survey of SDA drill logs indicates that, for most of these wells, circulation (i.e., air recovery) was partially or totally lost below about 18 m (60 ft). This meant that a large volume of air had been pumped into the subsurface at high pressures.

Vapor vacuum extraction is simulated in the model similar to the way air injection is handled. One difference with extraction is that phases are extracted rather than components. In this case, the gaseous phase is extracted, which is mostly air, but also includes any water or VOC vapor. Also, extraction is simpler because the extraction intervals do not change the way the injection intervals change when the well is drilled. Three historic vapor extraction tests were included in the calibration and base-case simulations, including the 1989 2-week test, the 1990 4-month test, and the 1993 Organic Contamination in the Vadose Zone Project treatability study. All of these tests pumped from Well 8901.

Vapor density gradients caused when high molecular weight compounds, such as carbon tetrachloride, are vaporized into the surrounding air, also cause vapor advection. Falta et al. (1989) and Mendoza and Frind (1990a, 1990b) suggest that density-driven gas flow will be significant where total gas density exceeds ambient gas density by more than 10% and the gas-phase permeability is greater

than 1×10^{-7} cm^2, which is within the range of fractured basalt permeability. Density-driven flow is likely to be important immediately below the source where concentrations are highest. Table 5-25 contains molecular weights of the VOCs.

Vapor advection caused by thermal gradients is not likely to be significant and was not included in the simulation study. The subsurface was assumed to be isothermal.

5.3.1.3.3 Aqueous Transport—Aqueous transport of VOCs can take place as a result of advection and diffusion, even though advection is typically much more rapid. Dissolved VOCs are transported by aqueous advection whenever water moves in the subsurface. Section 5.2 contains an extensive discussion of water movement in the vadose zone and aquifer. Aqueous diffusion acts the same as vapor diffusion, but aqueous-diffusion coefficients are usually four to five orders of magnitude less than vapor-diffusion coefficients. Aqueous-diffusion coefficients used in the RI/FS model were assigned a value four orders of magnitude less than the free-air-diffusion coefficients.

5.3.1.3.4 Degradation—Although degradation of carbon tetrachloride has probably occurred in the SDA subsurface, it was not included in the simulations because of uncertainty about the rate and mechanism. In the environment, carbon tetrachloride is degraded more readily under anaerobic conditions. In the SDA subsurface, aerobic conditions are likely to dominate; however, anaerobic conditions may occur in isolated locations, allowing for carbon tetrachloride degradation.

The presence of chloroform, a transformation product of carbon tetrachloride, is evidence that reductive dechlorination has occurred at the SDA subsurface. Historical records do not indicate chloroform disposal in the SDA, but chloroform has been detected in the groundwater and soil gas beneath the SDA. Neglecting degradation is conservative because byproducts of carbon tetrachloride degradation (i.e., chloroform, methylene chloride, and chloromethane) have transport properties similar to carbon tetrachloride, yet they are less toxic (i.e., have higher risk-based concentrations).

5.3.1.4 Boundary Conditions. Two types of boundary conditions were used in the VOC transport model: (1) a diffusion boundary condition on the surface and lateral boundaries and (2) a fluctuating surface pressure to mimic changes in barometric pressure. A diffusion boundary condition may be implemented in TETRAD to allow molecular diffusion across grid boundaries. The diffusion occurs as if there were an extra external gridblock with fixed saturation and mole fractions. The external gridblock at land surface in this case represents the atmosphere and was assumed to be completely saturated with air. This implies a zero concentration boundary for VOC vapor diffusion. The width of the external gridblock, which determines the diffusion length, is equal to the thickness of the uppermost gridblock in the model. Diffusion boundaries also were assigned to the lateral boundaries because of the relatively small domain compared to the size of the plume.

As mentioned previously, barometric pressure fluctuations were included in the VOC model calibration, but were not included in the base-case simulations due to the extremely long simulation times. Magnuson and Sondrup (1998) discusses in detail the assumptions and methodology for implementing barometric pressure fluctuations in the model. The effects of not including barometric pressure are discussed in Section 5.3.2.2.

5.3.1.5 Initial Conditions. Initial flow conditions were obtained from simulating a background infiltration rate of 1 cm/year (0.4 in./year) for 300,000 days (approximately 820 years). A longer time was used for the VOC runs because of the added time required for the dual continua to equilibrate.

5.3.1.6 Interface from Vadose Zone Model to Aquifer Model. Section 5.2.4.4.5 describes the process for transferring dissolved-phase simulation results from the vadose zone model to the aquifer model. In that case, the flux of water and the aqueous flux of contaminants from the fractured basalt were transferred from the vadose zone to the aquifer on a grid-by-grid basis. Because the VOC model has the added complexities of being dual continua, it was necessary to capture the flux of contaminant within the matrix domain. No gaseous-phase flux of contaminants is present in either the fracture or matrix domain because vapor-phase contaminants partition into the aqueous phase as water saturations increase near the water table and then advect out the bottom of the model domain. Direct partitioning from the vapor phase into the aquifer across the water table is not considered. Since contaminant mass advects out the bottom of the model domain without being influenced by contaminant mass already present in the aquifer, this approach is conservative because it maximizes aquifer concentrations. Direct partitioning would decrease overall as concentrations increase in the aquifer.

5.3.2 Volatile Organic Compound Transport Model Calibration

Calibration was achieved through a trial-and-error process of adjusting particular parameters within reasonable uncertainty ranges until the model results adequately agreed with observations of carbon tetrachloride in vadose zone soil-gas and aqueous concentrations in the aquifer. Carbon tetrachloride was chosen because it has the largest inventory and available data set for comparison and documentation of its disposal history and origin is better compared to other VOCs.

Calibration focused primarily on data collected through 1995, before the start of full-scale vapor vacuum extraction operations by Operable Unit 7-08. By doing this, calibration focused on matching data and trends that resulted from natural, ambient processes and not on artificial processes (e.g., vapor extraction). Comparisons were made of actual VOC mass removed to simulated mass removed, but parameter adjustments were not warranted based on the level of agreement.

The goal of calibration was to match observed general trends and not be overly concerned with matching values at specific points. Comparison of model results to observed data was both qualitative and subjective, relying primarily on visual observations of plots comparing model results to data. During the calibration of the IRA model (Magnuson and Sondrup 1998), several parameters were considered for use in calibrating the model. These included the following:

- Sediment tortuosity values
- Sorption coefficients (K_d values)
- Basalt matrix porosity
- Barometric pressure amplitude and wavelength
- Duration of air drilling.

The intent of VOC calibration was to not change anything that would impact water movement in the vadose zone. Relevant transport processes and geologic features were included in the model only if they could be represented with reasonable accuracy and they produced a measurable effect on the results.

For the RI/BRA VOC model calibration, only the sediment tortuosity values were adjusted. The final values from the IRA model calibration were used for the sorption coefficients, basalt matrix porosity, barometric pressure data, and duration of air drilling. Tortuosity values were adjusted and judged during the calibration process as to whether they were reasonable. The final tortuosity values are presented in Table 5-26.

During the calibration process, one other parameter was changed to obtain a better fit to the data. The fractured basalt permeability horizontal-to-vertical anisotropy ratio was changed from the value of 30:1, which was used in the IRA and ABRA models, to a value of 300:1. This change helped the model results better match the observed spreading of carbon tetrachloride in the vadose zone and demonstrated the linkage between the flow model described in Section 5.2 and the VOC transport model.

5.3.2.1 Comparison of Simulated and Observed Carbon Tetrachloride Concentrations.

This section presents final results from the VOC model calibration. Additional results of interim steps are presented by Magnuson and Sondrup (2006). Though nearly every soil-gas data point was used in the comparison to simulated values, not all the comparisons could be shown. This section contains selected results, but the results were taken from several different locations and depths to represent the entire plume. All the aquifer results are shown.

5.3.2.1.1 Vapor Concentration Vertical Profiles—Figure 5-70 shows a comparison of simulated concentrations at the simulation time of January 1, 1994, to time-averaged vertical profiles of the carbon tetrachloride concentration at selected wells. The measured data are the average of data collected over a 4-year period from January 1, 1992, to January 1, 1996. An average was taken because the concentration at a single point can vary considerably with time. Horizontal bars through each averaged data point indicate plus or minus 1 standard deviation for data at that port over the 4-year period. The 4-year averaging period was somewhat arbitrary, but was made large to represent as much data as possible, and remove influence of short-term events like the vapor extraction during the 1993 treatability study. Also, many monitoring wells were being drilled over this period, which can cause short-term variations in the data.

Data from wells near the center of the SDA were deemed to be more important for calibration, and more effort was focused on matching the profile of these wells. The model results compared well with measured concentrations in wells below the B-C interbed. However, above the B-C interbed, specifically toward land surface, the concentrations predicted by the model are greater than the measured data in many cases. This deviation is primarily due to discretization around the source areas (i.e., pits). In the model grid, monitoring wells are located in the same gridblocks that are designated as source gridblocks (i.e., pits). Because wells in the model were located as if they were drilled through the center of source pits, they showed a high concentration near land surface where the pits are located, especially because the source is still active (i.e., releasing mass). In reality, monitoring wells are located next to or between pits and concentrations near the surface would be lower than if the monitoring wells were drilled in the pits. At depth, differences in port locations and pit locations become less important because of the vertical distance from the source location.

Again, simulation results and data compare quite well at well locations inside and near the SDA. However, at wells such as Well M7S (approximately 914 m [3,000 ft] from the northeastern corner of the SDA), the simulation results are much lower than the data. In general, lateral spreading was less in the simulation results than is apparent in the data. This is one of the reasons that the larger basalt permeability anisotropy ratio of 300:1 was investigated and selected over the previously used 30:1. The larger horizontal-to-vertical permeability ratio was helpful in causing more lateral spreading in the model, but it still was not enough to produce the degree of spreading apparent in the data. However, as previously stated, matching concentrations in this region was secondary to obtaining a good match to concentration trends at the interior of the plume. Calibration produced a good match to vadose zone concentrations near to and below the burial pits where the majority of the mass exists and enters the aquifer.

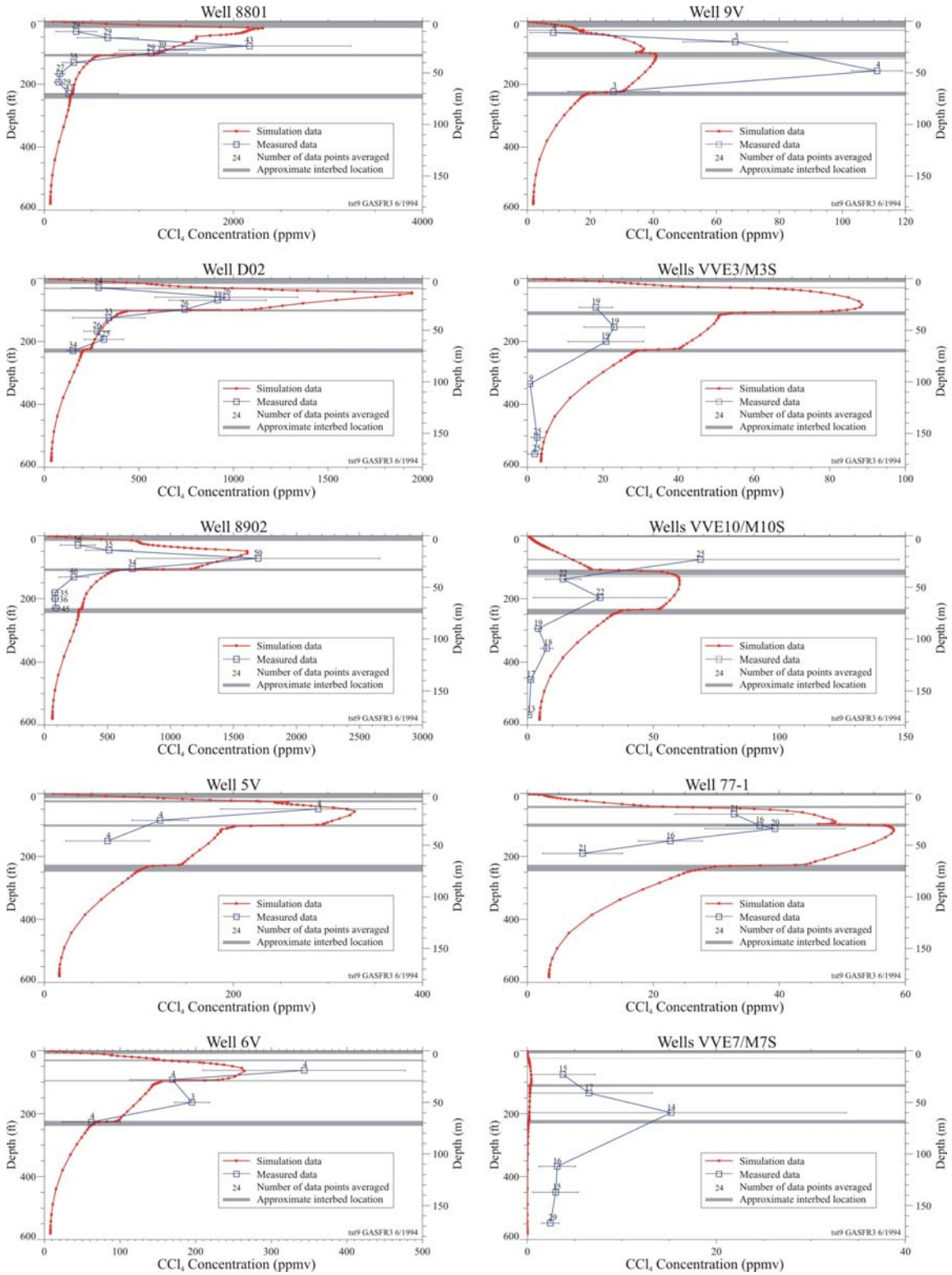

Figure 5-70. Comparison of simulated and measured carbon tetrachloride vapor concentration vertical profiles for select vapor monitoring wells near the Subsurface Disposal Area. The simulated data are from June 1994. The measured data were averaged over a 4-year period from January 1, 1992, to January 1, 1996. Error bars on the measured data represent plus or minus 1 standard deviation.

5.3.2.1.2 Vapor Concentration Time Histories—Figure 5-71 shows time-history comparisons for carbon tetrachloride vapor concentrations at several selected vapor ports in and around the SDA. Simulated data are plotted in the most refined grid that contains the monitoring port. In general, simulation results are in good agreement with measured data. The best agreement was obtained for ports closer to the source areas.

Perturbations in the modeled concentrations are due to air injection during well drilling and vapor vacuum extraction operations. In the model, data were saved roughly every 500 days (i.e., 1.4 years), except during some well-drilling events and vapor vacuum extraction events. In these cases, data were saved more often in an attempt to capture the higher frequency changes that occur as a result of the event. Variation in measured data is due to vapor vacuum extraction operations, well drilling, and barometric pressure fluctuations. Because it is not feasible to include actual barometric data in the simulation, changes in measured concentration caused by these data cannot be matched. Therefore, the purpose was to match the magnitude of the measured data.

5.3.2.1.3 Aquifer Concentration Time Histories—Figure 5-72 compares the time history of measured carbon tetrachloride concentrations to simulation results for aquifer wells near the SDA. The same data at respective well locations are shown in Figure 5-73. Model results and measured data shown through the year 2005, after the 1995 deadline for calibration data. Although the calibration focused on data collected before 1996, it is doubtful whether vapor vacuum extraction operations have impacted aquifer results significantly by 2005. In addition, some wells were drilled or began being monitored after 1995 (i.e., Wells M14S, M15S, M16S, M17S and OW2); therefore, no data exist for these wells from before 1995 to use for comparison.

Model results are a mixture of underpredictions, overpredictions, and good matches of the measured data. Only in a few cases do model results and measured data compare well in magnitude and trend because of the highly irregular and unpredictable distribution of carbon tetrachloride in the aquifer (see Section 4). The model underpredicts concentrations at Wells M3S, M6S, M7S, M16S, A11A31, USGS-88, USGS-120, and RWMC Production Well. However, the model matches the magnitude and trend of measured data quite well at Wells M1S, M4D, USGS-87, USGS-89, and USGS-90. The match is reasonable, but not quite as good, at Wells M14S, M15S, and OW2. The model overpredicts concentrations at Wells USGS-117 and USGS-119, and considerably overpredicts concentrations at Well M17S, which is the only aquifer well inside the SDA boundary. However, the measured concentrations at Well M17S seem unreasonably low given the close proximity of the well to the VOC sources.

In general, RI/FS model results are similar to IRA model results for the aquifer. Interim Risk Assessment model results at the RWMC Production Well agreed better because more VOCs in the IRA model were assigned to Pit 9, closer to the RWMC Production Well. However, knowledge of VOC waste-burial locations has vastly improved since the IRA model, and it is likely that if the current distribution of VOC waste were used in the IRA model, the results would be similar to the results obtained for the RI/FS model.

5.3.2.2 Effects of a Fluctuating Barometric Pressure Boundary Condition. Simulations were performed to quantify the impact of a fluctuating barometric pressure boundary condition. Figure 5-74 shows the mass flux of carbon tetrachloride to the aquifer both with and without a fluctuating barometric pressure boundary condition. The results show that when barometric pumping is not included in the simulation, the flux to the aquifer increases. The increase is approximately 40% in the year 2000 and 30% in the year 2125, when the flux to the aquifer peaks. The results for flux to the atmosphere are similar, but in this case the flux decreases when barometric pumping is not included. Therefore, not including barometric pumping is conservative for the groundwater pathway, but is not conservative for the air pathway.

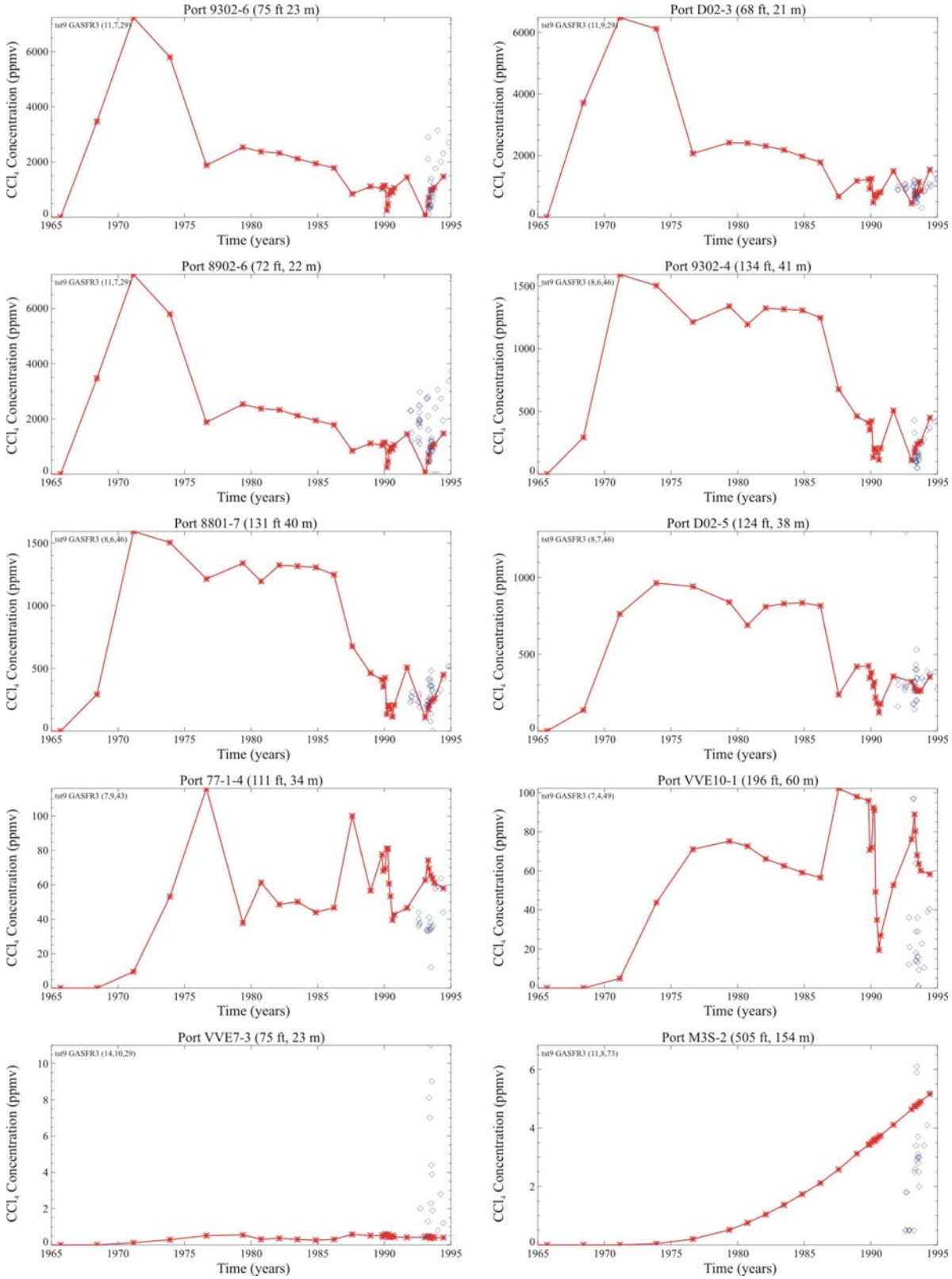

Figure 5-71. Comparison of simulated (red) and measured (blue) carbon tetrachloride vapor concentration time histories for select vapor monitoring ports near the Subsurface Disposal Area through the year 1995.

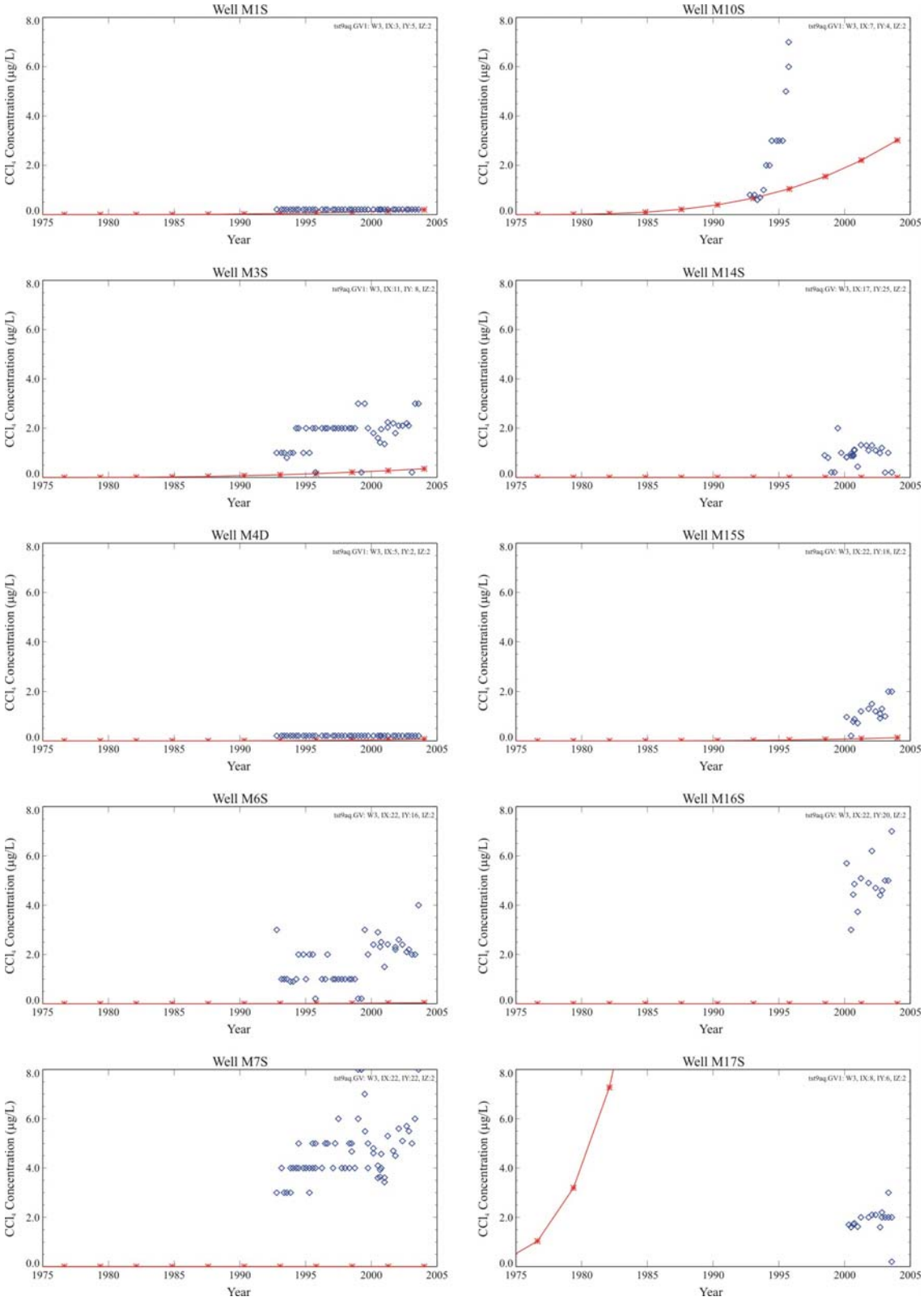

Figure 5-72. Time-history comparison of simulated (stars) and measured (diamonds) carbon tetrachloride concentrations in the aquifer at wells in and around the Subsurface Disposal Area through 2005.

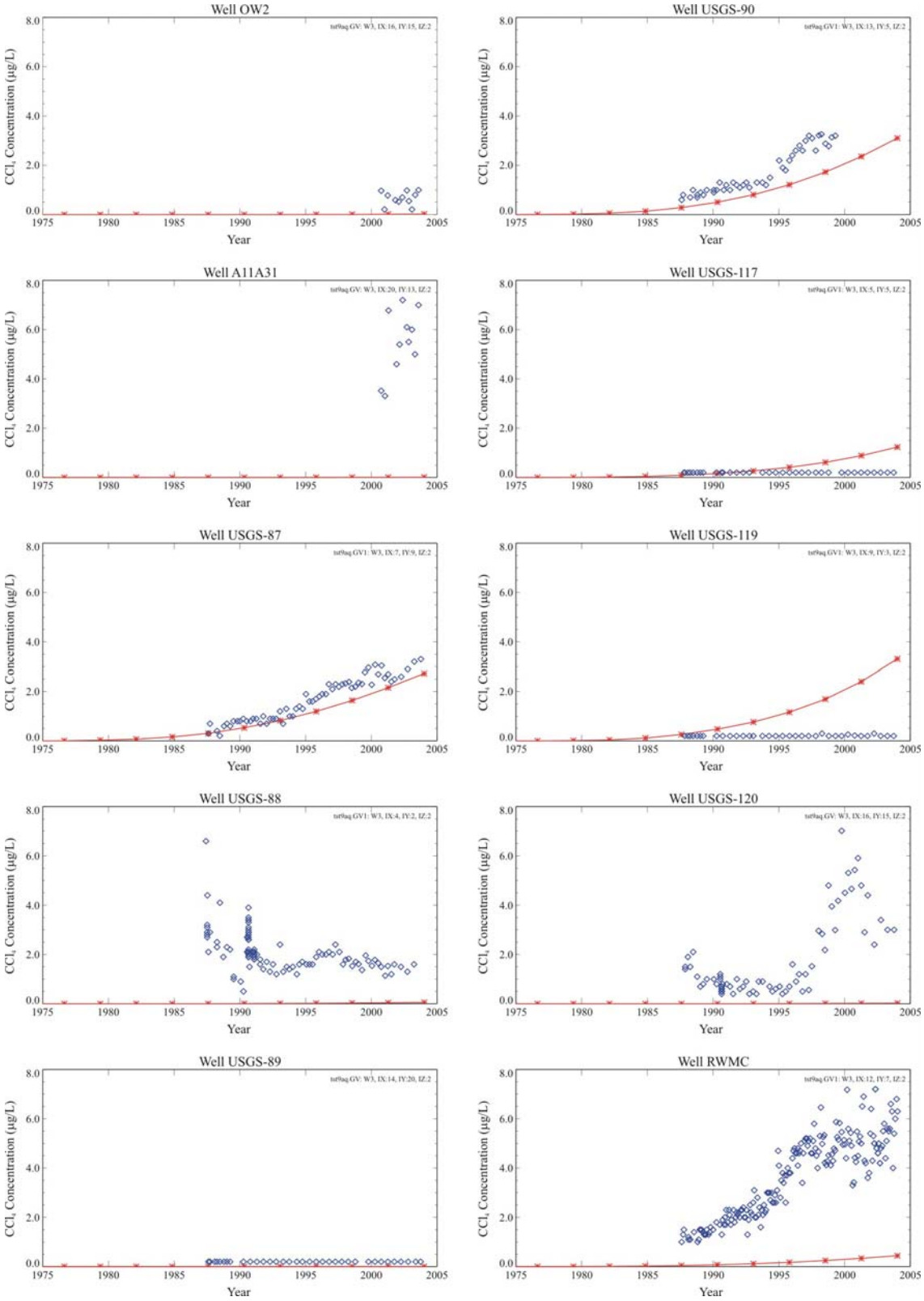

Figure 5-72. (continued).

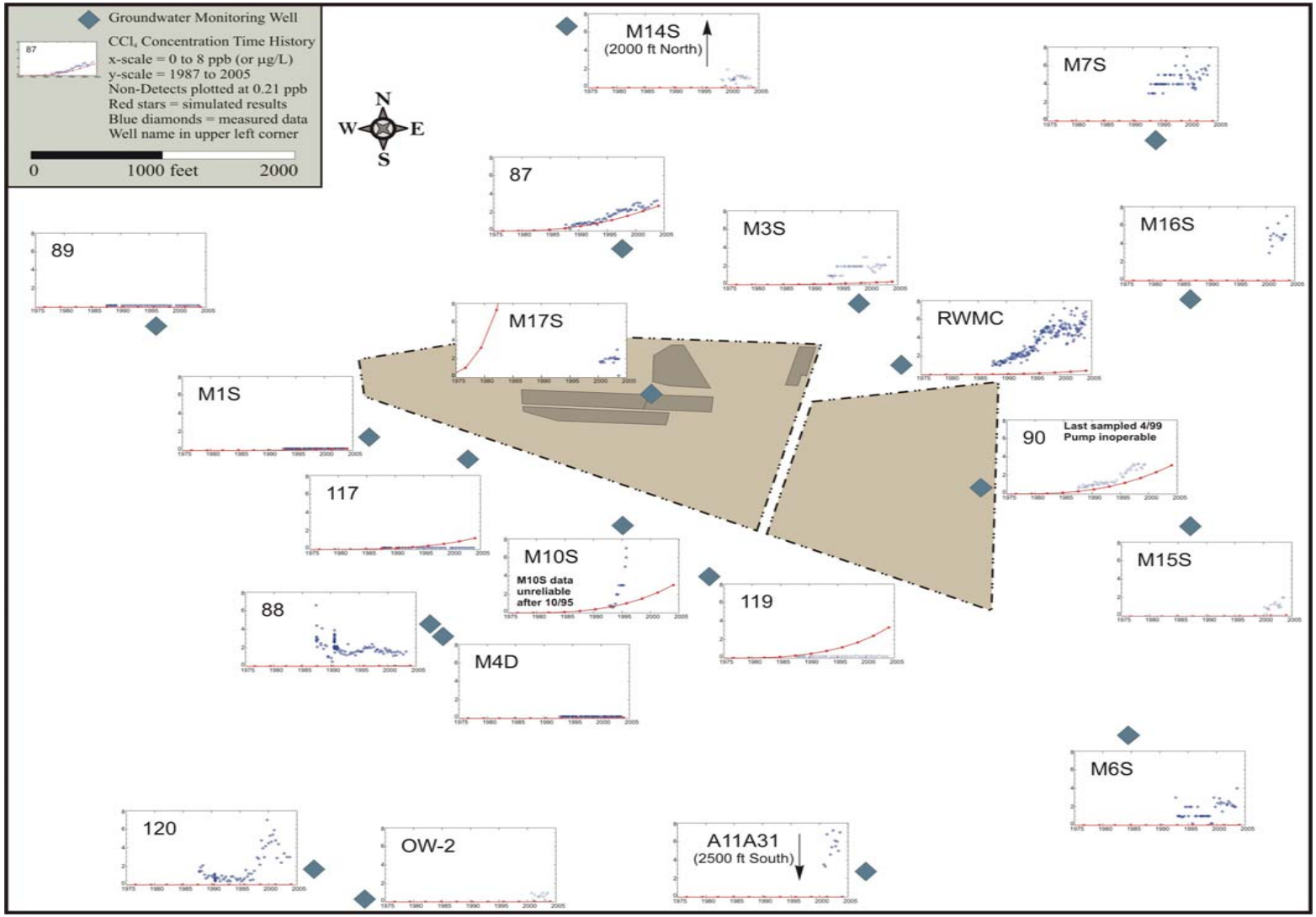

Figure 5-73. Time history of measured and simulated carbon tetrachloride concentrations in the aquifer at wells in and around the Subsurface Disposal Area. The source pits shaded in the SDA are the primary carbon tetrachloride source pits.

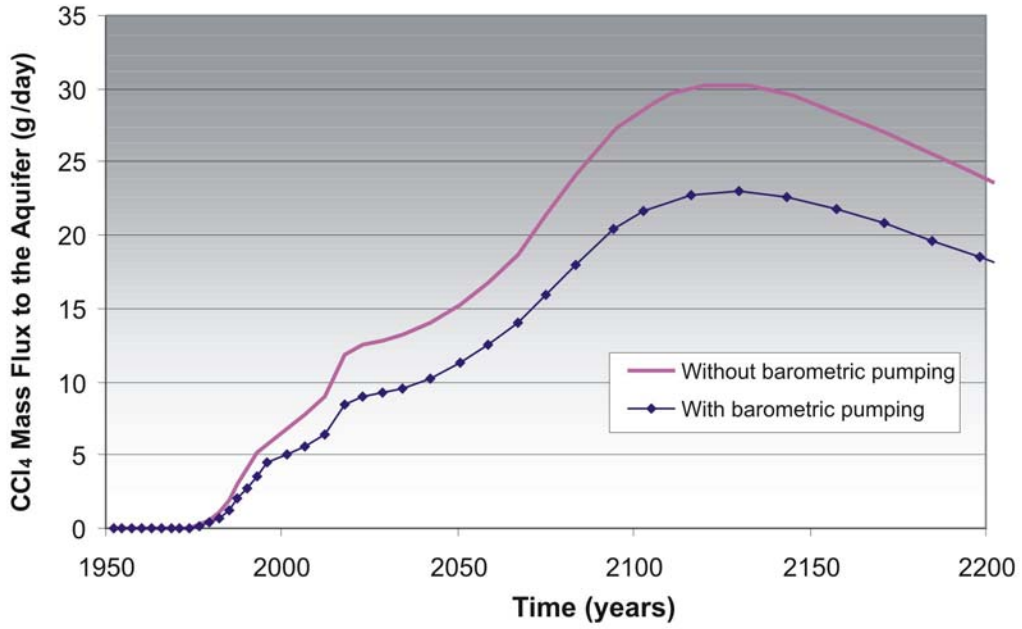

Figure 5-74. Time-history comparison of simulated carbon tetrachloride mass flux to the aquifer, with and without a surface barometric pressure fluctuation.

5.4 Gaseous-Phase Radionuclide Modeling

In the ABRA, C-14 was simulated as a strictly dissolved-phase contaminant. This meant that C-14 could not partition into the gaseous phase and undergo additional transport processes (e.g., diffusion in the gaseous phase). Therefore, C-14 could not diffuse out through the upper surface of the simulation domain. This was a conservative approach that maximized C-14 concentrations in the groundwater pathway. However, in the ABRA, the C-14 concentrations in the groundwater pathway were overpredicted by two to three orders of magnitude due to this conservatism when compared to currently observed concentrations from contaminant monitoring.

For the RI/FS model, the simulation of C-14 was modified to allow C-14 to partition into the gaseous phase. This meant that C-14 existed in both the aqueous and gaseous phase and underwent transport in both phases simultaneously. This approach to simulating C-14 was most easily accommodated by adopting the dual-continua model implemented for the VOC modeling previously described. Before simulating C-14 with the full-scale dual-continua vadose zone model, two interim simulation efforts were conducted to determine the appropriate partitioning parameters and the possible effect of increased diffusion across the near surface in the immediate vicinity of beryllium blocks, which contain a large fraction of the C-14 inventory. These two interim studies are briefly described first, followed by the implementation of C-14 in the dual-continua vadose zone model used for VOCs. Magnuson and Sondrup (2006) presents more detailed discussion of all three topics.

5.4.1 Carbon-14 Partitioning from Column Experiments

A simulation study was conducted to determine correct partitioning for C-14 in a combined aqueous- and gaseous-phase system. This simulation study used experimental data from a 3-m (9.8-ft) high × 0.9-m (3-ft) diameter mesoscale column where an aqueous-phase tracer (i.e., bromide), a gaseous-phase tracer (i.e., SF_6), and C-14, which partitioned into both phases, were monitored. The column experiment was designed to mimic conditions in the waste zone at the SDA and

had a constant low flux of water applied at the surface. The column experiment also allowed gaseous-phase diffusion out the surface. Inverse modeling was applied to this set of column data to match both the aqueous- and gaseous-phase transport. This inverse modeling study is documented in Martian (2003).

Parameters describing the partitioning of C-14 comprise the primary output from the inverse study used in RI/FS modeling. In Martian (2003), C-14 was treated as if it were carbon dioxide, with the partitioning estimated from Henry's Law. The resulting TETRAD input parameter A was 2.9×10^4 kPa and is essentially the inverse of the effective Henry's Law constant, assuming constant temperature and pressure.

The inverse modeling application resulted in excellent matches to observed water flux, breakthrough of the bromide and SF_6 tracers, and breakthrough of C-14 from the column in both the aqueous and gaseous phases. Because of this good agreement, a conclusion was made that the effective Henry's Law partitioning adequately described the partitioning of C-14 in the column and could be used, with the normal cautions on upscaling, for the RI/FS vadose zone modeling.

5.4.2 Carbon-14 Beryllium Near-Field Simulation

A significant portion of the C-14 buried in the SDA is in the beryllium reflector blocks. As beryllium corrodes, C-14 and tritium are released and partition into the aqueous and gaseous phases. With contaminant release concentrated in a small area within the surficial sediment, higher gaseous-phase concentration gradients would be established between release sites and the short distance to land surface, where movement of air maintains a gaseous-phase concentration of essentially zero. A hypothesis that this increased concentration gradient could result in additional release of C-14 from the subsurface was tested in a study documented by Nalla (2004). Subsurface and atmospheric sampling from an instrumented location in the SDA was used in an inverse modeling study.

Even with the less-than-desired match to observed C-14 and tritium migration behavior, it was concluded that a substantial fraction, on the order of 80% of the C-14 mass, is released to land surface through diffusion. This indicated that it was indeed important to include the diffusional loss through land surface in the RI/FS model. The Nalla (2004) recommendation to reduce C-14 release from beryllium reflector blocks by 80% for use in the subsurface model was not implemented; that implementation would have resulted in accounting doubly for the release to the atmosphere because surface diffusional losses also were included in the RI/FS model.

5.4.3 Carbon-14 Dual-Continua Vadose Zone Simulation

The VOC dual-continua model described in Section 5.3 was used to simulate transport of C-14. Using this dual-continua model takes advantage of additional calibration achieved in VOC modeling. Assigned contaminant mass locations for C-14 were different from locations for the strictly aqueous-phase contaminants, as discussed in Section 5.1.

5.4.3.1 Carbon-14 Model Boundary Conditions. Aqueous-phase boundary conditions were kept the same as the RI/FS VOC dual-continua model. Two changes were made to the gaseous-phase boundary conditions. First, the lateral zero-concentration boundaries were omitted because they were unnecessary for simulation of C-14. They were unnecessary because the C-14 contaminant mass did not reach the boundaries in appreciable quantities as it did for VOC contaminants. Second, similar to VOC modeling, barometric pressure fluctuations at land surface were eventually neglected in C-14 modeling. They were neglected primarily for computational expediency, because including barometric fluctuations required using a minimum 10-day time step, which resulted in long run times—on the order of 2 months of computer processing time—to achieve approximately 700 years of simulation time (the radionuclide

simulations for the base case and sensitivity simulations were all planned to be simulated to 1,000 years into the future, and out to peak concentrations within 10,000 years). This was not feasible within even the most generous time constraints. Fortunately, the effect of neglecting barometric fluctuations was conservative because more C-14 mass was retained in the simulation domain and migrated through the groundwater pathway.

The effect of not including barometric fluctuations was tested by making comparative simulations, with and without barometric pumping. These comparisons used the sensitivity simulation of the comparative base case (i.e., B4ng_g8), which comprised no removal of Pit 4 inventory and no grouting of beryllium blocks. Figure 5-75 shows a comparison of the maximum simulated aquifer concentration as a function of time at a depth of 12 m (39.3 ft) anywhere in the simulation domain, with and without barometric pumping. Concentrations for each simulation are extracted for both anywhere in the model domain and anywhere in the domain outside the SDA fence. The effect of not including barometric pressure fluctuations for locations outside the SDA fence was to increase the simulated aquifer concentration by approximately 20%. It was slightly larger inside the SDA, with an approximate 25% increase. Implementing C-14 simulations without barometric pressure fluctuations brought back some of the conservatism that had been reduced by simulating gaseous-phase partitioning.

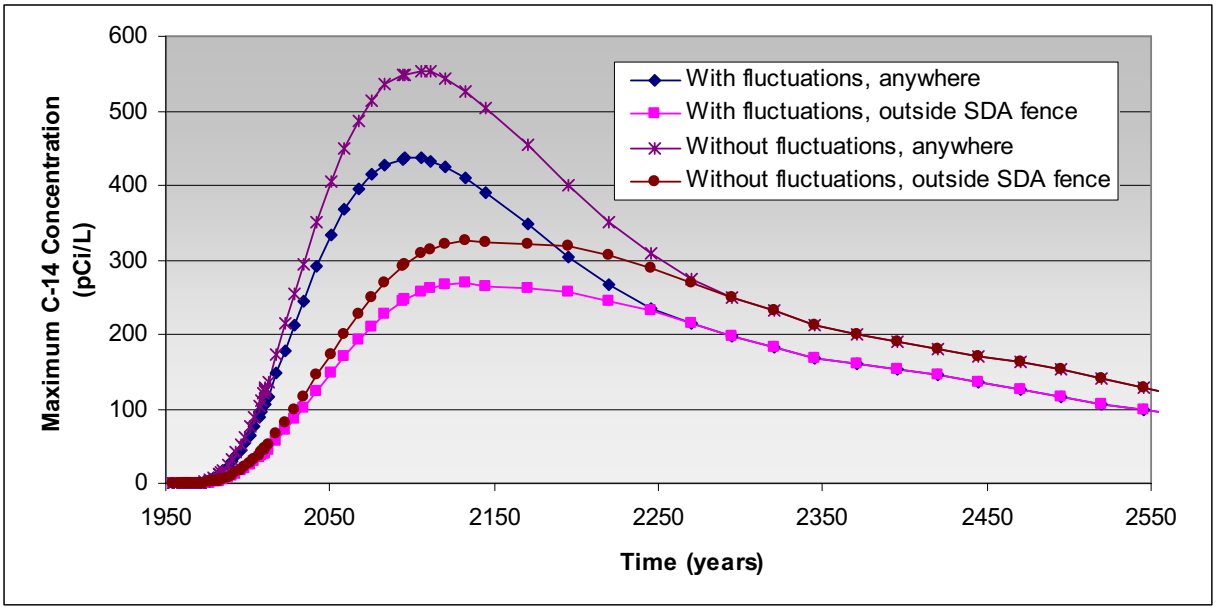

Figure 5-75. Maximum simulated aquifer carbon-14 concentration, anywhere in the simulation domain, at a depth of 12 m, with and without surface barometric pressure fluctuations.

5.4.3.2 Carbon-14 Comparison without Gaseous-Phase Partitioning. To demonstrate the effect of including gaseous-phase partitioning in the RI/FS model, an additional simulation was performed where the C-14 source release was imposed in the single-continua model used for contaminants that migrated strictly in the aqueous phase, essentially reverting to the method used in the ABRA for simulating C-14 migration. Figure 5-76 shows a comparison of the maximum simulated concentration anywhere in the aquifer for case B4ng_g8 with gaseous-partitioning in the vadose zone model and diffusion at land surface to the same simulation where gaseous-phase partitioning is not included. In the case where gaseous partitioning is not allowed, no diffusive loss to land surface occurs. The results are presented with both a linear and a logarithmic scale concentration axis because the difference is so large (i.e., approximately two orders of magnitude).

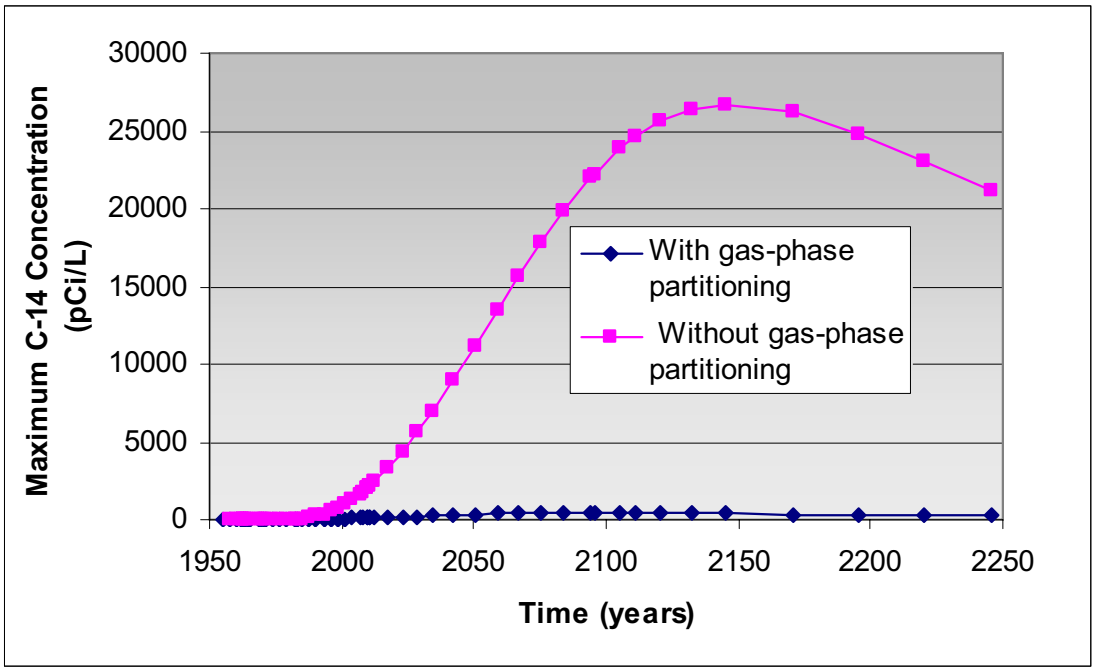

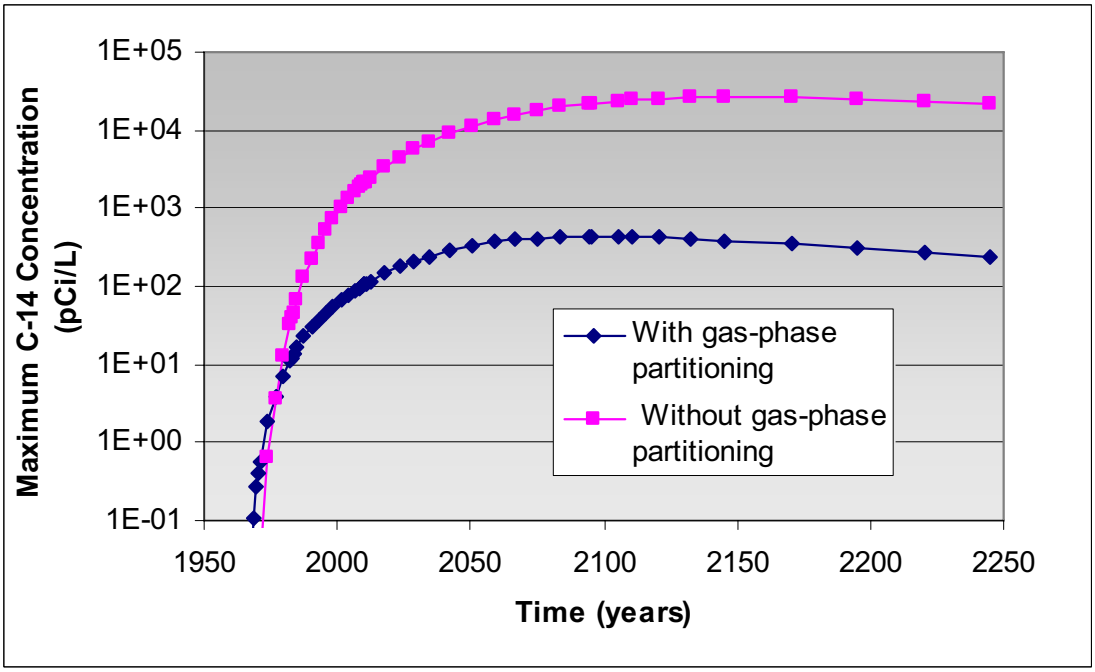

Figure 5-76. Maximum simulated concentration anywhere in the aquifer, with and without gaseous-phase partitioning in the vadose zone transport model.

5.4.3.3 Carbon-14 Model Remedial Investigation and Baseline Risk Assessment Base-Case Simulation Results. The base-case final simulation for C-14 did not include barometric pressure fluctuations. No consistently elevated concentrations or trends have been in evidence for C-14 monitoring in the vadose zone. One location that has shown detections is the perched water in Well USGS-92 above the C-D interbed. Figure 5-77 shows a comparison of the simulated C-14 aqueous-phase concentration at the gridblock representing this location to the monitoring results. No background concentration is added to the simulation results. Even with inclusion of gaseous-phase partitioning and diffusional losses to land surface, the simulated concentrations still overpredict the sporadic observed values, indicating the simulation result is still conservative.

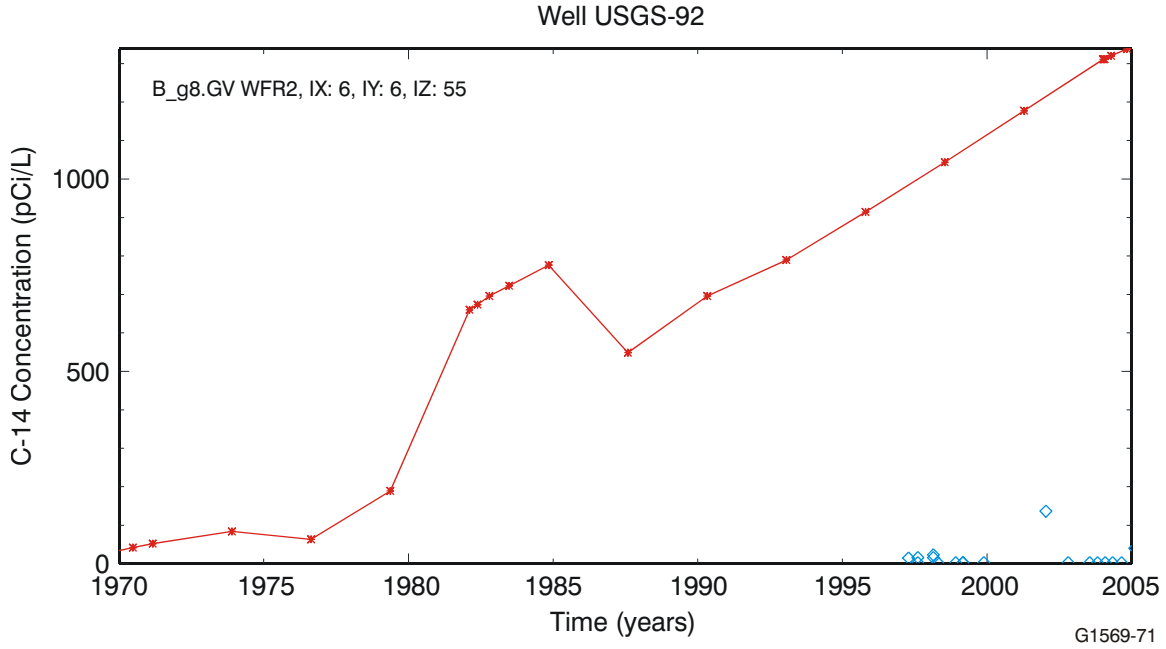

Figure 5-77. Time history of simulated (red line) and observed (blue diamonds) carbon-14 aqueous-phase concentrations at Well USGS-92.

Simulated aquifer concentration time histories for C-14 at locations containing aquifer monitoring wells are shown in Figure 5-77. Monitoring results for C-14 that represent 3σ detections, or greater, are included as blue diamonds on the time-history plots along with a whisker-style indication of their associated 1σ uncertainties. Results show the sporadic nature of detections and demonstrate that simulation results are conservative because they overpredict measured groundwater concentrations in Wells M17S and USGS-119, though not nearly to the degree recorded in the ABRA. The overprediction at Well M17S is consistent with the carbon tetrachloride results in that the model overpredicts measured data. Figure 5-77 shows simulated aquifer C-14 concentrations in the first-level refined grid for the aquifer domain. The simulated elevated concentrations are more centrally located beneath the southeastern corner of the SDA, when compared to other contaminants (e.g., nitrate).

5.5 Biotic Transport

Unlike other waste area groups, contaminants in Waste Area Group 7 are buried under an operational soil cover averaging 1.5 m (5 ft) deep. The contaminants must be brought to the surface to enable human contact with the contaminants. One possible mechanism for contaminants to be brought to the surface is biotic transport, which has been measured at the INL Site. The current 1.5-m (5-ft) soil cover at Waste Area Group 7 is not deep enough to prevent intrusion into the waste by deeper burrowing animals and deeper rooting plants; therefore, the DOSTOMAN biotic-pathway model was used to predict biotic transport of contaminants in the SDA.

Only the current cover is assessed for the RI/BRA. Programmatic guidelines specifying a surface barrier as a component of any remedial action ultimately implemented in the SDA have been adopted (Holdren and Broomfield 2004). Cover designs included as part of proposed remedial alternatives will be evaluated in the feasibility study.

5.5.1 Biotic Model Methodology

The biotic pathway takes available mass from the source-release model as input and computes surface soil concentrations. The biotic-uptake model is the same model used in previous risk assessments and is described in detail in the ABRA (Holdren et al. 2002). However, a review of the process identified that available mass from the source-release model, used as an input to the biotic model, might not be a conservative estimate. Therefore, the methodology used to estimate available mass was changed for this RI/BRA.

Previously, results from the source-release modeling were directly used as input into the biotic-transport model. In effect, this meant that contaminant mass was not available for transport until it had been released from the waste. However, in the case of some contaminants (e.g., Am-241 in sludge), plant roots could intrude into the waste and take up that contaminant before it was actually released from the waste. Therefore, the methodology was changed so that inventory released by the surface-wash mechanism is immediately available for transport by way of the biotic pathway. The inventory released by dissolution (e.g., Tc-99) in activated metal would not be available until the contaminant had released from the waste form. Therefore, output from source-release modeling is still used for dissolution release to provide input to the biotic model. Total input into the model is the sum of the surface wash, which is available immediately, and the dissolution release, which is still computed by the source-release model. To simplify the calculation of mass available from the surface-wash portion of the inventory, container failure rate is not used. No credit is taken for containers. This is more conservative than previous modeling because more mass is available sooner, and it simplifies the additional calculations required for input into the biotic model.

The DOSTOMAN code was used to predict the amount of contaminants brought to the surface. Yearly average concentrations were computed for the SDA. Four successive phases have been addressed that describe transition from the current disturbed setting back to a native vegetation mixture. Processes modeled using DOSTOMAN include animal burrowing, burrow collapse, plant uptake, radioactive decay, and leaching of contaminants from infiltrating water. Loss caused by erosion or surface runoff was not modeled. Neglecting erosion and surface runoff is conservative because it leads to higher surface concentrations in the SDA. The effect of including erosion would be to remove contaminant mass from the surface and, thereby, reduce the soil concentration to which the receptor would be exposed. The effect would be offset by reduced depth to the waste and enhanced intrusion. However, the erosion scenario is not appropriate because the SDA is a depositional environment (Hackett et al. 1995).

The SDA has been used for shallow land disposal since 1952. Animals and insects on or adjacent to the SDA could possibly serve as mechanisms of transport or accumulation of contaminants at the surface. The DOSTOMAN code was used to simulate the movement of contaminants by plant uptake, as well as animal and insect excavation, to evaluate the transport of contaminants through biota. Release of nonvolatile contaminants to the surface environment involves mechanical transport of waste to the surface. Mechanical transport can be simulated using a compartmentalized model that provides for flora to uptake waste and burrowing animals to burrow into the waste and deposit it at the surface. The compartmentalized modeling approach has been used (Shuman, Case, and Rope 1985) to model the movement of radionuclides at the INL Site with the DOSTOMAN code (Root 1981).

Subsurface contamination in the SDA can be moved to the surface and near-surface soil profile through root assimilation. Once transferred to aboveground plant structures, contamination may be transported by primary consumers through the food web or accumulate in the surface soil through plant death and decay. Most of the SDA has been seeded with crested wheatgrass (*Agropyron cristatum*) to reduce moisture infiltration and erosion. Russian thistle (*Salsola kali*) has invaded disturbed areas that have not been seeded successfully with grass. The vegetation surrounding the SDA is dominated by big sagebrush (*Artemisia tridentata)*, green rabbitbrush (*Chrysothamnus viscidiflorus*), and bluebunch wheatgrass (*Pseudoroegneria spicata*).

Redistribution of soil by burrowing animals may impact mobility of buried waste through transport enhancement, intrusion and active transport, and secondary transport (Arthur and Markham 1982; Cline et al. 1982). Four rodent species account for more than 90% of the composition of small mammals inhabiting the crested wheatgrass and Russian thistle habitat types in the SDA. These are Townsend's ground squirrel (*Spermophilus townsendii*) at 4%, Ord's kangaroo rat (*Dipodomys ordii*) at 10%, montane vole (*Microtus montanus*) at 23%, and the deer mouse (*Peromyscus maniculatus*) at 57% (Groves and Keller 1983).

Evidence suggests that harvester ants (*Pogonomyrmex salinus*) are active at the INL Site. The sampling of harvester ant nests at the Materials and Fuels Complex ponds suggests that the ants redistribute radionuclide concentrations in soil; the effect is seen mainly in the mound material (Blom, Johnson, and Rope 1991). In addition, harvester ants appear to have transported radioactive contaminants at the Boiling Water Reactor Experiment I site (Blom, Johnson, and Rope 1991) where a zone of surface contamination was covered with a layer of gravelly soil at least 15 cm (6 in.) deep. Harvester ants also exhibit a preference for disturbed conditions similar to those found in the SDA (Fitzner et al. 1979; McKenzie et al. 1982).

The DOSTOMAN code mathematically simulates movement of contaminants from subsurface source compartments to overlying sink compartments by solving a system of differential equations at specified time steps. The general equation is shown in Equation (5-4):

$$dQ_n/dt = \sum_{m=1}^{N} \lambda_{n,m} Q_m - \sum_{m=1}^{N} \lambda_{m,n} Q_n - \lambda_R Q_n \pm S_n \qquad (5\text{-}4)$$

where

Q_n = quantity of contaminant in compartment n (g)

Q_m = quantity of contaminant in compartment m (g)

$\lambda_{n,m}$ = rate constant for the transport of contaminants from compartment m to compartment n ($year^{-1}$)

$\lambda_{m,n}$ = rate constant for the transport of contaminants from compartment n to compartment m ($year^{-1}$)

λ_R = decay constant for the contaminant ($year^{-1}$)

S_n = source or sink term in compartment n (g/year)

N = total number of subsurface source compartments under consideration.

The first summation term in Equation (5-4) is the sum of all input rates to compartment n. The second summation term includes all rate-constant losses from compartment n. The remaining two terms include contaminant decay and the gain or loss in compartment n from sources or sinks.

At specified time increments, the system of differential equations presented by Equation (5-4) for n compartments can be solved to determine the contaminant inventory Q_n for each compartment. Details of the mathematical approach for determining a solution are given in Root (1981).

The DOSTOMAN model is represented graphically in Figure 5-78. Up to eight contaminants can be modeled in a single run. Figure 5-78 shows only two components that are part of a single decay chain. This simplification was used to illustrate how the model was set up. The first contaminant mass is contained in the dotted blue box at the left of Figure 5-78. Waste zones are represented by two red boxes at the bottom of the figure. Once mass is released from waste by the source-term model, the mass amount is input into the waste zones. Empty black boxes above the waste zone represent individual soil compartments. The green-shaded box at the upper left corner is the plant compartment. Contaminant mass is assimilated by plants and becomes part of the plant compartment, which is represented by the green lines that come from the waste zone and the individual soil zones to the plant compartment.

The mass of contaminant assimilated by plants is released when the plants die. Plant death is represented by the blue line from the plant compartment to the surface compartment. In reality, plant death contributes contaminant mass to all the soil compartments; however, for simplicity, the contaminant is shown as going only to the surface compartment.

Contaminant movement is represented by the purple line from the individual compartments to the surface compartment. Contaminant mass can be removed from an individual compartment by leaching or burrow collapse, which effectively moves mass to the next lower compartment and is represented by the gray lines in Figure 5-78.

Radioactive contaminants decay. If a stable isotope decays, the lost mass goes to the sink compartment (i.e., the stable isotopes are not hazardous and are no longer tracked). However, if another radioactive isotope in a decay chain decays, then mass is transferred to the set of compartments seen on the right of Figure 5-78 (in the purple dotted box labeled Contaminant 2). The contaminant mass can be transported by the same mechanisms as the original isotope. Transport rates are controlled by the properties (e.g., plant uptake factors or soil-to-water partition coefficient) of each isotope. Contaminant blocks were repeated for each contaminant modeled in a single simulation. Contaminants in any given compartment were assumed in the modeling to be available for transport by animals that burrow into a compartment even though they may not burrow as deeply as the waste. In addition, shallow-rooted plants were assumed to be able to uptake contaminants in nonwaste compartments.

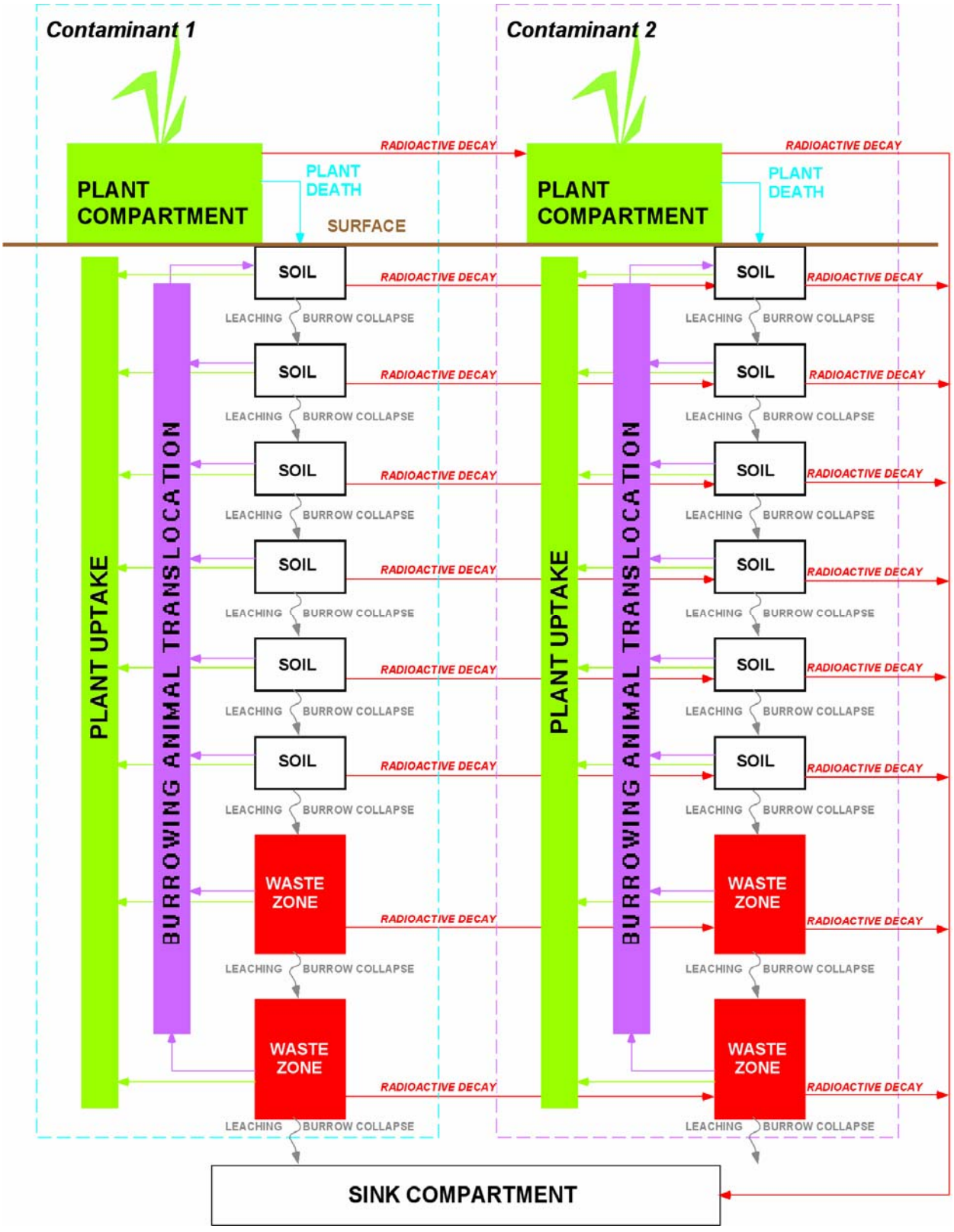

Figure 5-78. DOSTOMAN biotic modeling.

Uptake of contaminants by sagebrush was not modeled during the occupational period because it was assumed that current RWMC operations would inhibit growth of sagebrush during the period of institutional control. It also was assumed that maintenance of the SDA surface soil would continue during the institutional control period. Contaminant mass available is 23.2% of the mass released from the source-term model. This accounts for burying much of the waste more deeply than the plant roots or animal burrows are expected to go. Average depth to basalt is 5.3 m (17.5 ft) with 1.5 m (5 ft) of overburden and 0.6 m (2 ft) of underburden. The 1.5-m (5-ft) overburden is the weighted average of thickness of overburden based on recent survey results. The 0.6-m (2-ft) underburden is based on current operational practices. Therefore, the average waste thickness is 3.2 m (10.5 ft). Maximum depth of biotic intrusion is 2.3 m (7.6 ft) of which 1.5 m (5 ft) is overburden. Therefore, the fraction of the waste that is available for uptake is 0.8/3.2 m (2.6/10.6 ft) or 25%.

5.5.2 Methodology for Determining DOSTOMAN-Rate Constants

Transport and uptake parameters are determined using applicable literature. Biotic transport rate constants allow the determination of radionuclide and nonvolatile chemical movement between the contaminated waste compartment and overburden compartments. The generic symbol for the rate coefficient for compartment n to compartment m is $\lambda_{m,n}$. Specific coefficients for each process are defined below. A superscript is used to identify the coefficients for an individual process (e.g., plant uptake). For example, the plant uptake-rate coefficient for compartment n to compartment m is $\lambda_{m,n}^{PU}$.

These coefficients then are used as shown in Equation (5-1) to determine soil-contaminant concentrations. The plant death-rate constant determines the rate at which biomass dies and decays in the soil of each compartment. The rate constant is given by the Equation (5-5):

$$\lambda_{m,n}^{PD} = \sum_{i=1}^{N} [(1 - FBAG_i) \times FD_i \times FP_{i,m} + (FBAG_i \times FD_i)_{surface}] \qquad (5\text{-}5)$$

where

$\lambda_{m,n}^{PD}$ = death-rate constant for each plant in each compartment m ($year^{-1}$)

$FBAG_i$ = fraction of total aboveground biomass of plant species i

FD_i = fraction of belowground biomass of plant species i that dies annually ($year^{-1}$)

$FP_{i,m}$ = fraction of belowground mass of plant i in soil compartment m

N = number of plant species.

The second term in this expression is used only in the uppermost (surface) soil compartment. This term accounts for aboveground biomass that is assumed to enter the uppermost soil compartment (surface) at a rate equal to the annual death rate. The second term is deleted for all other soil compartments. The death-rate constant is calculated for each plant species and then summed to give an aggregate death-rate constant for each soil compartment.

Data for plant death and plant uptake were compiled from both INL Site-specific literature and outside literature. All source references, data reviews, and compilations have been summarized in Hampton and Benson (1995) and Hampton (2001).

The current scenario reflects plant production over a period of 100 years, during which time the current vegetation community is maintained. Community composition for future scenarios was modeled for four separate periods to replicate change in community structure over time (i.e., 100 to 130, 130 to 150, 150 to 200, and greater than 200 years).

Plant-age composition for current and future scenarios was assumed to remain constant over the modeled periods. Biomass calculations were based on a total community production and fractional contributions of individual plant species (NRCS 1981). Successional trends of the SDA from the current vegetation community were assumed to result in a natural community similar to sagebrush-grass communities surrounding RWMC and other parts of the region (Anderson 1991; Anderson and Inouye 1988; NRCS 1981).

Where possible, best-estimate input values from studies conducted in disturbed soil were used for the current scenario and values from undisturbed studies were used for 100-plus-year scenarios. Average values from studies with the greatest sample size were given preference, and the largest average was selected if sample sizes were consistent. If no average was reported, a median value was calculated from a published range. Otherwise, the smallest reported maximum value from all studies was selected. Data specific to the INL Site were selected over data from off the INL Site, unless the study was flawed or somehow less applicable (e.g., plants grown in media other than native soil).

Table 5-27. Fractional root distribution for individual plant species specific to the Idaho National Laboratory Site for the current scenario.

Depth (cm)	Crested Wheatgrass[a]	Russian Thistle[a]
0–15	0.35	0.22
15–30	0.25	0.21
30–45	0.10	0.21
45–90	0.23	0.23
90–135	0.04	0.10
135–180	0.03	0.03
180–225	0	0.02
225–270	0	0

a. Reynolds (1990).

5.5.3 Flora—Current Scenario

Vegetation cover on the SDA comprises two species: crested wheatgrass (*Agropyron cristatum*) and Russian thistle (*Salsola kali*) (Arthur and Markham 1982). Biomass and rooting depths for these species are summarized in Table 5-27. The total average community biomass (aboveground and belowground) was estimated as approximately 11,000 kg/ha (2.2 ton/ha) for current SDA conditions (Arthur and Markham 1982).

The composition was assumed to remain constant through 100 years of maintaining current conditions. Rooting depths and root-mass distribution are summarized on Table 5-28. The maximum rooting depth for crested wheatgrass is not expected to reach a depth sufficient to penetrate the waste matrix during the current scenario. However, Russian thistle can penetrate into the waste zone during the current occupational scenario. The establishment of sagebrush and other deeper rooting shrub species is controlled in the SDA; therefore, those species were not included as components for the current scenario.

5.5.4 Flora—100-Plus-Year Scenario

The 100-plus-year scenario for vegetation consists of several phases where transitional changes in the current SDA community composition result in reestablishment of a natural sagebrush and bunchgrass community (Anderson and Inouye 1988; Anderson et al. 1978; NRCS 1981). The composition of different species for communities modeled after 100 years is presented in Table 5-28, which summarizes biomass and maximum rooting depth of the individual species for each transitional phase. Composition and percent biomass for successive increments are based on Arthur and Markham (1982), Anderson and Inouye (1988), Hull and Klomp (1974), Anderson et al. (1978), and Anderson (1991).

Table 5-28. Fractional root distribution for individual plant species for the 100-plus-year scenario.

Depth (cm)	Crested Wheatgrass[a]	Russian Thistle[a]	Sagebrush[a]	Green Rabbitbrush[b]	Bluebunch Wheatgrass[a]	Needle and Thread Grasses[a]	Other Grasses[a]	Forbs[a]	Other Shrubs[b]
0–15	0.35	0.22	0.21	0.125	0.35	0.35	0.35	0.22	0.12
15–30	0.25	0.21	0.20	0.10	0.25	0.25	0.25	0.21	0.10
30–45	0.10	0.21	0.20	0.07	0.10	0.10	0.105	0.21	0.07
45–90	0.30	0.23	0.23	0.45	0.23	0.20	0.23	0.23	0.45
90–135	0	0.10	0.13	0.20	0.04	0.05	0.065	0.10	0.20
135–180	0	0.03	0.015	0.04	0.03	0.05	0	0.03	0.04
180–225	0	0	0.015	0.015	0	0	0	0	0.02
225–270	0	0	0	0	0	0	0	0	0

a. Reynolds (1990). Adjusted for maximum depths given on this table.
b. McKenzie et al. (1982).

Biomass calculations for the three periods (i.e., 130 to 150, 150 to 200, and greater than 200 years) are based on average yearly greater-than-land-surface estimates of 1,490, 2,030, and 1,000 kg/ha, respectively (see Table 5-28). Root-mass distribution with depth for this scenario is presented in Table 5-29. Sagebrush and similar shrubs (e.g., gray rabbitbrush [*Chrysothamnus nauseosus*]) are expected to attain maximum rooting depths with maximum shrub density developing at 200 years.

The other plant-rate constant is plant uptake, which simulates uptake of contaminants into the plant biomass. The death of the plant returns the contaminants to the soil compartments. Equation (5-6) describes the uptake constant:

$$\lambda_{m,n}^{P^U} = \sum_{i=1}^{N} (B_V \times PP_i \times FP_{i,m}) / MS_m \qquad (5\text{-}6)$$

where

$\lambda_{m,n}^{P^U}$ = plant uptake rate constant ($year^{-1}$)

B_V = plant bioaccumulation factor ([mg/g plant]/[mg/g soil])

PP_i = annual plant productivity (g/year) for all plants of species i

$FP_{i,m}$ = fraction of root mass of all plant species i in soil compartment m

MS_m = mass of soil in compartment m (g)

N = number of species.

Table 5-29. Estimated parameters for the uptake of plant species for the Subsurface Disposal Area for current and 100 to 200-plus-year scenarios.

Plant Species	Root-to-Shoot Ratio	Fraction Litterfall ($Year^{-1}$)[a]	Fraction Root Death ($Year^{-1}$)[b]	Current Scenario		100-Plus-Year Scenarios			
				Maximum Root Depth (cm)	Fraction of Total Biomass[c]	Maximum Root Depth (cm)	Fraction of Total Biomass (130 years)[d]	Fraction of Total Biomass (150 years)[d]	Fraction of Total Biomass (200 plus years)[d]
Crested wheatgrass	8[e]	1	0.5	**150**[f]	**0.75**	75[g]	**0.55**	**0.30**	—
Russian thistle	1.4[b]	1	1	172[h]	**0.25**	172[h]	**0.15**	—	—
Sagebrush	1.3[e]	0.50[f]	0.5	—	—	220[f]	**0.05**	**0.10**	**0.20**
Green rabbitbrush	1.3[e]	0.85[f]	0.5	—	—	200[f]	**0.11**	**0.06**	**0.05**
Bluebunch wheatgrass	8[e]	1	0.5	—	—	150[j]	**0.03**	**0.05**	**0.10**
Needle and thread grasses	9[i]	1	0.5	—	—	139[j]	**0.02**	**0.09**	**0.10**
Other grasses	9[i]	1	0.5	—	—	100[f,j]	**0.05**	0.20	**0.29**
Forbs	1.5[b]	1	0.8[a]	—	—	145[h]	**0.02**	**0.10**	**0.15**
Other shrubs	1.5[b]	1	0.8[a]	—	—	183[k]	**0.02**	**0.10**	**0.11**
Community aboveground biomass (kg/ha)				—	**1,490**	—	**1,490**	1,700	800
Community root-to-shoot ratio				—	**6.35**	—	5.57	5.70	5.22

Note: Data in **bold** are specific to the Idaho National Laboratory Site.

a. Estimate based on root-to-shoot and fractional root depths for grass and shrub species presented in Becker et al. (1994).
b. Becker et al. (1994).
c. Arthur (1982); Arthur and Markham (1982).
d. Composition and percent biomass based on successive increments based on data presented in Arthur (1982), Anderson and Inouye (1988), and Anderson (1991).
e. Hull and Klomp (1974).
f. Reynolds and Fraley (1989).
g. Abbott, Fraley, and Reynolds (1991).
h. Klepper, Gano, and Cadwell (1985).
i. Pearson (1965).
j. McKenzie et al. (1982).
k. For gray rabbitbrush from Klepper et al. (1979).

— = Plant species is not present for this scenario.

The annual plant productivity (PP_i) can be found by using Equation (5-7):

$$PP_i = SB_i \times (RS_i + 1) \times FN_i \times SA \quad (5\text{-}7)$$

where

PP_i = annual plant productivity

SB_i = shoot biomass per unit area for species i (g/m^2)

RS_i = root-to-shoot ratio for species i

FN_i = fraction of total biomass produced each year (1/year)

SA = surface area of the SDA (m^2).

Mass of soil in compartment m (MS_m) can be found by using Equation (5-8):

$$MS_m = VC_m \times \rho \quad (5\text{-}8)$$

where

MS_m = mass of soil in compartment m

VC_m = volume of compartment m (cm^3)

ρ = density of soil (1.5 g/cm^3).

Plant uptake constants are determined for each plant species in each compartment and then summed to produce the aggregate uptake-rate constant for that compartment.

Movement of contaminants by burrowing animals and ants requires soil transport rate constants. Equation (5-9) describes the soil transport rate constant:

$$\lambda^{\beta}_{m,n} = \sum_{i=1}^{N} (I_i \times MB_i \times FNB_i \times FB_{i,m}) / MS_m \quad (5\text{-}9)$$

where

$\lambda^{\beta}_{m,n}$ = soil transport rate constant ($year^{-1}$)

I_i = number of individual animals in species i

MB_i = mass of soil moved to the surface per individual by species i (g)

FNB_i = fraction of new burrows per year for species i ($year^{-1}$)

$FB_{i,m}$ = fraction of burrows of species i in soil compartment m

MS_m = mass of soil in compartment m (g)

N = number of species.

A soil transport rate constant is calculated for each compartment for each burrowing species in that compartment. Constants for each species are summed to produce the aggregate soil transport rate constant for each compartment. The predominant effect produced by this constant occurs when a burrowing animal digs directly into the waste and transports it to the surface.

Burrowing animals enhance waste transport through intrusion activities that move contaminants to the surface. The DOSTOMAN biotic transport model includes contributions of both burrowing mammals and harvester ants. Data were compiled from SDA and INL Site-specific literature and outside literature.

5.5.5 Fauna—Current Scenario

Composition of burrowing species, population density, burrow volumes, and average burrow depths reflecting estimated current burrowing activity in the SDA are shown in Table 5-30. Burrow distribution with depth for individual species is listed in Table 5-31. Burrow distributions, with depth, for the current scenario are based on average burrow depths, and the soil profile was assumed to be disturbed. No animals are expected to attain burrow depths sufficient to exceed the current overburden thickness of 1.5 m (5 ft) (calculated average). The deepest average burrow depths are 1.4 m (4.5 ft) for harvester ants and 1.3 m (4.3 ft) for Townsend's ground squirrels (see Table 5-30). Species densities (see Table 5-32) are based primarily on previous studies of the SDA by Groves (1981), Groves and Keller (1983), Koehler (1988), Boone (1990), and Boone and Keller (1993). Burrow volume, depth, composition, and average population densities were assumed to remain constant for 100 years, assuming that institutional controls maintain current conditions over that period (see Tables 5-31 and 5-32).

Table 5-30. Small animal density and burrowing parameters for the current scenario.

Burrowing Animal Species[a]	Population (individuals per hectare)[a]	Maximum Depth (cm)	Burrow Volume (L)	Number of New Burrows (per year)[b]
Townsend's ground squirrel	**5**	**130**[c]	**9.4**[c]	0.75
Ord's kangaroo rat	**5**	**90**[c]	**7.3**[c]	0.87
Deer mouse	**17**	**50**[c]	**1.3**[c]	0.87
Montane and sagebrush voles	**30**	**40**[c]	**2.1**[c]	0.87
Great Basin pocket mouse	**15**	77[d]	6.8[d]	0.75
Western harvester ant (nests)	**13**[e]	138[f]	2.4[g]	0.1[e]

Note: Data in **bold** are specific to the Idaho National Laboratory Site.

a. Mammal species composition and populations are based on studies conducted in the Subsurface Disposal Area by Groves (1981), Groves and Keller (1983), Koehler (1988), Boone (1990), and Boone and Keller (1993).
b. McKenzie et al. (1982).
c. Reynolds and Laundré (1988).
d. Landeen and Mitchell (1981).
e. Blom, Clark, and Johnson (1991).
f. Gaglio et al. (1998).
g. Fitzner et al. (1979).

Table 5-31. Burrow volume and fraction of volume excavated at depth by small animals for the current scenario.

Depth of Disturbed Soil (cm)	Townsend's Ground Squirrel[a]	Ord's Kangaroo Rat[a]	Deer Mouse[a]	Voles[a]	Great Basin Pocket Mouse[b]
	Fraction of Volume				
0–15	0.06	0.16	0.38	0.46	0.24
15–30	0.18	0.13	0.29	0.46	0.24
30–45	0.34	0.23	0.25	0.08	0.24
45–90	0.24	0.47	0.08	0	0.29
90–135	0.18	0	0	0	0
135–180	0	0	0	0	0
180–225	0	0	0	0	0
225–270	0	0	0	0	0
Total burrow volume (L)	**9.4**	**7.3**	**1.3**	**2.1**	**6.8**

a. Reynolds and Laundré (1988), Reynolds and Wakkinen (1987).
b. McKenzie et al. (1982).

Table 5-32. Small animal density and burrowing parameters for the Subsurface Disposal Area 100-plus-year scenario.

Species[a]	Current/100-plus Years (number per hectare[a])	Average Depth (cm)	Burrow Volume (L)	New Burrows (year^{-1})[b]
Badger	1/3	180[c]	318.0[b,d] (diameter =30 cm, length = 450 cm)	3
Deer mouse	**17/30**	**24**[e]	**1.7**[e]	0.87
Great Basin pocket mouse	**15/25**	44.4[f]	**5.6**[f]	0.75
Least chipmunk	**3/8**	**17.5**[g]	**5.5**[g]	0.75
Montane and sagebrush voles	**30/10**	**23**[c]	**1.5**[c]	0.87
Northern pocket gopher	**7/7**	13.4[h]	5.5[h,d]	0.75
Ord's kangaroo rat	**8/5**	**34**[i]	**7.2**[i]	0.87
Rabbits	8/20	150	87.0[d] (length = 170 cm)	0.75
Townsend's ground squirrel	**5/5**	**128**[e]	8.2[e]	0.75
Western harvester ant (nests)	20[j]/36[j]	138[k]	7.0[l,d]	0.1

Note: Data in **bold** are specific to the Idaho National Laboratory Site.

a. Compiled from Groves (1981), Groves and Keller (1983), Koehler (1988), Boone (1990), and Boone and Keller (1993), unless otherwise noted.
b. Lindzey (1976).
c. McKenzie et al. (1982).
d. Calculated from data presented in reference.
e. Reynolds and Wakkinen (1987).
f. Landeen and Mitchell (1981).
g. Laundré (1989a).
h. Winsor and Whicker (1980).
i. Reynolds and Laundré (1988).
j. Blom, Clark, and Johnson (1991).
k. Gaglio et al. (1998).
l. Fitzner et al. (1979).

5.5.6 Fauna—100-Plus-Year Scenario

Composition of the animal community for the 100-plus-year scenario was altered to reflect changes as the vegetation community is transformed to simulate conditions at the INL Site if institutional controls were discontinued. The composition, burrow depth, volume, and density of species for the 100-plus-year modeled periods are summarized in Table 5-33. The fractional burrow distribution for each individual species is presented in Table 5-33. Burrow distributions, with depth, for the 100-plus-year scenario are based on average burrow depths and profiles of undisturbed soil. While rodent populations fluctuate widely from year to year (Boone and Keller 1993), population densities presented are average species compositions and population levels over time.

Leaching from a compartment is computed using Equation (5-10):

$$\lambda^{L}_{m,m+1} = \frac{P}{\theta R\, T_m} \tag{5-10}$$

where

$\lambda^{L}_{m,m+1}$ = leach rate coefficient for compartment m (year-1)

P = net infiltration (m/year)

θ = volumetric moisture content (unitless)

R = contaminant-specific retardation coefficient (unitless)

T = thickness of compartment m (m).

Burrow collapse is computed using the burrow compartment mass excavation given in Equation (5-11). The lowest compartment receives mass from the middle compartment equal to the amount of soil moved to the surface from the lowest compartment. The middle compartment receives mass from the upper compartment equal to mass moved to the surface from both the first and second compartments. This way mass removed by burrowing is replaced by burrow collapse from the compartment above. Total mass moved into any compartment by burrow collapse is equal to mass removed from that compartment plus total mass moved to the surface from all compartments below. Equation (5-11) is used for computing the burrow collapse for a compartment:

$$\lambda^{c}_{m,n} = \sum_{i=1}^{nl} \lambda^{\beta}_{m,i} \frac{T_n}{T_i} \tag{5-11}$$

where

$\lambda^{c}_{m,n}$ = burrow collapse-rate constant ($year^{-1}$)

$\lambda^{\beta}_{m,i}$ = soil transport rate constant for compartment i ($year^{-1}$) for burrowing animals

T_n = thickness of compartment n (m)

T_i = thickness of compartment i (m)

nl = number of compartments lower than compartment i.

Table 5-33. Burrow volume and fraction of volume excavated at depth by small animals for the 100-plus-year scenario in undisturbed soil.

Depth of Undisturbed Soil (cm)	Townsend's Ground Squirrel[a]	Ord's Kangaroo Rat[a]	Deer Mouse[a]	Voles[a]	Great Basin Pocket Mouse[b]	Northern Pocket Gopher[b]	Least Chipmunk[c]	Badger[b]	Rabbits[d]	Western Harvester Ant
	Fraction of Volume									
0 to 15	**0.08**	**0.21**	**0.32**	**0.46**	0.32	0.98	**0.48**	0.21	**0.17**	0.21
15 to 30	**0.18**	**0.29**	**0.68**	**0.54**	0.31	0.02	**0.52**	0.21	**0.17**	0.21
30 to 45	**0.08**	**0.14**	**0**	**0**	0.37	0	**0**	0.20	**0.17**	0.21
45 to 90	**0.11**	**0.36**	**0**	**0**	0	0	**0**	0.19	**0.17**	0.15
90 to 135	**0.55**	0	0	0	0	0.	**0**	0.10	**0.17**	0.12
135 to 180	**0**	0	0	0	0	0	**0**	0.09	**0.15**	0.10
180 to 225	**0**	0	0	0	0	0	**0**	0	**0**	0
225 to 270	**0**	0	0	0	0	0	**0**	0	**0**	0
Total burrow volume (L)[e]	**8.2**	**7.2**	**1.7**	**1.5**	5.6	5.5	**5.5**	170	**87**	2.4

Note: Data in **bold** are specific to the Idaho National Laboratory Site.

a. Reynolds and Laundré (1988).
b. McKenzie et al. (1982).
c. Laundré (1989a; 1989b).
d. Wilde (1978).
e. Total burrow volumes from Table C-3 of Appendix C in Hampton (2001).

5.5.7 Biotic-Model Calibration

The biotic model was not calibrated for two reasons. First, data from surface sampling are inconsistent and probably reflect past operational releases and flooding events rather than biotic uptake. In addition, repeated recontouring has made data for surface concentrations less useful for calibration purposes. Concentrations of Cs-137 and Co-60 decrease more rapidly than can be accounted for by decay or leaching. Rapid decrease is believed to be caused by having sampled clean soil used in recontouring. Second, a surface barrier will be a component of the remedial action ultimately implemented in the SDA (Holdren and Broomfield 2004). Any additional cover would tend to eliminate the potential for biotic intrusion into the waste. Therefore, calibration of the biotic model was not attempted.

5.5.8 Summary

The DOSTOMAN biotic model was used to predict surface soil concentrations for use in the exposure assessment. Soil concentrations are believed to be conservative for the processes modeled. The methodology used to produce inputs to the model is more conservative than previous modeling efforts. The biotic model was not calibrated to measured soil concentrations because (1) soil data were inconsistent for many contaminants, (2) the SDA surface is routinely modified by subsidence repair and recontouring, and (3) some form of covering with additional material (i.e., a surface barrier) will be implemented as a component of any remedial action in the SDA. An appropriately designed cover would eliminate the possibility of biotic intrusion into the waste.

5.6 Summary and Conclusions

Modeling presented in Section 5 is the basis for analysis of risk in Section 6. With changes to the surface infiltration boundary condition and to the source term to reflect possible remedial alternatives, these models also will form the basis for remedial decisions for Operable Unit 7-13/14. Many aspects of the source-release and groundwater-pathway modeling have been improved compared to the ABRA model. However, uncertainties are and always will be associated with predicting movement of contaminants in the subsurface; therefore, conservatism is retained in the modeling and is demonstrated through comparison to monitoring. The primary improvement over the ABRA model was in the knowledge of inventory, waste-disposal streams, and disposal locations within the SDA. These improvements in the inventory and results of characterization activities have been successfully incorporated into the source-release model and the interface with the vadose zone model. Improvements also have been made in groundwater-pathway modeling; however, those improvements have had a lesser impact on predicted concentrations. For groundwater-pathway modeling, updating the VOC modeling and including gaseous-phase C-14 transport were the primary improvements. Table 5-34 summarizes the improvements in RI/FS modeling. However, results must be considered in the context of uncertainties inherent in the modeling relative to conceptual models and parameterization of the conceptual model that was implemented. Section 6 provides a discussion of uncertainties.

In each case, best judgment was used in implementing the source-release model and the subsurface flow and transport model. Lack of data for calibrating the source-release model and the subsurface flow and transport model for strictly dissolved contaminants continues to require that modeling primarily rely on individual comparisons to field data instead of calibration to a contaminant plume. The ongoing monitoring program and evaluation of monitoring results represent considerable time and expense. Results of these monitoring activities have shown promise in identifying trends in contaminant behavior that are useful for determining the relative conservatism in modeling. Fortunately, from an environmental consequence perspective, the movement of contaminants in the vadose zone and aquifer beneath the SDA is slow, and no extensive dissolved-phase-contaminant plume is available against which to calibrate.

Table 5-34. Summary of improvements in the remedial investigation and feasibility study models compared to the Interim Risk Assessment and Ancillary Basis for Risk Analysis models.

Topic	ABRA Approach	Modifications for the RI/BRA	Bases for Improvement
Contaminant screening	Simulated fate and transport for contaminants in seven groups. Only surface pathway risk was assessed for Cs-137 and Sr-90 (human health) and ecological contaminants of potential concern using DOSTOMAN. Risk estimates for the three VOC contaminants of potential concern were scaled from the IRA and not remodeled by Operable Unit 7-13/14.	ABRA risk estimates were used to eliminate contaminants of potential concern. Full decay chains were simulated so that some isotopes, which are not contaminants of potential concern, were simulated.	Used results of previous assessments, including the ABRA, to eliminate contaminants that would not affect the total risk.
Source-term inventory	Corrected Contaminant Inventory Database for Risk Assessment best-estimate inventories were used to generate base-case risk estimates. Uncertainties in inventories were assessed by simulating corrected upper-bound quantities and the projected maximum limits on the facility disposal quantities.	Waste inventories from INL Site waste generators were corrected and incorporated into the Waste Information and Location Database. This provides better estimates of the inventory of fission and activation products. Upper-bound inventory quantities were used to assess uncertainty.	Complete revision of the inventories for Materials and Fuels Complex, Idaho Nuclear Technology and Engineering Center, Naval Reactors Facility, Test Reactor Area, and Test Area North.
Source discretization	Contaminant Inventory Database for Risk Assessment inventories were proportioned into 13 discrete source areas based on shipping information in the WasteOScope database.	The Waste Information and Location Database inventory was proportioned into 18 discrete source areas. The additional areas are used to better define the location of INL Site-generated waste.	Development of Waste Information and Location Database, which contains inventory revisions and location information.
C-14 risk	Based on Contaminant Inventory Database for Risk Assessment best-estimate inventories and release rates from literature reviews of corrosion data.	Revised inventory and mobility (K_d) and used the RI/BRA dual-continua model to include gaseous-phase partitioning, which allowed vapor-phase diffusion through land surface.	Revised inventory (see above) and mobility, and included additional processes to be more representative.

Table 5-34. (continued).

Topic	ABRA Approach	Modifications for the RI/BRA	Bases for Improvement
VOC mass remaining in the waste	The IRA assumed that essentially no remaining source was left in the waste zone. The IRA used a VOC source that underestimated the mass of VOC buried in the SDA. Therefore, it was necessary to release all the VOC mass to calibrate to observed subsurface concentrations.	Used Miller and Varvel (2005) and Varvel (2005) updated estimates of total buried inventories. Sondrup et al. (2004) provided a basis for 50% mass remaining in 2000, which was used for modeling.	Additional evidence suggested substantial VOC mass remaining in the waste zone. Evidence included observations from the Operable Unit 7-10 Glovebox Excavator Method Project and data from Type A and B probing in the Pit 4 Series 743 Focus Area. Also, a Geologic and Environmental Probe System lysimeter in Pit 10 yielded free product.
VOC groundwater-pathway modeling	Scaled IRA concentrations and risk bases concentrations on inventory corrections. Did not account for the VOC mass removed by ongoing extraction.	Updated VOC modeling to use RI/BRA dual-continua simulation domain. VOC mass removed by ongoing operations, and projected future operations were included in the RI/BRA base case.	Using consistent domains between Operable Units 7-13/14 and 7-08. Making use of additional operation results.
Uranium risk	Addressed solubility limits in uncertainty based on Eh and pH combinations possible in waste.	Reduced solubility limits to account for competition between isotopes.	Including a more representative process.
Interbed hydrologic and transport properties	Included spatial variability in hydrologic properties in the B-C and C-D interbeds.	Corrected implementation errors for including spatial variability in hydrologic properties in the B-C and C-D interbeds. Used additional core data to compare to previous kriged estimates.	Analyzed cores collected in 2003 to profile hydrologic properties and provide basis for comparison to previous kriging estimates.
Interbed lithology	Kriged available values.	Performed extensive evaluation to provide a pedigree for all the lithologic selections used in developing the RI/FS model, including selecting new SDA wells drilled since 2003.	Questions on process used to make previous selections resulted in need for evaluation effort.

Table 5-34. (continued).

Topic	ABRA Approach	Modifications for the RI/BRA	Bases for Improvement
Infiltration rates	Infiltration across the SDA was varied spatially, and if averaged, would have a value of 8.5 cm/year. Spatially varying infiltration rates were averaged to obtain a unique infiltration rate for each of the 13 source areas.	Infiltration across the SDA was varied spatially and, if averaged, would have a value of 5.0 cm/year. Spatially-varying infiltration rates were averaged to obtain a unique infiltration rate for each of the 18 source areas for aqueous-phase transport and nine source areas for combined aqueous- and gaseous-phase radionuclide transport.	Reevaluation of infiltration-rate estimates from several neutron probe access tube-based monitoring events were discounted due to instruments being in ditches or low-lying areas and, therefore, are not representative of infiltration through waste.
Aquifer-simulation domain	Extended domain to the INL Site boundary; resulted in risk isopleth contour level 1E-05 extending past edge of domain.	Extended domain west and south to ensure risk isopleth contour level 1E-05 would be contained within the domain.	Removed perception of indefinite extent of a key risk isopleth-contour level.
Upgradient contributions	Upgradient contribution assumed not to occur.	Searched for upgradient contributions, but detected no discernible impact.	Issue is still unresolved, and therefore, it is appropriate to continue neglecting possible contribution from upgradient sources and presuming contaminants in the aquifer are from the SDA.
Sporadic low-level detections of actinides in aquifer	Assumed to be anomalous.	Assumed to be anomalous.	Isotopic analysis (thermal ionization mass spectrometry) of aquifer samples from the immediate vicinity of the SDA indicated no impact of uranium in the aquifer.
Calibration of vadose zone flow model	Used perched water locations and temporal behavior as calibration targets with poor results.	Water potentials from the deep tensiometer network inside and outside the SDA were used to calibrate the vadose zone flow model and corroborate the conceptual model that had a higher infiltration rate inside the SDA than outside the SDA. The presence and absence of perched water was used in a comparative sense to compare against simulated moisture contents in the B-C and C-D interbeds.	Used a consistent set of field monitoring data to refine model parameters controlling the movement of water in the subsurface.
Distribution coefficient assignments	Used data from Dicke (1997), except for revised value for C-14.	Values refined for C-14, Ac-227, Am-241, Am-243, Np-237, plutonium, and uranium.	Use of additional site-specific information from core-interbed sample analysis and column studies.

Table 5-34. (continued).

Topic	ABRA Approach	Modifications for the RI/BRA	Bases for Improvement
Facilitated transport of plutonium	Evaluated as sensitivity cases.	Included in RI/BRA base case using evaluation of Batcheller and Redden (2004).	Inclusion of additional processes to be more representative.
Spreading area influences	Included influence as part of base case.	Neglected influence because additional water at depth only served to dilute the groundwater-pathway concentrations.	Conservative assumption.

ABRA = Ancillary Basis Risk Analysis
INL = Idaho National Laboratory
IRA = Interim Risk Assessment (Becker et al. 1998)
RI/BRA = remedial investigation and baseline risk assessment
SDA = Subsurface Disposal Area
VOC = volatile organic compound

Results of these models are a reasonable basis for estimating potential risk to human health and the environment and for assessing appropriate remedial alternatives to mitigate unacceptable risk. However, results must be considered in light of uncertainties associated with this analysis. Existing data sets for dissolved-phase contaminants were inadequate for model calibration; therefore, model parameters were not adjusted in an attempt to achieve calibration by improving agreement between simulated and observed results. Instead comparisons were made to assess model predictions relative to observed results. Modeling results consistently overpredict aquifer concentrations (neglecting sporadic detections), overpredict at some vadose zone monitoring locations, and underpredict at other vadose zone monitoring locations. The latter is likely due to a combination of highly heterogeneous waste disposal and gridblock averaging that reduces simulated concentrations due to large gridblock volumes relative to the point-scale monitoring results from the vadose zone network. Based on this, the groundwater-pathway modeling results are generally conservative. This conservatism primarily results from overestimating contaminant source release, having rapid vertical transport in the fractured basalt portions of the vadose zone, and including the extensive low-permeability region in the aquifer domain, which limits dilution.

Relative to sensitivity results, the source inventory and release mechanism have the largest impact on predicted groundwater-pathway concentrations. In terms of water movement and its impact on the subsurface pathway, two primary features of the models impact predicted concentrations. First, the amount of water that contacts waste influences groundwater-pathway concentrations. This water serves as the driving force to move aqueous-phase contaminants along the groundwater pathway. Sensitivity simulations show that additional water in the vadose zone that does not contact the waste primarily results in dilution of groundwater-pathway concentrations. Second, the low-permeability region in the aquifer has a substantial impact on predicted concentrations. This low-permeability region reduces dilution that would otherwise occur and results in increased concentrations that are more reflective of the concentration of water influxing from the vadose zone.

The source inventory and release mechanism having the largest impact on the groundwater pathway indicates that efforts expended since the ABRA on identifying waste inventories and locations has been justified. The importance of quantifying the amount of water contacting the waste also justifies the efforts expended to place probes in the waste and shows promise for improved results with the Geologic and Environmental Probe System probes. Obtaining samples of leachate for contaminant analyses will substantiate the results of groundwater-pathway monitoring.

In terms of uncertainty, given the lack of quantitative uncertainty assessment, all uncertainty discussions have to be qualitative. Given that the model overpredicts current concentrations in the aquifer, it is certain that model results are conservative at the present time. The amount of uncertainty in the predictive results undoubtedly increases with time, decreasing the level of confidence that the model remains conservative over time. Monitoring over time and comparing monitoring results against model predictions will be an important aspect of post-record of decision monitoring.

5.7 References

Abbott, M. L., L. Fraley Jr., and T. D. Reynolds, 1991, "Root Profiles of Selected Cold Desert Shrubs and Grasses in Disturbed and Undisturbed Soils," *Environmental and Experimental Botany*, Vol. 31, pp. 165–78.

Adler Flitton, M. K., C. W. Bishop, R. E. Mizia, L. L. Torres, and R. D. Rogers, 2001, *Long Term Corrosion/Degradation Test Third-Year Results*, INEEL/EXT-01-00036, Rev. 0, Idaho National Engineering and Environmental Laboratory.

Anderson, Danny L. and Bruce H. Becker, 2006, *Source Release Modeling Report for OU 7-13/14,* ICP/EXT-05-01039, Rev. 0, Idaho National Laboratory, Idaho Cleanup Project.

Anderson, J. E., 1991, *Vegetation Studies to Support the NPR Environmental Impact Statement*, NPR-DEIS-SR-003, Environmental Science and Research Laboratory.

Anderson, J. E., R. J. Jeppson, R. J. Rjwilkosz, G. M. Marlette, and K. E. Holte, 1978, *Trends in Vegetation Development on the Idaho National Engineering Laboratory Site*, Idaho National Engineering Laboratory.

Anderson, J. E. and R. Inouye, 1988, *Long-Term Dynamics of Vegetation in Sagebrush Steppe of Southeastern Idaho, Final Report*, Contract No. C84130479, Department of Biological Sciences, Idaho State University.

Anderson, S. R., D. J. Ackerman, M. J. Liszewski, and R. M. Freiburger, 1996, *Stratigraphic Data for Wells at and Near the Idaho National Engineering Laboratory, Idaho*, Open File Report 96-248, U.S. Geological Survey, DOE/ID-22127, U.S. Department of Energy Idaho Operations Office.

Ansley, Shannon L., Catherine M. Helm-Clark, and Swen O. Magnuson, 2004, *Updated Stratigraphic Selections for Wells in the Vicinity of the Subsurface Disposal Area*, ICP/EXT-04-00207, Rev. 0, Idaho National Engineering and Environmental Laboratory, Idaho Completion Project.

Arnett, R. C. and R. P. Smith, 2001, "WAG 10 Groundwater Modeling Strategy and Conceptual Model," INEEL/EXT-01-00768, Rev. Draft B, Idaho National Engineering and Environmental Laboratory.

Arthur, W. J. III, 1982, "Radionuclide Concentrations in Vegetation at a Solid Radioactive Waste-Disposal Area in Southeastern Idaho," *Journal of Environmental Quality*, Vol. 11, No. 3, pp. 394–399.

Arthur, W. J. and O. D. Markham, 1982, "Ecological Vectors of Radionuclide Transport at a Solid Radioactive Waste Disposal Facility in Southeastern Idaho," *Proceedings of the International Conference on Radioactive Waste Management*, *Winnipeg, Manitoba, Canada*, *September 12–15, 1982*, Canadian Nuclear Society.

Baca, R. G., S. O. Magnuson, H. D. Nguyen, and P. Martian, 1992, *A Modeling Study of Water Flow in the Vadose Zone Beneath the Radioactive Waste Management Complex*, EGG-GEO-10068, Rev. 0, Idaho National Engineering Laboratory.

Batcheller, Thomas A. and George D. Redden, 2004, *Colloidal Plutonium at the Operable Unit 7-13/14 Subsurface Disposal Area: Estimate of Inventory and Transport Properties*, ICP/EXT-04-00253, Idaho National Engineering and Environmental Laboratory, Idaho Completion Project.

Becker, B. H., 1997, *Selection and Development of Models Used in the Waste Area Group 7 Baseline Risk Assessment*, INEEL/EXT-97-00391, Idaho National Engineering and Environmental Laboratory.

Becker, B. H., C. A. Loehr, S. M. Rood, and J. A. Sondrup, 1994, *Risk Assessment of Remedial Objectives for Nontransuranic Waste in Pit 9*, EGG-ER-11093, Rev. 1, Idaho National Engineering Laboratory.

Becker, B. H., T. A. Bensen, C. S. Blackmore, D. E. Burns, B. N. Burton, N. L. Hampton, R. M. Huntley, R. W. Jones, D. K. Jorgensen, S. O. Magnuson, C. Shapiro, and R. L. VanHorn, 1996, *Work Plan for Operable Unit 7-13/14 Waste Area Group 7 Comprehensive Remedial Investigation/Feasibility Study*, INEL-95/0343, Rev. 0, Idaho National Engineering Laboratory.

Becker, B. H., J. D. Burgess, K. J. Holdren, D. K. Jorgensen, S. O. Magnuson, and A. J. Sondrup, 1998, *Interim Risk Assessment and Contaminant Screening for the Waste Area Group 7 Remedial Investigation*, DOE/ID-10569, Rev. 0, U.S. Department of Energy Idaho Operations Office.

Blom, P. E., W. H. Clark, and J. B. Johnson, 1991, "Colony Densities of the Seed Harvesting Ant Pogonomyrmex salinus (Hymenoptera: Formicidae) in Seven Plant Communities on the Idaho National Engineering Laboratory," *Journal of the Idaho Academy of Science*, Vol. 27, No. 1, pp. 28–36.

Blom, P. E., J. B. Johnson, and S. K. Rope, 1991, "Concentrations of ^{137}Cs and ^{60}Co in Nests of the Harvester Ant, Pogonomyrex Salinus, and Associated Soils near Nuclear Reactor Waste Water Ponds," *American Midland Naturalist*, Vol. 126, pp. 140–151.

Boone, J. D., 1990, *Ecological Characteristics and Preferential Edge Use of Small Mammal Populations Inhabiting a Radioactive Waste Disposal Area*, M. S. Thesis: Idaho State University, Pocatello, Idaho.

Boone, J. D. and B. L. Keller, 1993, "Temporal and Spatial Patterns of Small Mammal Density and Species Composition on a Radioactive Waste Disposal Area: The Role of Edge Habitat," *Great Basin Naturalist*, Vol. 53, No. 4, pp. 341–349.

Case, Marilyn J., Arthur S. Rood, James M. McCarthy, Swen O. Magnuson, Bruce H. Becker, and Thomas K. Honeycutt, 2000, *Technical Revision of the Radioactive Waste Management Complex Low-Level Waste Radiological Performance Assessment for Calendar Year 2000*, INEEL/EXT-2000-01089, Idaho National Engineering and Environmental Laboratory.

Cecil, L. D., J. R. Pittman, T. M. Beasley, R. L. Michel, P. W. Kubik, P. Sharma, U. Fehn, and H. Gove, 1992, "Water Infiltration Rates in the Unsaturated Zone at the Idaho National Engineering Laboratory Estimated from Chlorine-36 and Tritium Profiles, and Neutron Logging," *Proceedings of the 7th International Symposium on Water-Rock Interaction*, *Park City, Utah,* WRI-7, Rotterdam: Balkema.

Cline, J. F., F. G. Burton, D. A. Cataldo, W. E. Skiens, and K. A. Gano, 1982, *Long-Term Biobarriers to Plant and Animal Intrusion of Uranium Tailings*, DOE/UMT-0209, Pacific Northwest National Laboratory.

Colwell, F. S., 1988, *Final Report: Microbial Examination of the RWMC Surface and Subsurface Soils and Biodegradation of Low Molecular Weight Hydrocarbons Using Microorganisms Indigenous to RWMC*, ST-BEG-03-88, Idaho National Engineering Laboratory.

Dicke, C. A., 1997, *Distribution Coefficients and Contaminant Solubilities for the Waste Area Group 7 Baseline Risk Assessment*, INEEL/EXT-97-00201, Rev. 0, Idaho National Engineering and Environmental Laboratory.

DOE-ID, 2004a, *Action Memorandum for Accelerated Retrieval of a Described Area within Pit 4*, DOE/NE-ID-11179, Rev. 0, U.S. Department of Energy Idaho Operations Office.

DOE-ID, 2004b, *Idaho National Engineering and Environmental Laboratory Operable Unit 10-08 Sitewide Groundwater Model Work Plan*, DOE/NE-ID-11188, Rev. 0, U.S. Department of Energy Idaho Operations Office.

EPA, 1999, *Understanding Variation in Partition Coefficient, K_d Values*, EPA 402-R-99-004A&B, U.S. Environmental Protection Agency.

Fabryka-Martin, J., G. Gee, and A. Flint, 1999, *Peer Review Team Report on Conceptual Models and Field Verification of Radionuclide Transport through the Vadose Zone at INEEL*, Final Report, November 5, 1998, Administrative Record No. 531975, prepared by Los Alamos, U.S. Geological Survey, and Pacific Northwest National Laboratory for Idaho National Engineering and Environmental Laboratory.

Falta, R. W., I. Javandel, K. Pruess, and P. A. Witherspoon, 1989, "Density-Driven Flow of Gas in the Unsaturated Zone due to the Evaporation of Volatile Organic Compounds," *Water Resources Research*, Vol. 25, No. 10.

Fitzner, Richard E., Ken A. Gano, William H. Rickard, and Lee E. Rogers, 1979, *Characterization of the Hanford 300 Area Burial Grounds, Task IV-Biological Transport*, PNL-2774, Pacific Northwest National Laboratory.

Fjeld, Robert J., John T. Coates, and Alan W. Elzerman, 2000, *Final Report, Column Tests to Study the Transport of Plutonium and Other Radionuclides in Sedimentary Interbed at INEEL*, INEEL/EXT-01-00763, Rev. 0, prepared by the Department of Environmental Engineering and Science, Clemson University for Idaho National Engineering and Environmental Laboratory.

Freeze, R. A. and J. A. Cherry, 1979, *Groundwater*, Englewood Cliffs: Prentice-Hall.

Gaglio, M. D., W. P. Mackay, E. A. Osorio, and I. Iniguez, 1998, "Next Populations of Pogonomyrmex salinus Harvester Ants (Hymenoptera: Formicidae)," *Sociobiology,* Vol. 332 pp. 459–463.

GE, 1989, *Nuclides and Isotopes Fourteenth Edition Chart of the Nuclides*, General Electric Nuclear Energy.

Gelhar, L. W., 1986, "Stochastic Subsurface Hydrology from Theory to Applications," *Water Resources Research*, Vol. 22, No. 9, August 1986 Supplement, pp. 135S–145S.

Grossman, Christopher J., Robert A. Fjeld, John T. Coates, and Alan W. Elzerman, 2001, *The Sorption of Selected Radionuclides in Sedimentary Interbed Soils from the Snake River Plain, Final Report,* INEEL/EXT-01-01106, prepared by Clemson University, Clemson, South Carolina, for Idaho National Engineering and Environmental Laboratory.

Groves, C. R., 1981, *The Ecology of Small Mammals on the Subsurface Disposal Area, Idaho National Engineering Laboratory Site*, M.S. Thesis: Idaho State University, Pocatello, Idaho.

Groves, C. R. and B. Keller, 1983, "Ecological Characteristics of Small Mammals on a Radioactive Waste Disposal Area in Southeast Idaho," *American Midland Naturalist*, Vol. 109, No. 2, pp. 253-265.

Hackett, W. R., J. A. Tullis, R. P. Smith, S. J. Miller, T. V. Dechert, P. A. McDaniel, and A. L. Falen, 1995, *Geologic Processes in the RWMC Area, Idaho National Engineering Laboratory: Implications for Long Term Stability and Soil Erosion at the Radioactive Waste Management Complex*, INEL-95/0519, Idaho National Engineering Laboratory.

Hampton, H. L. and T. A. Benson, 1995, *SDA Biotic Data Compilation,* EDF ER-WAG7-76, INEL-95/139, Rev.1, Idaho National Engineering Laboratory.

Hampton, N. L., 2001, *Biological Data to Support Operable Unit 7-13/14 Modeling of Plant and Animal Intrusion at Buried Waste Sites*, INEEL/EXT-01-00273, Rev. 0, Idaho National Engineering and Environmental Laboratory.

Hanson, Duane, G. E. Matthern, N. A. Yancey, and D. L. Knudson, 2004, *Evaluation of the Durability of WAXFIX for Subsurface Applications*, ICP/EXT-04-00300, Rev. 0, Idaho National Engineering and Environmental Laboratory, Idaho Completion Project.

Holdren, K. Jean, Bruce H. Becker, Nancy L. Hampton, L. Don Koeppen, Swen O. Magnuson, T. J. Meyer, Gail L. Olson, and A. Jeffrey Sondrup, 2002, *Ancillary Basis for Risk Analysis of the Subsurface Disposal Area*, INEEL/EXT-02-01125, Rev. 0, Idaho National Engineering and Environmental Laboratory.

Holdren, K. Jean and Barbara J. Broomfield, 2004, *Second Addendum to the Work Plan for the Operable Unit 7-13/14 Waste Area Group 7 Comprehensive Remedial Investigation/Feasibility Study*, DOE/ID-11039, U.S. Department of Energy Idaho Operations Office.

Hubbell, J. M., M. J. Nicholl, J. B. Sisson, and D. L. McElroy, 2004, "Application of a Darcian Approach to Estimate Liquid Flux in a Deep Vadose Zone," *Vadose Zone Journal*, Vol. 3, pp. 560–569.

Hull, A. C. Jr. and G. J. Klomp, 1974, "Yield of Crested Wheatgrass under Four Densities of Big Sagebrush in Southern Idaho," Technical Bulletin No. 1483, U.S. Department of Agriculture.

Hull, Larry, Idaho National Engineering and Environmental Laboratory, to K. Jean Holdren, Idaho National Engineering and Environmental Laboratory, September 25, 2003, "Plutonium Kd Post Tally Jenkin's Comment."

Klepper, E. L., L. E. Rogers, J. D. Hedlund, and R. G. Schreckhise, 1979, *Radioactivity Associated with Biota and Soil of the 216-A- 24 Crib*, PNL-1948, Pacific Northwest National Laboratory.

Klepper, E. L., K. A. Gano, and L. Cadwell, 1985, *Rooting Depth and Distributions of Deep-Rooted Plants in the 200 Area Control Zone of the Hanford Site*, PNL-5247, Pacific Northwest National Laboratory.

Knobel, L. L., B. R. Orr, and L. D. Cecil, 1992, "Summary of Background Concentrations of Selected Radiochemical and Chemical Constituents in Groundwater from the Snake River Plain Aquifer, Idaho: Estimated from an Analysis of Previously Published Data," *Journal of the Idaho Academy of Science*, Vol. 28, No. 10.1, pp. 48.

Koehler, D. K., 1988, *Small Mammal Movement Patterns Around a Radioactive Waste Disposal Area in Southeastern Idaho*, M.S. Thesis: University of Wyoming, Laramie, Wyoming.

Kozak, Dr. Matt, Dr. Man-Sung Yim, and Dr. Terry Sullivan, 2003, *Independent Peer Review of Source-term Modeling for the INEEL Subsurface Disposal Area*, ICP/EXT-03-00081, Rev. 0, prepared by Brookhaven National Laboratory for Idaho National Engineering and Environmental Laboratory.

Kudera, D. E. and B. W. Brown, 1996, *Volatile Organic Compounds Disposed of from 1952 Through 1983 at the Radioactive Waste Management Complex: Quantities Forms, Release Mechanisms and Rates*, ER-WAG7-90, Idaho National Engineering Laboratory.

Landeen, D. S. and R. M. Mitchell, 1981, "Invasion of Radioactive Waste Burial Sites by the Great Basin Pocket Mouse (Perognathus parvus)," *International Symposium on Migration in the Terrestrial Environment of Long-lived Radionuclides from the Nuclear Fuel Cycle*, *Knoxville, Tennessee*, *July 27–31, 1981*, Vol. RHO-SA-211.

Laundré, J. W., 1989a, "Burrows of Least Chipmunks in Southeastern Idaho," *Northwestern Naturalist*, Vol. 70, pp. 18–20.

Laundré, J. W., 1989b, "Horizontal and Vertical Diameter of Burrows of Five Small Mammal Species in Southeastern Idaho," *Great Basin Naturalist*, 1989, Vol. 49, pp. 646–649.

Leecaster, Molly K., 2002, *Geostatistic Modeling of Subsurface Characteristics in the Radioactive Waste Management Complex Region, Operable Unit 7-13/14*, INEEL/EXT-02-00029, Rev. 0, Idaho National Engineering and Environmental Laboratory.

Leecaster, Molly K., 2004, *Fiscal Year 2004 Geostatistical Modeling of Lithologic Characteristics in the Radioactive Waste Management Complex for Operable Unit 7-13/14*, ICP/EXT-04-00494, Idaho National Engineering and Environmental Laboratory, Idaho Completion Project.

Leecaster, Molly K. and Larry C. Hull, 2004, *Spatial Distribution of Neptunium and Uranium Partition Coefficients (K_d) for Interbed Sediments at a Radioactive Waste Subsurface Disposal Area*, ICP/EXT-03-00088, Rev. 0, Idaho National Engineering and Environmental Laboratory, Idaho Completion Project.

Lerman, A., 1988, *Geochemical Processes Water and Sediment Environments,* Reprint ed., Melbourne, Florida: Krieger Publishing Company.

Lindzey, F. G., 1976, "Characteristics of the Natal Den of the Badger," *Northwest Science*, Vol. 50, No. 3, pp. 178–180.

Loomis, Guy G., James J. Jessmore, Jerry R. Weidner, Christopher M. Miller, and Allen L. Sehn, 2002, *Final Results Report for In Situ Grouting Technology for Application in Buried Transuranic Waste Sites, Volume 1, Technology Description and Treatability Study Results for Operable Unit 7-13/14*, INEEL/EXT-02-00233, Rev. 1, Idaho National Engineering and Environmental Laboratory.

Lopez, S. L., William H. Landman, Donald E. Sebo, and Vivian G. Schultz, 2005, *Summary Report for the OU 7-13/14 Early Actions Beryllium Encapsulation Project*, ICP/EXT-04-00646, Idaho National Laboratory, Idaho Completion Project.

Lopez, Steve L., 2004, *Action Memorandum for the OU 7-13/14 Early Actions Beryllium Encapsulation Project*, DOE/NE-ID-11162, U.S. Department of Energy Idaho Operations Office.

Magnuson, S. O., 1995, *Inverse Modeling for Field-Scale Hydrologic and Transport Parameters of Fractured Basalt*, INEL-95/0637, Idaho National Engineering Laboratory.

Magnuson, S. O., 1998, *Sensitivity of the SDA Flow and Transport Simulator to the Low Permeability Region in the Aquifer*, INEEL/INT-98-01066, Idaho National Engineering and Environmental Laboratory.

Magnuson, S. O. and D. L. McElroy, 1993, "Estimation of Infiltration from In Situ Moisture Contents and Representative Moisture Characteristic Curves for the 30', 110', and 240 Interbeds," EDF-RWM-93-001, Idaho National Engineering Laboratory.

Magnuson, S. O. and A. J. Sondrup, 1998, *Development, Calibration, and Predictive Results of a Simulator for Subsurface Pathway Fate and Transport of Aqueous- and Gaseous-Phase Contaminants in the Subsurface Disposal Area at the Idaho National Engineering and Environmental Laboratory*, INEEL/EXT-97-00609, Idaho National Engineering and Environmental Laboratory.

Magnuson, Swen O. and A. Jeffrey Sondrup, 2006, *Subsurface Flow and Transport Modeling for the OU 7-13/14 Remedial Investigation and Feasibility Study,* ICP/EXT-05-01016, Rev.0, Idaho National Laboratory, Idaho Cleanup Project.

Martian, P., 1995, *UNSAT-H Infiltration Model Calibration at the Subsurface Disposal Area, Idaho National Engineering Laboratory*, INEL-95/0596, Idaho National Engineering Laboratory.

Martian, P., 2003, "Simulation of Carbon-14 Transport in a Mesoscale Experiment," MCP-3394, Rev. 0, Idaho National Engineering and Environmental Laboratory.

McCarthy, J. M., R. C. Arnett, R. M. Neupauer, M. J. Rohe, and C. Smith, 1995, *Development of a Regional Groundwater Flow Model for the Area of the Idaho National Engineering Laboratory, Eastern Snake River Plain Aquifer*, INEL-95/0169, Rev. 1, Idaho National Engineering Laboratory.

McCarthy, J. M., B. H. Becker, S. O. Magnuson, K. N. Keck, and T. K. Honeycutt, 2000, *Radioactive Waste Management Complex Low-Level Waste Radiological Composite Analysis*, INEEL/EXT-97-01113, Rev. 0, Idaho National Engineering and Environmental Laboratory.

McElroy, D. L. and J. M. Hubbell, 1990, *Hydrologic and Physical Properties of Sediments at the Radioactive Waste Management Complex*, EGG-BG-9147, Idaho National Engineering Laboratory.

McElroy, Deborah L. and Joel M. Hubbell, 2003, *Advanced Tensiometer Monitoring Results from the Deep Vadose Zone at the Radioactive Waste Management Complex*, INEEL/EXT-02-01276, Rev. 0, Idaho National Engineering and Environmental Laboratory.

McKenzie, D. H., L. L. Caldwell, Jr., C. E. Cushing, R. Harty, Jr. W. E. Kennedy, M. A. Simmons, J. K. Soldat, and B. Swartzman, 1982, *Relevance of Biotic Pathways to the Long-Term Regulation of Nuclear Waste Disposal*, NUREG/CR-2675, U.S. Nuclear Regulatory Commission.

McKenzie, M. Doug, Donald E. Sebo, Kirk M. Green, and Vivian G. Schultz, 2005, *Waste Information and Location Database for the OU 7-13/14 Project*, ICP/EXT-04-00271, Idaho National Laboratory, Idaho Cleanup Project.

Mendoza, C. A. and E. O. Frind, 1990a, "Advective-Dispersive Transport of Dense Organic Vapors in the Unsaturated Zone, 1, Model Development," *Water Resources Research*, Vol. 26, No. 3.

Mendoza, C. A. and E. O. Frind, 1990b, "Advective-Dispersive Transport of Dense Organic Vapors in the Unsaturated Zone, 2, Sensitivity Analysis," *Water Resources Research*, Vol. 26, No. 3.

Merck, 1989, *An Encyclopedia of Chemicals, Drugs, and Biologicals,* 11th ed., Rahway, New Jersey: Merck & Co. Publishing.

Miller, Eric C. and Mark D. Varvel, 2005, *Reconstructing the Past Disposal of Series 743 Waste in the Subsurface Disposal Area for Operable Unit 7-08, Organic Contamination in the Vadose Zone*, INEEL/EXT-01-00034, Rev. 1, Idaho National Laboratory, Idaho Completion Project.

Millington, R. J., 1959, "Gas Diffusion in Porous Media," *Science*, Vol. 130.

Nagata, P. K. and J. Banaee, 1996, *Estimation of the Underground Corrosion Rates for Low-Carbon Steels; Types 304 and 316 Stainless Steels; and Inconel 600, 601, and 718 Alloys at the Radioactive Waste Management Complex*, INEL 096/098, Idaho National Engineering Laboratory.

Nalla, Gopi, 2004, *Near-Field Simulation of Carbon-14 and Tritium Migration from Buried Beryllium Blocks in the Subsurface Disposal Area*, ICP/EXT-04-00321, Rev. 0, Idaho National Engineering and Environmental Laboratory, Idaho Completion Project.

Nimmo, J. R., K. S. Perkins, P. A. Rose, J. P. Rousseau, B. R. Orr, B. V. Twining, and S. R. Anderson, 2001, "2001 Kilometer-Scale Rapid Flow in a Fractured-Basalt Unsaturated Zone at the Idaho National Engineering and Environmental Laboratory," edited by B. H. Kueper, K. S. Novakowski, and D. A. Reynolds., *2001 Conference Proceedings*, *Toronto, March 26-28, 2001*.

NRCS, 1981, *NRCS Range Site Descriptions for MLRA*, BLM-BLMB-B11b, National Resource Conservation Service.

Oztunali, O. I. and G. W. Roles, 1985, *Update of Part 61 Impacts Analysis Methodology,* NUREG/CR-4370, Vol. 1, U.S. Nuclear Regulatory Commission.

Pearson, L. C., 1965, "Primary Production in Grazed and Ungrazed Desert Communities of Eastern Idaho," *Ecology*, Vol. 46, pp. 278–285.

Plummer, M. A., L. C. Hull, and D. T. Fox, 2004, "Transport of Carbon-14 in a Large Unsaturated Column," *Vadose Zone Journal*, Vol. 3, No. 1, pp. 109–121.

Reynolds, T. D., 1990, "Root Mass and Vertical Root Distribution of Five Semi- Arid Plant Species," *Health Physics*, Vol. 58, No. 2, pp. 191–197.

Reynolds, T. D. and W. L. Wakkinen, 1987, "Characteristics of the Burrows of Four Species of Rodents in Undisturbed Soils in Southeastern Idaho," *American Midland Naturalist*, Vol. 118, No. 2, pp. 245–260.

Reynolds, T. D. and J. W. Laundré, 1988, "Vertical Distribution of Soil Removed by Four Species of Burrowing Rodents in Disturbed and Undisturbed Soils," *Health Physics*, Vol. 54, No. 4, pp. 445–450.

Reynolds, T. D. and L. L. Fraley Jr., 1989, "Root Profiles of Some Native and Exotic Plant Species in Southeastern Idaho," *Environmental and Experimental Botany*, Vol. 29, No. 2, pp. 241–248.

Roback, R. C., T. M. Johnson, T. L. McLing, M. T. Murrell, Shangde Luo, and Teh Lung Ku, 2001, "Uranium Isotopic Evidence for Groundwater Chemical Evolution and Flow Patterns in the Eastern Snake River Plain Aquifer," *Idaho-Geological Society of America Bulletin*, Vol. 113, No. 9, pp. 1133–1141.

Robertson, J. B., 1974, *Digital Modeling of Radioactive and Chemical Waste Transport in the Snake River Plain Aquifer at the National Reactor Testing Station, Idaho,* Open-File Report IDO-22054, U.S. Geological Survey.

Robertson, J. B., R. Schoen, and J. T. Barraclough, 1974, *The Influence of Liquid Waste Disposal on the Geochemistry of Water at the National Reactor Testing Station, Idaho, 1952-1970*, Open-File Report IDO-22053, U.S. Geological Survey.

Rodriguez, R. R., A. L. Schafer, J. M. McCarthy, P. Martian, D. E. Burns, D. E. Raunig, N. A. Burch, and R. L. Van Horn, 1997, *Comprehensive RI/Feasibility Study for the Idaho Chemical Processing Plant Operable Unit 3-13 at the INEEL–Part A, RI/BRA Report*, DOE/ID-10534, U.S. Department of Energy Idaho Operations Office.

Rood, A. S., 1999, *GWSCREEN: A Semi-Analytical Model for Assessment of the Groundwater Pathway from Surface or Buried Contamination, Theory and User's Manual Version 2.5,* INEEL/EXT-98-00750, Idaho National Engineering and Environmental Laboratory.

Root, R. W. Jr., 1981, *Documentation and User's Guide for DOSTOMAN–A Pathways Computer Model of Radionuclide Movement*, DPST-81-549, Savannah River Laboratory.

Rousseau, Joseph P., Edward R. Landa, John R. Nimmo, L. DeWayne Cecil, LeRoy L. Knobel, Pierre D. Glynn, Edward M. Kwicklis, Gary P. Curtis, Kenneth G. Stollenwerk, Steven R. Anderson, Roy C. Bartholomay, Clifford R. Bossong, and Brennan R. Orr, 2005, *Review of the Transport of Selected Radionuclides in the Interim Risk Assessment for the Radioactive Waste Management Complex, Waste Area Group 7 Operable Unit 7-13/14, Idaho National Engineering and Environmental Laboratory, Idaho*, Scientific Investigations Report 2005-5026, U.S. Geological Survey, DOE/ID-22192, U.S. Department of Energy Idaho Operations Office.

Shuman, R. D., M. J. Case, and S. K. Rope, 1985, *Documentation of a Simple Environmental Pathways Model of the Radioactive Waste Management Complex at the Idaho National Engineering Laboratory*, EGG-WM-6916, Idaho National Engineering Laboratory.

Smith, R. P., 2002, *Variability of the Aquifer Thickness Beneath the Idaho National Engineering and Environmental Laboratory (INEEL)*, INEEL/EXT-02-01022, Idaho National Engineering and Environmental Laboratory.

Sondrup, A. Jeffrey, Eric C. Miller, Edward H. Seabury, and Nick Josten, 2004, *Estimating Carbon Tetrachloride and Total Volatile Organic Compound Mass Remaining in Subsurface Disposal Area Pits*, ICP/EXT-04-00396, Idaho National Engineering and Environmental Laboratory, Idaho Completion Project.

Sullivan, T. M., 2006, *DUSTMS_D—Disposal Unit Source Term—Multiple Species—Distributed Failure Data Input Guide*, Rev. 1, BNL-75554-2006, Brookhaven National Laboratory.

Varvel, Mark D., 2005, *Mass Estimates of Organic Compounds Buried in the Subsurface Disposal Area for Operable Units 7-08 and 7-13/14*, INEEL/EXT-01-00277, Rev. 1, Idaho National Laboratory, Idaho Completion Project.

Vigil, M. J., 1988, *Estimate of Water in Pits during Flooding Events*, EDF-BWP-12, Idaho National Engineering Laboratory.

Vinsome, P. K. and G. M. Shook, 1993, "Multi-Purpose Simulation," *Journal of Petroleum Science and Engineering*, Vol. 9, pp. 29–38.

Visual Numerics, Inc., 2001, PV-WAVE User's Guide, unpublished work, 1990–2001.

Whitmire, D. L., 2001, *Summary Report: Simulation of Groundwater Flow near the Subsurface Disposal Area at the Idaho National Engineering and Environmental Laboratory,* INEEL/EXT-01-01643, Rev. 0, prepared by North Wind Environmental for Idaho National Engineering and Environmental Laboratory.

Wilde, D. B., 1978, *A Population Analysis of the Pygmy Rabbit (Sylvilagus idahoensis) on the INEL Site*, Ph.D. Dissertation: Idaho State University, Pocatello, Idaho.

Winsor, T. F. and F. W. Whicker, 1980, "Pocket Gophers and Redistribution of Plutonium in Soil," *Health Physics*, Vol. 39, pp. 257–262.

Wylie, A. H. and J. M. Hubbell, 1994, *Aquifer Testing of Wells M1S, M3S, M4D, M6S, M7S, and M10S at the Radioactive Waste Management Complex*, ER-WAG7-26, Rev. 1, Idaho National Engineering Laboratory.